Chemical Looping Combustion of Biomass: Thermodynamic Analysis and Metal Oxide Synthesis

Submitted in partial fulfilment of the requirements

for the award of the degree of

DOCTOR OF PHILOSOPHY

in

CHEMICAL ENGINEERING

by

Mr. SHAILESH SINGH SIKARWAR

(Roll No. 717141)

Supervisor

Dr. Vooradi Ramsagar

Associate Professor

Co- Supervisor

Prof. Venkata Suresh Patnaikuni

Professor

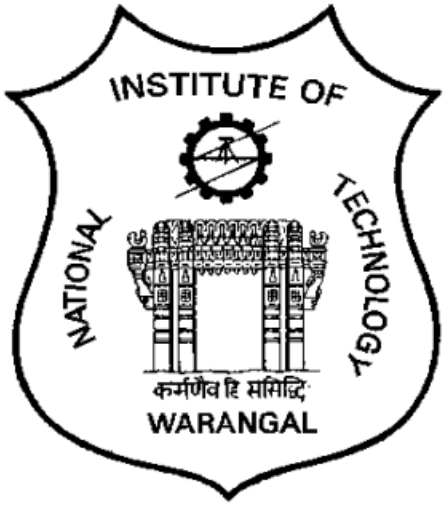

Department of Chemical Engineering

National Institute of Technology Warangal

Warangal-506004, Telangana, India

January – 2024

Dedicated

to

My parents

DECLARATION

This is to certify that the work presented in the thesis entitled "***Chemical Looping Combustion of Biomass: Thermodynamic Analysis and Metal Oxide Synthesis***" is a bonafide work done by me under the supervision of ***Dr.Vooradi Ramsagar and Prof. Venkata Suresh Patnaikuni*** and was not submitted elsewhere for award of any degree.

I declare that this written submission represents my ideas in my own words and where others' ideas or words have been included, I have adequately cited and referenced the original source. I also declare that I have adhered to all principles of academic honesty and integrity and have not misrepresented or fabricated or falsified any idea/data/fact/source in my submission. I understand that any violation of the above will be a cause for disciplinary action by the Institute and can also evoke penal action from the sources which have thus not been properly cited or from whom proper permission has not been taken when needed.

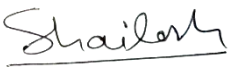

Shailesh Singh Sikarwar

(717141)

ACKNOWLEDGEMENT

I take this opportunity to express my sincere gratitude to my respected supervisors ***Dr.Vooradi Ramsagar and Prof. Venkata Suresh Patnaikuni***, Department of Chemical Engineering, National Institute of Technology (NIT), Warangal, India for giving me an opportunity to pursue doctoral thesis work under their esteemed supervision. Their outstanding guidance, constant support, patience, motivation and immense knowledge extremely helped me in all the time of research and writing of this thesis. I could not have imagined having better mentor for my PhD study.

I wish to sincerely thank university authorities, ***Prof. Bidyadhar Subudhi***, Director, NIT Warangal, ***Prof. N.V. Ramana Rao***, former Director, NIT Warangal and other top officials who gave me an opportunity to carry out research work. I wish to express my sincere and whole hearted thanks and gratitude to my doctoral scrutiny committee (DSC) members**, *Prof. A. Sarat Babu***, Department of Chemical Engineering, ***Dr. S. Vidyasagar,*** Associate Professor, Department of Chemical Engineering, ***Dr. D. Jaya Krishna,*** Associate Professor Department of Mechanical Engineering, NIT Warangal for their kind help, encouragement and valuable suggestions for successful completion of research work. I would like to express heart-felt thanks to former DSC member ***Prof. Y. Pydi Setty***, Department of Chemical Engineering, NIT Warangal for his suggestions, support and encouragement. I wish to express my profound thanks to the entire Faculty, Scholars, Non-teaching staff and all others in the Chemical Engineering Department and in the Institute who directly and indirectly helped me during the course of my research work at NIT Warangal.

I wish to express sincere thanks to my beloved friends and lab mates *Dr. Gajanan Dattarao Suryawanshi, Dr. B. Basant Kumar Pillai, Mr. Kiran Donthula* and *Ms. Snigdha Saha* for their constant encouragement and help acquired during my research period at NITW.

I take this opportunity to sincerely acknowledge the ***Ministry of Education (MoE), Government of India*** for providing the financial assistance in the form of stipend. Last but not the least; I would like to express my profound gratitude to my family members: my father ***Mr. Govind Singh Sikarwar***, my mother ***Mrs. Shailaja Sikarwar***, my wife ***Mrs. Anupam Parmar*** and other members of my family for their support and continuous encouragement throughout my years of study and through process of researching and writing this thesis.

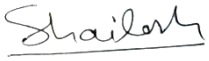

Shailesh Singh Sikarwar

Abstract

The most bothersome challenge for sustaining life on Earth is global warming caused by greenhouse gas emissions. Most countries currently rely on coal as their principal fossil fuel source for electricity generation. Coal-fired power stations release significant amounts of greenhouse gases, making the power industry a key contributor to anthropogenic CO_2 emissions. To successfully restrict global warming, a significant transition to renewable energy sources is required. Agricultural biomass might be a viable alternative to fossil fuels for low-capacity energy generation. This strategy not only minimizes reliance on fossil fuels, but it also acts as a dependable supplement to solar and wind energy during the off-season, solving both energy needs and waste management concerns at the same time. As a result, there is an urgent need to improve power generation capabilities utilizing biomass, which is a carbon-negative and renewable fuel. Furthermore, incorporating a CO_2 capture unit into this technology has the potential to change it from carbon-neutral to carbon-negative, giving a sustainable solution to decreasing CO_2 emissions. Chemical Looping Combustion (CLC) is a contemporary method in which fuels generate both heat and power without any carbon emissions.

The CLC method is fundamentally based on merging oxy-combustion and pre-combustion capture techniques. This eliminates direct air participation in the combustion process. Metal oxide is used in fuel reactors to provide oxygen for combustion of the fuel while the air reactor oxidizes the reduced form of metal oxide. Hydrogen is widely employed in the petrochemical sector for the upgrading of fossil fuels and the production of ammonia and methanol. It is also an ecologically friendly energy source for transportation and electricity generation. The three reactor Biomass Direct Chemical Looping (BDCL) system is a particularly efficient alternative when seeking to co-produce power and hydrogen utilizing CLC technology.

This study uses aspenONE v10.0 to synthesis and simulate CLC-based power plants and BDCL plants. A rigorous parametric study is undertaken to discover opportunities for improving overall plant performance. The range of plant variations studied within this project falls into the subsequent four categories: 1) Conventional BFPP without CO_2 capture, 2) CLC based BFPP with power generation alone, 3) CLC based BFPP with hydrogen and power co-generation, 4) CLC based BFPP with hydrogen and power co-generation coupled with CO_2 utilization plant. The overall performances of these configurations are examined based on the

energy, exergy, and environmental analyses. The first objective of the thesis is addressed by conducting the performance evaluation and comparison of conventional and CLC based BFPP combined with an Organic Rankine Cycle (ORC) system. The proposed CLC based BFPP is extended for co-generation of hydrogen and power in the second objective of thesis. Furthermore, the utilization of the produced hydrogen and carbon dioxide for the synthesis of methane and ammonia is also explored. The third objective of the thesis is addressed by conducting the performance evaluation and comparison of CLC based biomass fired power plants with different oxygen carriers. The fourth objective of the thesis is focused on the experimental studies to synthesize and performance assessment of novel nanofibrous oxygen carriers.

Based on the research findings, it can be concluded that CLC based BFPP configuration is energetically, exergetically and environmentally efficient compared to the conventional BFPP. Furthermore, the net energy and exergy efficiencies of the three-reactor CLC plant with hydrogen co-generation are found to be 33.72% and 28.99%, respectively. These efficiencies are greater by 12.13% and 10.43% compared to CLC based BFPP. Also, the CLC based plants integrated with methane and ammonia synthesis may not be a better choice for power production due to significant loss in energy. It is also revealed that the bimetallic oxygen carrier (10% CuO + 90% Fe_2O_3) is a better option for achieving high process efficiency without considerably inflating overall operational costs as iron ore is largely available in India at lower cost as compared to copper ore. During CLC experimental tests with gaseous fuel, it is evident that the Fe_2O_3/Al_2O_3 composite nanofibres are more resistant to thermal sintering than the nanoparticles. Hence, these nanostructured oxygen carriers could be a promising option for lengthy CLC operations.

This study demonstrates the superiority of chemical looping combustion-based biomass fired power plant for CO_2 capture coupled with the carbon dioxide utilization plant over the conventional plant. The outcome of this study can provide the basis for potential improvement of CLC based BFPP. Additionally, the findings show great promise and open the way for a new direction in the creation of nanostructured OCs capable of exhibiting extraordinary redox cyclic stability.

Table of Content

List of Figures

List of Tables

Nomenclature

BDCL	Biomass Direct Chemical Looping
BEHP	biomass electrolysis for hydrogen production
BFPP	Biomass Fired Power Plants
CCR	carbonation-calcination reaction
CCU	Carbon capture and utilization
CFB	circulating fluidized bed
CFPP	Coal-Fired Power Plants
CLC	Chemical Looping Combustion
CLG	Chemical Looping Gasification
CLHP	chemical looping hydrogen production
CLOU	Chemical Looping with Oxygen Uncoupling
CNF	Composite nanofibers with 60 wt.% Fe_2O_3 and 40 wt.% Al_2O_3
CNP	Composite nanoparticles with 60 wt.% Fe_2O_3 and 40 wt.% Al_2O_3
CCS&U	CO_2 capture, storage and utilization
CHP	combined heat and power
EDAX	Energy dispersive X-ray spectroscopy
FBFCs	flow biomass fuel cells
GHG	greenhouse gas
HHV	Higher Heating Value
iG-CLC	in-situ Gasification-Chemical Looping Combustion
IEA	International Energy Agency
MEA	monoethanolamine
MCFC	Molten Carbonate Fuel Cells
OC	oxygen carrier
ORC	Organic Rankine Cycle
SEM	Scan electron microscopy
PNF	Pure Fe_2O_3 nanofibers

PNP	Pure Fe_2O_3 nanoparticles
PVP	Polyvinylpyrrolidone
SOFC	solid oxide fuel cell
XRD	X-Ray diffraction analysis

Symbols

$\dot{m}_n$	Mass flow rate
$\dot{E}$	Energy flow
$\dot{W}$	Power output
η	Energy efficiency
Ex	Exergy
ψ	Exergy efficiency
$SCEx$	Standard specific exergy
LHV_b	Lower heating value of biomass
HHV_b	Higher heating value of biomass
E_{CO_2}	Specific CO_2 emission
$\varepsilon_{af.CO_2}$	Annual CO_2 emissions rate per unit of biomass
n	number of components
N	nitrogen
O	oxygen
R	universal gas constant, kJ/kmol K
S	specific molar entropy, kJ/kmol K
S	sulphur
T	temperature, K
P	Pressure
U_f	Fuel utilization factor
F	Faraday constant
V	Voltage
λ	Latent heat of vaporization
w	moisture content, %
x	mole fraction

Chapter 1
Introduction

As per the International Energy Agency (IEA) 2010 recommendation, by the 2050th year, the CO_2 emissions from the power plants need to be reduced to 20% of the 2009 emissions (IEA, 2010). At present in most of the countries, coal is the primary fossil fuel source for power generation. Figure 1.1 Shows the global CO_2 emissions from different sectors. The coal-fired power plants cause enormous greenhouse gas (GHG) emissions, hence the power sector has major share in anthropogenic CO_2 emissions.

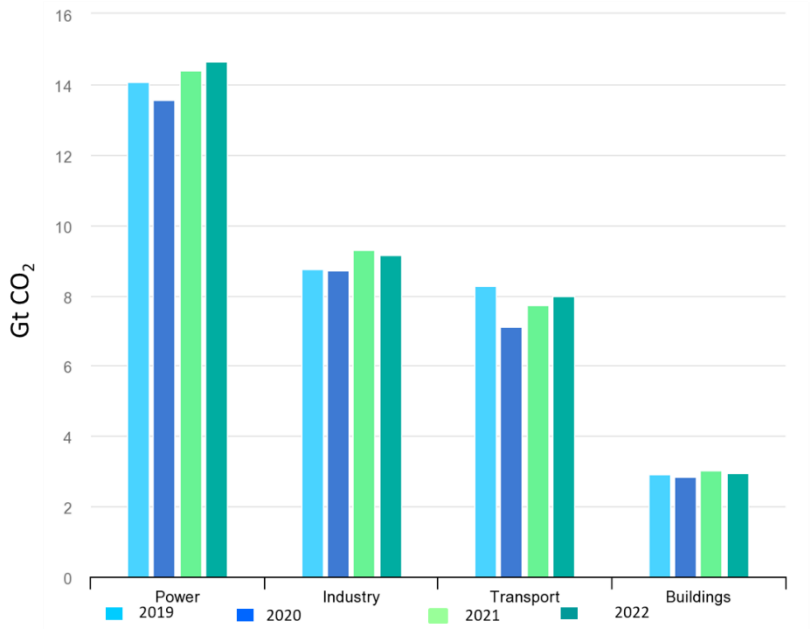

Figure 1.1 Share of global CO_2 emissions by different sectors (IEA, 2023a).

As fossil-based fuels still remain as our primary source of energy in this century, the emission of CO_2 into the atmosphere leading to climate change and global warming has become a global colossal issue, which requires immediate attention (Jain, 2019).India stands as the fourth largest emitter of CO_2 in the world after China, the US and the EU as per the EC, Emissions database for global atmospheric research, 2019. To curtail the CO_2 emissions and to limit the global temperature rise to 2 °C by end of this century as per the Paris agreement in CoP-21, 2015, countries should adopt multi-pronged strategies including use of alternative energy sources (e.g., solar, wind and geothermal) and renewable (e.g., biomass and biofuel); integration of CO_2 capture, storage and utilization (CCS&U) and improving process efficiencies to reduce energy consumption (Razi and Dincer, 2022). Consequently, India reaffirmed its commitment at the CoP-26 conference held in Nov 2021 at Glasgow, Scotland, to obtain 50% of its energy from renewable resources and to reduce total projected carbon emissions by one billion tons by 2030. It also pledged to achieve net zero emission status by 2070 (Dwivedi et al., 2022). Recently, the Indian government initiated a National Green Hydrogen Mission with an aim to make India as a global hub for production, utilization and export of green hydrogen and its derivatives.

To effectively limit the global temperature rise to the critical threshold of 2°C by the end of this century, the imperative is clear: a substantial shift towards renewable energy sources is paramount. This transition necessitates not only a reduction in the unrestrained consumption of fossil fuels but also a robust embrace of diverse renewable sources (Sharif et al., 2021). However, the prevailing strategy of centralized energy generation, particularly in the realm of electricity, proves to be an unsuitable avenue for the efficient harnessing of renewables, and this is attributed to a combination of compelling factors: (i) The requirement for ample space to accommodate high-capacity power plants stands as a significant limitation in the current context. The substantial land footprint needed for such installations raises concerns about the utilization of valuable areas and the environmental impact of such large-scale facilities (Rahaman et al., 2022). (ii) Critical efficiency consideration revolves around heating applications. In this context, the direct utilization of renewable energy sources exhibits a clear advantage over the more intricate route of converting renewable energy to electricity and then further converting it to heat. This direct application approach is not only more straightforward but also ensures minimal energy losses in the transformation process. (iii) The intermittent nature of renewable energy, largely determined by geographical location and seasonal variations, creates a formidable challenge (Azarpour et al., 2013). The inconsistency in energy production from a single renewable source renders it inadequate to meet the continuous, centralized demand characteristic of the current energy consumption model. The reliance on a singular renewable source becomes impractical, necessitating a more diverse and adaptable approach.

To effectively address these limitations and unlock the full potential of renewables, the development of intelligent, sustainable energy systems becomes an inevitability. These smart systems operate on the fundamental principle of tailoring energy solutions to the specific needs of a given region or locality (Dincer and Acar, 2017). The viability of such systems hinges on the availability of local resources, making resource assessment and allocation a critical determinant of their feasibility. Moreover, as a pivotal step in this transformative journey, the utilization of environmentally benign resources and the implementation of waste-to-energy policies assume paramount importance (Gungor and Dincer, 2021; Gungor and Dincer, 2022). These strategies hold the potential to significantly alleviate the environmental burdens arising from conventional landfilling practices, thereby playing a vital role in the reduction of greenhouse gas emissions. Solar and wind energy serve as exemplary cases of these environmentally friendly resources, boasting zero carbon emissions. However, their inherent seasonality introduces challenges in maintaining a consistent power supply to meet continuous demand, particularly during periods of reduced sunlight or wind. To bridge this gap and ensure

a dependable energy supply throughout the year, the utilization of biomass emerges as a compelling alternative (Hossen et al., 2022). Various forms of biomass, such as agricultural waste, forest waste, municipal solid waste, and sewage waste, can be harnessed for power production. This approach not only reduces dependence on fossil fuels but also serves as a reliable complement to solar and wind energy during off-seasons, thus addressing both energy requirements and waste management challenges simultaneously.

The global potential of biomass as a renewable energy source is vast, with significant contributions from various regions. In North America, Canada utilizes agricultural and forest residues, producing 27 million tons of biomass annually with over 200 firms generating $1.3 billion in sales from bioproducts. The United States leads in bioethanol production, primarily using corn, contributing 43% to the total renewable energy produced domestically (Gielen et al., 2019). In South America, Brazil's energy matrix prominently features renewable resources, with sugarcane biomass playing a critical role, making it a leading producer of bioethanol (Brinkman et al., 2018). Asia also shows substantial potential, with China leveraging its vast agricultural residues to produce bioethanol and biogas, and India focusing on crops like Jatropha and sugarcane for biodiesel and ethanol production, respectively. Malaysia, with its extensive oil palm plantations, is pivoting towards biomass for energy to reduce reliance on finite fossil fuels. Europe, aiming for 32% renewable energy by 2030, heavily relies on agricultural and forest residues, with France and Germany being significant contributors (Scarlat et al., 2019). The European Union also dominates global wood pellet production, further highlighting the continent's commitment to biomass as a key component of its renewable energy strategy.

Bioenergy with Carbon Capture and Sequestration (BECCS) combines the generation of bioenergy with carbon capture and storage technology to achieve negative CO_2 emissions. Biomass absorbs CO_2 from the atmosphere as it grows, which is then captured and sequestered when the biomass is converted into energy, preventing it from returning to the atmosphere (Babin et al., 2021). The BECCS concept has the following clear advantages: (a) Negative Emissions: BECCS can remove CO2 from the atmosphere, helping to reduce overall greenhouse gas concentrations (Fajardy et al., 2017). (b) Renewable Energy Source: Biomass is a renewable resource that can be replenished, offering a sustainable energy alternative. (c) Energy Production: BECCS generates energy in the form of heat, electricity, or biofuels while capturing carbon (Pröll and Zerobin, 2019). (d) Climate Mitigation: It can contribute significantly to meeting climate targets, such as those set by the Paris Agreement (Moriarty and Honnery, 2016). (e) Economic Potential: Provides opportunities for economic growth in the bioenergy sector and related industries (Al-Qayim et al., 2015; Portugal-Pereira et al., 2015).

However, the implementation of BECCS at large scale may disturb the eco system and has the following negative impacts: (a) Land Use: Large-scale BECCS requires substantial land, which can lead to deforestation, loss of biodiversity, and competition with food production (Fajardy and Mac Dowell, 2017). (b) Water Consumption: BECCS has a high water footprint, exacerbating water scarcity issues, especially in agriculture-intensive regions (Gerbens-Leenes et al., 2009). (c) Energy Efficiency: The energy return on investment (EROI) for biofuels is relatively low compared to fossil fuels, which can make BECCS energy-intensive and less efficient (Hall et al., 2014). (d) Collateral Emissions: Processes involved in BECCS, such as biomass transportation and processing, can produce additional CO_2 emissions, potentially offsetting the benefits (Fajardy and Mac Dowell, 2017). (e) Economic Costs: High costs associated with biomass cultivation, carbon capture, and storage technology can make large-scale BECCS implementation economically challenging. (f) Negative Emission Potential: Achieving true negative emissions is complex and requires meticulous management to avoid collateral emissions and other unforeseen environmental impact (Fajardy and Mac Dowell, 2017).

In summary, the imperative to restrict global temperature rise necessitates a multifaceted approach that leverages the immense potential of renewables. The development of adaptable and resource-aware smart energy systems, coupled with the strategic utilization of environmentally friendly resources and the integration of waste-to-energy principles, provides a comprehensive framework to achieve this critical goal. By embracing renewable diversity, optimizing energy usage, and mitigating environmental impacts, we can chart a course toward a more sustainable energy future, effectively combating climate change while ensuring reliable energy access for generations to come.

The remaining portion of this chapter is structured as follows: Section 1.1 delves into the current utilization of fossil energy (coal, natural gas) and biomass in India and globally for electricity generation along with the recent trends in greenhouse gas emissions both in India and worldwide. In Section 1.2, deals with the most promising CO_2 mitigation techniques, such as CCS, CCU, and CCHC. It also provides a comprehensive overview of potential CO_2 utilization strategies. Finally, Section 1.3 outlines the overall structure and organization of the thesis.

1.1. Electricity generation from fossil fuels and biomass

Currently and in the near future, fossil fuels remain the primary energy sources for electricity generation in developing nations. In 1971, fossil fuels accounted for 88% of global energy consumption, a figure that decreased to 86% in 2015 when the Paris Agreement was signed, and further dropped to 83% by 2020 (Dale, 2021; IEA, 2020). Over the past two years,

electricity generation from coal-fired power plants has reached an all-time high due to the Russia-Ukraine conflict. Although this surge is a temporary disruption, the overall trajectory is not aligned with the Net Zero Emissions by 2050 Scenario. This scenario necessitates immediate reductions, aiming for a global decline of approximately 55% in unabated coal-fired generation by 2030 compared to 2022 levels, with a complete phase-out by 2040 (IEA 2023b). India possesses about 7.1% of the world's total coal reserves (IEA, 2020), and as of 2020, 75% of its total power generation comes from coal-fired power plants (Statistical-Review-of-World-Energy, 2017). Figure 1.2 provides CO_2 emission statistics in India for the year 2019 across various sectors. In the power sector alone, coal-fired power plants emitted a substantial amount of CO_2.

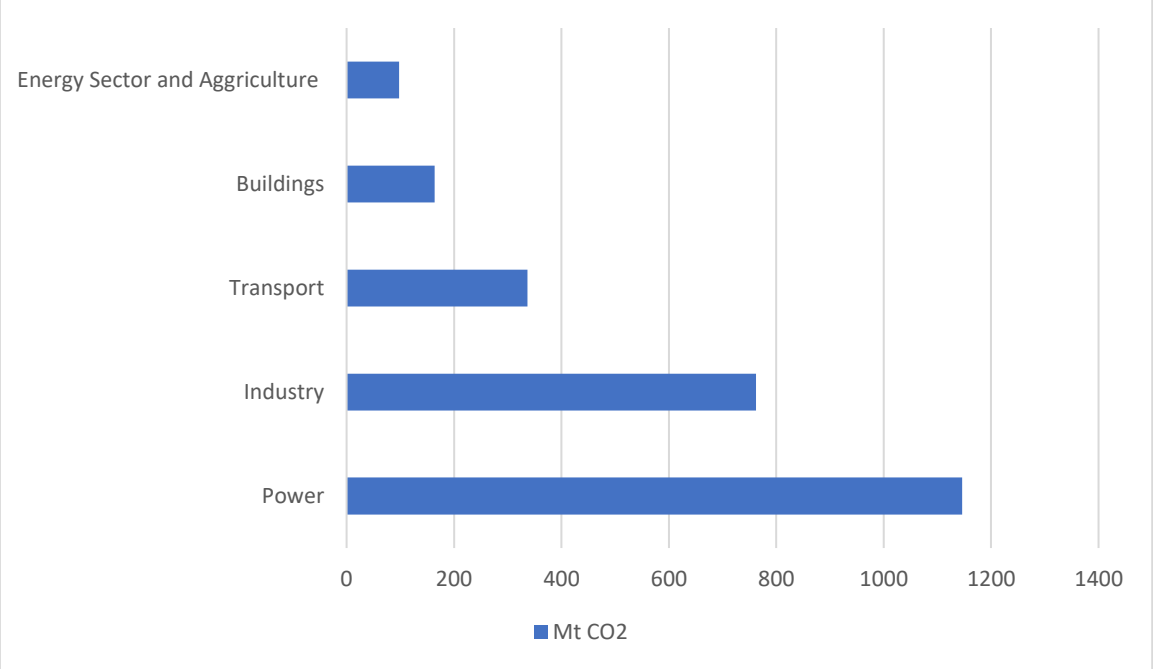

Figure 1.2: CO_2 emission statistics in India in the year 2019

Considering the fact that India has large coal reserves and its main source of electricity is thermal power plants using coal, it may not be possible to completely switch the power production from coal to renewable sources, at least for the next three to four decades. It ultimately calls for integration of emerging, futuristic and energy efficient CCS&U technologies into the thermal power plants. Furthermore, there is an urgent need to develop power production capabilities using biomass, which is a carbon negative and renewable fuel. Government of India has taken steps toward this by issuing a regulation on 9th Oct 2021 that all coal-fired thermal power plants must implement co-firing of biomass with coal up to 5% by energy within a year from regulatory date and 7% within two years. The substantial increase of biomass share in blended fuels drives the thermal power generation technology towards carbon neutral as it is, or carbon negative with CO_2 capture (Pillai et al., 2019; IEA, 2015; Sing, 2016; Annual report MNRE, 2017-2018).

In India, approximately 32% of the primary energy supply is derived from biomass, effectively meeting the energy requirements of over 70% of its population, as outlined in the IEA's India Energy Outlook (IEA, 2015). Notably, India possesses a potential bioenergy capacity of around 25 GW from commercially viable sources. Figure 1.3 provides an overview of India's electricity generation capacity, categorized by various energy resources, as of the year 2018. Countries with a strong agricultural base, like India, tend to produce substantial amounts of biomass. Annually, India generates 145.02 million tons of agricultural surplus dry biomass and 59.68 million tons from forest resources. In the Indian bioenergy sector, bagasse cogeneration currently contributes 8.7 GW, while non-bagasse biomass contributes only 0.662 GW in grid-connected mode and 0.16 GW in captive or off-grid mode (Annual report MNRE, 2017-2018). Apart from bagasse, the untapped potential of other available biomass resources in India remains underutilized. This inefficiency is attributed to various factors, including a lack of proper planning, suboptimal biomass management, and unfavorable policies (Singh, 2016). Transitioning from scattered domestic biomass use, the implementation of small-scale and grid-independent biomass-based power generation enhances utilization efficiency and addresses rural energy demand challenges. Furthermore, integrating a CO_2 capture unit with this technology has the potential to transform it from being carbon-neutral to carbon-negative, offering a sustainable approach to mitigating CO_2 emissions (Pillai et al., 2019).

1.2.Carbon Capture Technologies

Carbon dioxide emissions arise from both natural sources, such as decomposition, ocean release, and respiration, and human activities that include cement production, deforestation, and the combustion of fossil fuels like coal, oil, and natural gas. The accumulation of greenhouse gases contributes to the warming of our planet. Over the past 150 years, human activities have been the predominant drivers of the increased greenhouse gas levels in the atmosphere, notably CO_2, which is a major contributor to global warming. The consequences of this warming extend globally, affecting the environment, economy, and society as a whole. Therefore, carbon capture is recognized as a crucial and effective strategy for reducing CO_2 emissions and mitigating their detrimental effects (Gür, 2022; Sifat and Haseli, 2019).

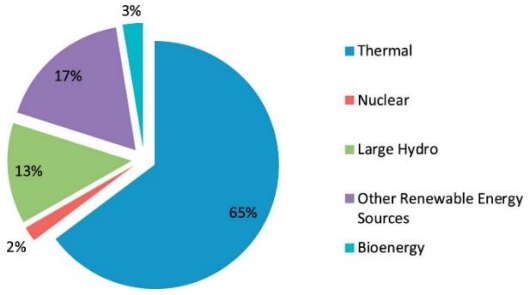

Figure 1.3: Electrical generation capacity in India (Annual report MNRE 2017-2018).

The technological landscape of CO_2 capture can be broadly classified into three main categories: pre-combustion, oxy-combustion, and post-combustion approaches. These technologies offer attractive CO_2 reduction potential but come with a notable energy penalty. Post-combustion capture targets direct CO_2 removal from flue gases after the combustion process, pre-combustion capture focuses on CO_2 extraction during the fuel conversion process before combustion, and oxy-combustion capture employs pure oxygen instead of air to generate a concentrated CO_2 gas stream (Madejski et al., 2022; Gizer et al., 2022).

Beyond these primary approaches, numerous alternative CO_2 capture methods have emerged. Examples include CO_2 permeable membranes (Hafeez et al., 2021), Molten Carbonate Fuel Cells (MCFC) (Odunlami et at., 2022), high-pressure solvent absorption from pressurized combustion/power generation exhaust gases (de Meyer and Jouenne, 2022), supersonic flow-driven CO_2 deposition, and more. A wide array of separation methods can be applied, predominantly utilizing post-combustion and pre-combustion approaches. These methods involve gas-phase separation, absorption in various solvents (e.g., amines, potassium carbonate, ammonia, sodium hydroxide) (Peu et al., 2023), adsorption on sorbents (e.g., molecular sieve, activated carbon) (Al Mesfer et al., 2018), as well as membrane-based or hybrid processes combining chemical absorption and membranes (Bhattacharyya et al., 2022). In addition to the well-established absorption techniques, other separation methods have emerged, such as Chemical Looping Combustion (CLC) (Daneshmand-Jahromi et al., 2023) and hydrate-based separation (Cheng et al., 2022). CLC, also known as unmixed combustion, employs oxygen carriers (metal oxides like Fe_2O_3, NiO, CuO, and Mn_2O_3) to indirectly provide oxygen for combustion. Hydrate-based separation involves injecting gas streams at high pressure to force CO_2 into water, subsequently separating and releasing CO_2 from the hydrate.

Among these methods, post-combustion capture as shown in Figure 1.4(a) stands out as a versatile choice, easily retrofitted into existing power plants to capture CO_2 from flue gas streams after combustion. This process generates a concentrated CO_2 stream that can be compressed, transported, and stored or sequestered. The typical coal/biomass based power plant process generates CO_2 containing flue gas streams at ambient pressure, which can be subjected to various separation techniques, including low-temperature adsorbents, physical/chemical absorption solvents, high-temperature sorbents, ionic liquids, CO_2 separation membranes, molecular filtration, and more. Some commercially deployed or pilot-demonstrated post-combustion capture technologies include carbonation-calcination reaction (CCR) systems, chilled ammonia, and monoethanolamine (MEA) (Chao et al., 2021).

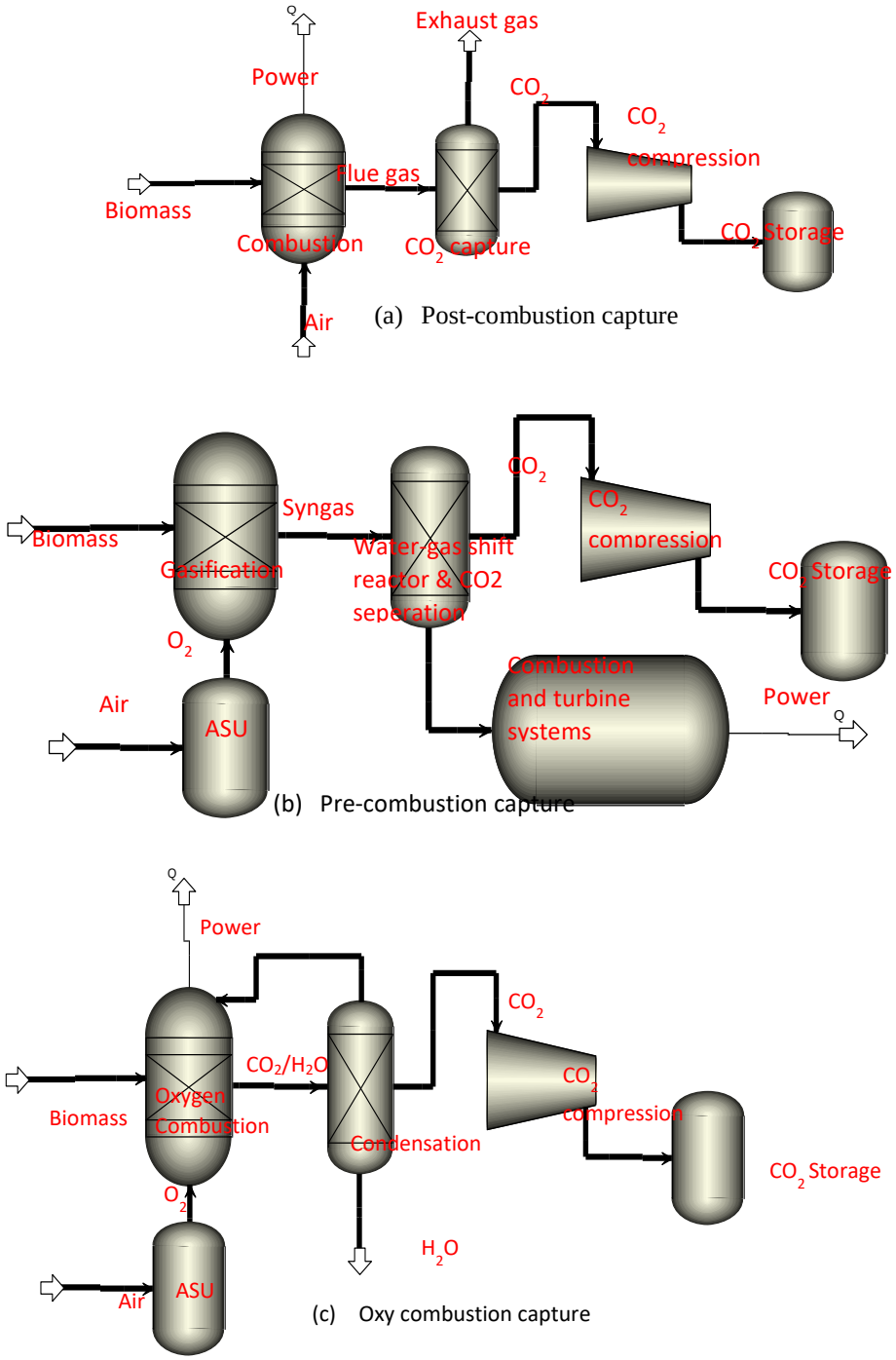

Figure 1.4. Flow diagram of CO_2 capture technologies (a) post-combustion, (b) pre-combustion and (c) oxy-combustion techniques

Pre-combustion capture as shown in Figure 1.4(b) operates by having coal/biomass react with pure oxygen (extracted from air separation units) in the presence of steam, resulting in syngas (composed of CO and H_2) (Olabi et al., 2022). The CO in the syngas is then converted into CO_2 and H_2 through the water gas shift reaction, yielding a concentrated CO_2 containing exit gas stream. Physical absorption-based processes (Selexol, Rectisol, etc.) or chemical absorption-based processes (methyldiethanolamine, MEA, etc.) can be employed to separate CO_2 and H_2S from this stream, resulting in concentrated hydrogen, which is utilized in combined cycle power

generation systems to generate electricity. The oxy-combustion capture scheme as shown in Figure 1.4(c), initially proposed by Horn and Steinberg in 1982, involves burning coal/biomass with high-purity oxygen (approximately 95%) instead of air. A portion of the flue gas stream is recycled back to the combustor to maintain the temperature. Unlike the post-combustion capture technique, the flue gas stream in the oxy-combustion process is not diluted by nitrogen, resulting in a composition primarily comprised of CO_2 and steam (Dziejarski et al., 2023).

These diverse carbon capture technologies, spanning pre-combustion, post-combustion, and oxy-combustion approaches, along with innovative alternative methods, hold immense potential for reducing CO_2 emissions, enhancing sustainability, and mitigating the global impacts of greenhouse gases (Sifat and Haseli , 2019). At present, the post combustion CO_2 capture by chemical absorption using amine-based solvents was one among the matured CO_2 capture technologies. However, the process is energy intensive and solvents are corrosive in nature are the major problems associated with this technology (Mazari et al., 2015). These unavoidable limitations indeed motivated the researchers to develop 2nd generation CO_2 capture technologies aiming at lower energy and economic penalties. Currently, Chemical Looping Combustion is attracting significant attention as a promising combustion technology for thermal power plants, due to its low energy penalty and the ability for inherent 100% CO_2 capture using metal oxides as oxygen carriers (Alalwan and Alminshid 2021).

1.2.1. Chemical looping combustion

In the realm of advanced combustion technologies, CLC has emerged as a standout contender, drawing significant attention as a highly promising option for thermal power plants. The distinctive feature of CLC lies in its impressive capability to simultaneously achieve minimal energy penalties and inherent 100% CO_2 capture, achieved through the utilization of efficient metal oxides as oxygen carriers. The fundamental concept of the CLC process is combining the oxy-combustion and pre-combustion capture techniques. Instead of direct air supply, CLC employs metal oxide/oxygen carrier particles to facilitate the conversion/oxidation of fuel into CO_2 and steam within the fuel reactor. This innovative approach has sparked heightened research interest in the combustion of gaseous, liquid, and solid fuels using CLC technology over the past few decades.

In the CLC scheme, the sold/gaseous fuel and oxygen carrier are introduced directly into the fuel reactor. Within this reactor, fuel undergoes combustion, and the oxygen carrier is simultaneously reduced. The reduced oxygen carrier is subsequently re-oxidized in the air reactor in the presence of air. The resulting exit streams from the fuel and air reactors exhibit a CO_2-rich composition and a N_2-rich composition, respectively. The block diagram for this two

reactor configuration is shown in Figure 1.5(a). A wide range of oxygen-carrying metal oxides, including copper oxides, iron oxides, manganese oxides, and magnesium oxides, can be effectively employed within the two-reactor CLC system. Importantly, the CLC technology has not only found its place in conventional power generation but is also being actively explored for cogeneration applications (He et al., 2020; Li et al., 2019).

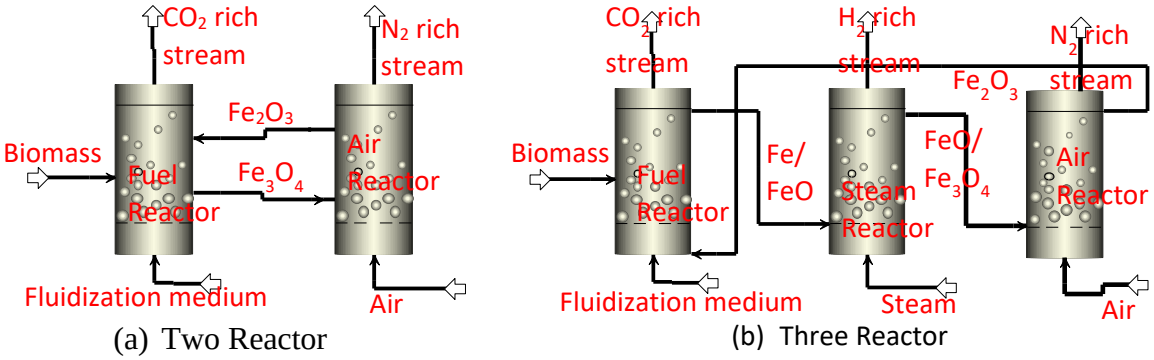

Figure 1.5: Different CLC process configurations

In the context of solid fuel CLC for power generation and hydrogen production, an intriguing extension introduces a third reactor, aptly named the steam reactor, situated between the air and fuel reactors as shown in Figure 1.5(b) (Li et al., 2019). Typically, Fe_2O_3, known for its diverse reducing states (FeO, Fe, and Fe_3O_4), serves as the preferred metal oxide for the three-reactor CLC system. The intricate steps of reduction and oxidation unfolds as Fe_2O_3 first undergoes reduction to FeO/Fe in the fuel reactor, facilitated by the presence of fuel and CO_2/steam as fluidizing agents. This reduced oxygen carrier then undergoes partial oxidation to Fe_3O_4/FeO in the steam reactor in the operating temperature range of 750 K to 850 K, utilizing steam. For temperatures above approximately 840 K, the reaction scheme for the iron-steam reaction becomes more complex. In this scenario, iron is oxidized by steam in two distinct steps as shown in Equations 1.1 and 1.2. Similar to the two-reactor CLC system, the air reactor re-oxidizes the completely reduced oxygen carriers, now in the presence of air. The streams emanating from the fuel and steam reactors, following steam condensation, yield pure carbon dioxide and hydrogen, respectively.

$$0.947Fe + H_2O\ (g) \leftrightarrow Fe_{0.947}O + H_2 \quad (1.1)$$

$$3.808Fe_{0.947}O + H_2O\ (g) \leftrightarrow 1.202Fe_3O_4 + H_2 \quad (1.2)$$

The merits of CLC extend beyond efficient CO_2 and hydrogen separation. The technology offers a significant advantage in reducing nitrous oxide (NO_x) emissions by preventing the formation of nitrogen oxides from the direct combustion of atmospheric nitrogen and oxygen. Additionally, it enables the effective control of other airborne pollutants, positioning CLC as an environmentally favourable solution for clean energy generation. The profound potential of CLC in revolutionizing energy generation while addressing environmental concerns makes it

an intriguing prospect in the ongoing quest for sustainable and cleaner energy solutions (Joshi et al., 2021). However, the successful integration of CLC into coal, natural gas, and Biomass Fired Power Plants (BFPP) pivots on several critical factors, primarily energy integration between the process units, char reaction enhancement, oxygen carrier particle reactivity, solid conversion, fate of the pollutants and ash, thermal stability of oxygen carriers, and oxygen carrying capacity.

1.2.2. CO_2 utilization

Carbon capture and utilization (CCU) encompasses a spectrum of applications where captured CO_2 is used directly or indirectly in various products. However, the conversion of carbon dioxide (CO_2) into valuable products faces a significant obstacle: a lack of comprehensive understanding regarding the range of products that can be derived from CO_2, the necessary catalysts, and the kinetics of associated reactions. This limitation has resulted in the current state of carbon dioxide conversion technologies, which are predominantly in their early developmental stages. Consequently, the scope of carbon dioxide conversion processes has primarily been constrained to the production of bulk chemicals like urea, methanol, syngas, and DMC. Currently, approximately 230 Mt of CO_2 per year are utilized, with primary application areas being the fertilizer industry (for urea manufacturing, constituting around 130 Mt) and enhanced oil recovery (approximately 80 Mt). It is worth noting, however, that in theory, numerous chemicals could be synthesized through carbon dioxide conversion reactions (Otto et al., 2015). Notably, there is a dearth of process-level studies focused on the production of CO_2-based fine chemicals, and the instances of industrial applications are limited, such as the CO_2-based methanol plants in Iran, Qatar, and Iceland (Aasberg-Petersen et al., 2008; Al-Hitmi, 2012; Carbon Recycling International, 2016).

While conversion processes have been successfully employed for the industrial production of urea and certain carbonates (Mikkelsen et al., 2010), the advancement of this technology to encompass a wider array of products remains relatively restricted. Methanol production stands as the most mature technology in this domain. However, even if conversion processes for various products become both mature and sustainable, the potential reduction in emissions is still hampered by the ongoing demand for these products. A comprehensive shift from conventional production to conversion processes would result in only a 1% reduction in emissions (Frauzem et al., 2017). This limitation could be significantly ameliorated by discovering more sustainable pathways for fuel production. In this context, the conversion of CO_2 into biofuels presents an attractive solution, albeit one that necessitates sustainability and the generation of net-negative CO_2 emissions.

Excitingly, novel pathways for utilizing CO_2 in the production of synthetic fuels, chemicals, and building aggregates are gaining significant traction. Projections suggest that by 2030, around 10 Mt of CO_2 per year could be captured for these innovative purposes, including approximately 7 Mt CO_2 for synthetic fuel production. However, this approach does not provide a permanent solution, as the combustion of synthetic fuels and the decomposition of chemicals release CO_2 back into the atmosphere. The aggregate impact of these projects, if fully realized, would approach half the CO_2 utilization target for synthetic fuel production by 2030 outlined in the Net Zero Emissions by 2050 (NZE) Scenario. It is crucial to note that, to align with the NZE Scenario, all captured CO_2 must originate from air or biogenic sources, a condition currently met only by a fraction of the planned CCU capacity for fuels by 2030 (IEA, 2023b).

In this context, the viability of capturing CO_2 from biomass-based power plants using chemical-looping combustion technology is particularly noteworthy. This approach not only offers a more practical avenue for CO_2 capture but also demonstrates synergistic benefits, such as the utilization of renewable energy sources and minimization of waste. In comparison to CO_2 capture from air, this approach holds significant promise, indicating a potentially more feasible and impactful pathway forward.

1.3. Organization of the thesis

The structure of this thesis is designed to provide a comprehensive exploration of the research area, encompassing seven distinct chapters. Each chapter addresses crucial aspects of the subject matter, from the broader context down to specific analyses, comparisons, and experimental investigations. An expanded overview of the content covered in each chapter is given below:

Chapter 1: Introduction and Context

In this chapter, the focus is on laying the foundation for the research by discussing the broader significance and relevance of the chosen area of study. The chapter begins by providing a detailed overview of power production, emphasizing the use of various fuels in both the Indian and global contexts. A particular emphasis is placed on highlighting the pressing concern of greenhouse gas emissions within this energy sector. The discussion introduces the pivotal role of chemical looping combustion and carbon capture and utilization as a potential solution to mitigate these emissions. Additionally, this chapter touches on the technical challenges associated with CLC when using solid fuels.

Chapter 2: Literature Review

This chapter undertakes a thorough literature review, covering a wide spectrum of carbon capture technologies, with a focus on CLC of solid fuels in general and biomass in particular and with different oxygen carriers. The discussion extends to CLC's integration with hydrogen

generation systems and CO_2 utilization technologies. Furthermore, the chapter concludes by outlining the motivation drawn from the comprehensive literature review, which directly informs the research objectives that have guided the entire study.

Chapter 3: Methodology and Analysis Techniques

In this chapter, the research methodology, system descriptions, and the analytical techniques employed for the study are meticulously elucidated. The focus is on the methods used to compute critical parameters such as energy, exergy, and environmental factors. Furthermore, detailed information regarding the validation data and operational conditions used for developing the aspenONE flowsheet models is provided, enhancing the credibility and reliability of the subsequent analyses.

Chapter 4: Novel CLC and ORC Integrated Biomass Power

This chapters presents a detailed description of the innovative integration of CLC and Organic Rankine Cycle (ORC) in a biomass-based power generation setup. A comprehensive performance assessment of this novel configuration is conducted, involving a direct comparison with conventional biomass-fired power plants. Key parameters derived from energy, exergy, environmental, and sensitivity analyses are used to evaluate the efficacy of the proposed system, aligning with the proposed Objective I .

Chapter 5: Power and Hydrogen Co-Generation

Building upon the findings from Chapter 4, Chapter 5 takes the most suitable CLC-based plant configuration and extends it to develop a biomass-fired power plant that focuses on both electricity and hydrogen co-generation. This chapter also explores the potential utilization of CO_2 to produce valuable products. A comparison of different cases is conducted based on energy, exergy, and environmental analyses, providing insights that address Objective II.

Chapter 6: Performance Assessment with Different Oxygen Carriers

The performance evaluation of the proposed CLC configuration from Chapter 4 is extended in Chapter 6 by considering different oxygen carriers, including Fe_2O_3, CuO, NiO, Co_3O_4, and a mixture of Fe_2O_3 and CuO. The study includes analyses of oxygen carriers blends, aiming to determine sustainable metal oxide input for biomass-based thermal power plants. A comprehensive comparison of various cases is conducted based on energy, exergy, and environmental analyses.

Chapter 7: Performance of Integrated System and Experimental Investigation

This chapter centres on a thorough performance assessment of an integrated system encompassing steam gasification of biomass, CLC of syngas, and ORC units for power production. To assess the real-time performance of metal oxides as oxygen carriers, an experimental investigation is carried out, focusing on synthesis of novel nanostructured

Fe_2O_3@Al_2O_3 metal oxides. Furthermore, the cyclic redox stability and reactivity of metal oxides are explored within the CLC environment, using gaseous fuel.

Chapter 8: Conclusions and Future Work

The final chapter presents the overarching conclusions drawn from the entirety of the research work. It provides a concise summary of the key findings, highlighting the significance and implications of the study's outcomes. Additionally, this chapter offers insights into potential avenues for future research, suggesting areas where the current study can be extended or deepened, thereby contributing to the advancement of knowledge in the field.

Chapter 2
Literature Review

Chapter 2

Literature review

Chapter 1 highlights the pivotal role of biomass-based power plants in addressing the urgent challenge of reducing CO_2 emissions. Moreover, it highlights the potential of integrating carbon capture and utilization technologies with thermal power plants to further enhance our efforts in mitigating these emissions. Within the scope of this chapter, a comprehensive survey of existing biomass-based power plant technologies and their integration with CO_2 capture and utilization schemes is meticulously detailed, while also highlighting the critical research gaps that need to be addressed.

Subsequent sections within this chapter place a strong emphasis on exploring the utilization of chemical looping technology for power generation from biomass, a process that inherently captures CO_2. To facilitate clarity, the chapter is organized into five distinct sections, each serving a specific purpose and providing essential insights into the considered topics. Section 2.1 explores the broader landscape of biomass-based thermal power plants, extensively exploring the intricacies of their integration with CO_2 capture technologies. Key aspects such as the underlying working principles, feasibility considerations, the technology readiness level, and other pertinent factors are comprehensively examined in this section. In Section 2.2, a comprehensive overview of the promising realm of hydrogen and power cogeneration from biomass is presented. This section goes beyond mere exposition, offering a meticulous comparative assessment of various configurations that have evolved over time, encompassing diverse power cycles. This comparison serves to provide valuable insights into the performance of these configurations. Section 2.3, on the other hand, takes on the role of conducting a thorough literature review, elucidating the current state of metal oxide synthesis and evaluating their viability within the context of our goals. These reviews are instrumental in setting the stage for the subsequent discussions by establishing the current landscape and identifying gaps in our understanding. Section 2.4 encapsulates the identified gaps, and provides a concise overview of the objectives and the scope of the present study, setting the stage for the exploration and analysis that follows.

2.1. Biomass based power plants

Traditional energy production for electricity heavily relies on turbine-based generators fuelled by the combustion of fossil oil and coal. However, the imperative to curb pollutant and greenhouse gas emissions has prompted countries to actively seek ways to reduce their dependence on fossil fuels within conventional power plants. This has led to a notable surge in the exploration of alternative sources like nuclear, wind, hydro, and solar energy, as they

promise a more sustainable future. Within this landscape, biomass has emerged as a pivotal sustainable resource, encompassing materials like wood, grass, agricultural residues, animal and human waste, and even algae. These resources are naturally replenished on a large scale across many regions (Situmorang et al., 2020), rendering biomass an attractive candidate for energy production. The versatility of biomass extends to its processing, with multiple pathways such as combustion, gasification, pyrolysis, and more. These methods yield final products including heat, power, and usable fuel, augmenting the appeal of biomass as a renewable energy source (Osman et al., 2019). Recent reviews highlight the current status, scope and technical challenges associated with the utilization of biomass for power production. Singh (2015) highlighted the importance of agricultural biomass as a renewable energy source with potential to replace fossil fuels, benefitting energy security and employment in agricultural societies without harming the environment. The review focused on Punjab, estimating crop residue production through the residue-to-product ratio method, considering competitive uses and harvesting practices. Approximately 40.17% (22.315 Mt) of the total biomass potential (55.396 Mt) is surplus, mainly from cereals, cotton, and sugarcane. This surplus biomass can provide 2000-3000 MW of electricity with varying thermal efficiency. The importance of utilizing residues for environmental preservation, methodology for estimating biomass availability, and the technical and economic considerations for decentralized power plants in Punjab are highlighted. Liu et al., (2020) highlighted the potential of biomass for energy production and its role in generating heat, electricity, and hydrogen. The review emphasized the challenges in improving conversion efficiency and minimizing environmental impacts. Two emerging research areas, flow biomass fuel cells (FBFCs) and biomass electrolysis for hydrogen production (BEHP), are discussed in terms of technological advancements and need for further research to overcome the existing challenges. Tahir et al., (2023) explored the potential of biomass as a renewable energy source in Pakistan, focusing on its current energy landscape and future prospects. The study highlighted chemical looping technology for cleaner fuel production and pollution control, with a specific focus on hydrogen generation. This study suggested that, in Pakistan biomass can be seen as a viable alternative in contrast to more expensive renewable options like solar and wind. The study highlighted the benefits of using biomass in chemical looping gasification, highlighting its positive environmental impact and potential to combat climate change. Further, the challenges and considerations in choosing appropriate oxygen carrier materials for chemical looping technologies are discussed. Ultimately, biomass's role in chemical looping gasification is presented as a promising avenue for sustainable energy and environmental preservation in Pakistan. Malico et al., (2019) explored the potential for bioenergy utilization in Europe's industrial sector to achieve a low-

carbon economy. The review suggested that biomass utilization is technically feasible across various energy intensive industries, depending on technology, scale, and economics. Research directions outlined to further integrate biomass into industry by developing advanced conversion technologies, optimizing system operation, establishing efficient supply chains, and designing market-based mechanisms to promote bioenergy investment.

At present, direct combustion stands out as the predominant thermochemical route for biomass conversion, accounting for over 97% of global biomass energy utilization (Pan et al., 2020). This method aligns well with conventional thermal power generation practices (Zhu et al., 2019), and projections indicate that biomass power may encompass more than 15% of industrialized nations' electricity supply by the close of 2020 (Liu et al., 2020). A notable advantage of biomass power generation is its carbon-neutral characteristic, alongside lower sulfur and nitrogen content compared to fossil fuels, contributing to emissions reduction. To gain insight into the landscape of biomass-based power production technologies, Table 2.1 presents a comprehensive overview. It details various aspects including feedstock type, energy conversion mechanisms, energy efficiency, operational capacity, and CO_2 capture considerations, providing a holistic snapshot of the diverse avenues within this promising realm.

Depending on the availability of biomass, the biomass-fired power plants are being used for the electricity generation for small to medium scale capacity. Most of the BFPPs have power capacities between less than 1 MW to 25 MW (Kumar et al., 2015). These small to medium scale capacities are effectively being handled by integrating the Organic Rankine Cycle (ORC) with combustion system. ORC is similar to Rankine cycle in working mechanism except the working fluid is high molecular weight organic fluid with lower boiling point than water. Integration of ORC unit, eliminates the need of superheating which ultimately avoids higher capital investment for the machineries like high temperature and pressure steam boilers (Morrone et al., 2018; Liu,et al., 2011; Preißinger et al., 2012). In addition, lack of condensation of working fluid reduces corrosion and enhances the operational life of turbines (Bundela and Vivek, 2010). Another advantage of ORC is it does not require recirculation in boilers due to low gravity difference between vapor and liquid phases of the organic fluid (Quoilin et al., 2013).

Table 2.1. Technologies for power production from biomass.

Feed stock and methodology	Power production mechnisam	Capacity	Energy Efficiency	CO_2 capture	Reference
Modelled biomass (Torrefied wood) gasification process integrated with methanol synthesis and power production.	Integrated Gasification Combined Cycle (IGCC) and Inverted Brayton Cycle (IBC) turbine	4 to 5.5 MW	--	Not modelled	(Del Grosso et al., 2020)
Experimental investigation of biomass (Scratched construction wood) gasification process integrated with stirling engine.	updraft fixed bed gasifier followed by combustor integrated to stirling engine for power production	25 kW	20% (electrical)	Not modelled	(Lin, 2007)
Investigated the emission characteristics of particulate matter from biomass (Dry bark feedstocks) based power production.	Not modelled.	-	-	Focus is on emission characteristics of particulate matter	(Hu et al., 2020)
Investigated the performance of natural gas, coal and biomass (US forestry residue) fired power plants integrated with CO_2 capture.	Supercritical power plant	800 MW	28.1 (electrical)	Amine based CO_2 capture and compression	(Ali et al., 2017)
Thermodynamic analysis of low capacity biomass fired (olive cake and date seed mixture) power plant	Steam cycle	1 kW	12 (electrical)	CCS system not modelled	(Al Asfar et al., 2020)

Thermodynamic assessment of cogeneration system for power and hot water production based on biomass gasification and syngas combustion	Gas turbine as the topping cycle and the S-CO_2 cycle as the bottoming cycle	--	40.11 (energy)	CCS system not modelled	(Gholamian et al., 2016)
Proposed a configuration consist of Biomass (HHV-16.038MJ/kg) gasification, chemical looping air separation, steam cycle and SOFC.	Steam cycle and SOFC	--	51.7 (electric)	Chemical looping air separation	(Yan et al., 2019)
Exergy, exergy and environmental analysis of biomass based multigeneration system for production of hot water and hydrogen	ORC cycle	671kW	22 (exergy)	CCS system not modelled	(Ahmadi et al., 2013)
Biomass gasification based multigeneration system for heating, cooling, electrical power, and hydrogen generation	ORC Cycle	--	21.89 (exergy)	CCS system not modelled	(Khanmohammadi et al., 2016)
biomass gasification system for power and water generation	ORC cycle, Bryton cycle	--	42 (exergy)	CCS system not modelled	(Khanmohammadi and Atashkari, 2018)
Integrated biomass gasification combined cycle with CO_2 removal	Bryton cycle and steam cycle	191 MW	33.94	chemical absorption	(Carpentieri et al., 2005)

Performance assessment of coal-biomass cofiring power plant	Steam cycle	500 MW	38	Chemical absorption	(Bui et al., 2018)
CO_2 recycling biomass (Coconut shell) gasification based carbon-negative power plant	Bryton cycle	--	39.03	CCS system not modelled	(Prabowo et al., 2015)
Energy and exergy analysis of double calcium looping integrated biomass (sugarcane bagasse) fired power plant	ORC cycle	162 kW	7	Ca-looping system	(Pillai et al., 2019).
Performance of biomass (Wood pellets) fired power plant is compared with coal fired power plant.	Replaced conventional steam cycle with sCO_2 cycle	458 MW	28.05 (electrical)	Oxy combustion	(Wei et al., 2020).
Performance assessment of palm tree based biomass power plant.	Steam cycle	67.65 MW	--	CCS system not modelled	(Hayati et al., 2020).
Experimental investigation of micro cogeneration system consists of biomass boiler and ORC units	ORC cycle	2.5 kW	7.4 (electric)	CCS system not modelled	(Carraro et al., 2020).

Numerous studies are available on the conventional direct-biomass fired power plant using ORC unit. The first biomass fuelled ORC unit was installed in Biere, Switzerland in the year 1998 (Colonna et al., 2015). The increase in number of academic documents and patents published was at a slow pace from 1987 to 2009, while the increase was rapid from the year 2009 to 2012 (Fu et al., 2014). Most of the studies focused on combined heat and power (CHP) cogeneration plants, with an objective to improve efficiency by cycle modification, selection of working fluid and optimization of operating conditions/design parameters as shown in Table 2.2. The presented literature also highlights that the overall energy efficiency of simple ORC integrated BFPP varies in the range of 5 to 13%.

Table 2.2. Literature summary of ORC based BFPPs

Research Focus	Author	Key outcomes
Cycle modification	*Algieri (2016)*	Performance of Subcritical and Transcritical ORC cycles were compared and the influence of internal regeneration (i.e. utilization of heat from turbine outlet to preheat the working fluid before entering the evaporator) was evaluated. The results showed that the Transcritical cycle with internal regeneration offered the maximum electric performance compared to subcritical cycle. On the other hand, a conventional saturated ORC cycle guaranteed the highest thermal efficiency.
	Al-Sulaiman et al., (2012)	Energy and exergy analyses were carried out for the following four biomass fired power systems integrated with ORC cycle: electrical-power, cooling-cogeneration, heating-cogeneration and trigeneration. This study demonstrated that the maximum exergy efficiency of the ORC was 13% and, the efficiency increased to 28% with trigeneration. The study also revealed that the biomass combustion unit and ORC evaporator have highest exergy destruction contributing to 93% of total exergy destruction.

	Nur et al., (2019)	An ORC based small scale power plant was designed to generate electricity by using empty fruit bunch and palm oil shells as biomass fuel. Integration of a recuperator between expander and condenser results in higher thermal efficiency and less fuel consumption than without recuperator.
	Jang and Lee (2018)	Thermodynamic analysis was carried out for ORC-based biomass CHP system. The plant performance was analysed using eight different working fluids at the fixed electricity and heat production capacities. The fluids with higher latent heat had better performance with highest ORC efficiencies in the range from 5.95% to 7.29%.
Selection of working fluid	*Borsukiewicz-Gozdur et al., (2014)*	Three CHP system variants: A) wet working fluids; dry working fluids B) with and C) without internal regeneration were considered for wood processing plants to produce electricity and to heat the air used for wood drying. The performance of each configuration was analyzed on the basis of three parameters, i.e. electric power output, heat flux supplied to the dryer and the air temperature. It was observed that use of dry working fluids (variant B & C) generated more electric power output than variant A. However, the wet working fluids resulted in high heat transfer flux in drying chamber. Further, high-temperature drying conditions were observed in the absence of regeneration.
	Sotomonte et al., (2011)	Two ORC configurations, with and without regenerator in combination with various organic working fluids were assessed based on the second law of thermodynamics. The results showed that family of alkyl-benzenes offered around 5 percent higher exergetic efficiencies than siloxanes.

	Wang et al., (2019)	A novel domestic CHP system using biomass as a fuel was proposed and sensitivity analysis was performed to investigate the effects of key operating parameters such as expander inlet pressure and temperature, extracting ratio and low-pressure expander inlet pressure. An optimization algorithm using the principles of thermodynamics and economics was also developed to find the operating conditions for optimum performance.
Optimization of operating conditions/design parameters	*Ahmadi et al., (2013)*	A multi-generation ORC based BFPP integrated with an absorption chiller and a proton exchange membrane (PEM) electrolyzer was assessed thermodynamically. The effects of pinch point temperature, the ORC turbine inlet pressure, and the ORC pump inlet temperature on the system performance were investigated. The results showed that combustor and ORC evaporator were the main sources of irreversibility and exergy destruction.
	Pezzuolo et al., (2016)	Various plant configurations of ORC integrated CHP system with biomass as a fuel were compared in terms of energy, exergy and economics. A mathematical model for the ORC unit and the boiler was developed using MATLAB to determine the best plant configuration. The efficient plant configuration was with recuperator between expander and condenser.

2.1.1. Chemical looping combustion of biomass for power generation and CO_2 capture

To minimize the energy penalty in BFPP integrated CO_2 capture, Chemical-looping combustion technology can also be considered as potential alternative (Adanez et al., 2012). Thus technology facilitates the inherent CO_2 capture mechanism, hence, except condensation, no additional separation processes are required to obtain the CO_2 in pure form. The reduced metal oxides from fuel reactor and oxidized metal oxides from air reactor are separated by using cyclone separators (Fan, 2010). In the last few decades, substantial developments have been noticed on the combustion of coal using CLC technology (Surywanshi et al., 2019),

however relatively lesser attention has been given towards the design and development of CLC integrated BFPPs (Adánez et al., 2018).

The following literature highlights the recent developments on CLC integrated BFPP. Mercado et al., (2023) studied the performance of a kilowatt-hour biomass based CLC plant. Comparisons between coal-based power plants, coal-based CLC plants, and biomass-based CLC plants showed that biomass-based CLC had the least environmental impact, though water consumption was a drawback. The environmental impacts of coal-based systems largely stemmed from upstream processes like mining and processing. Using rice husks as feedstock led to net negative emissions. A life cycle assessment (LCA) model was developed to compare biomass-based CLC with conventional coal power and coal-based CLC, using a cradle-to-grave approach and validated through a global warming potential study. Pérez-Astray et al., (2020) tested two manganese-based ores as oxygen carriers with different biomasses (pine sawdust and almond shells) in a 0.5 kWth CLC unit, achieving nearly 100% CO_2 capture. Recycling the fuel reactor outlet reduced oxygen demand by 30%, with no NOx emissions and low tar levels detected. Pérez-Astray et al., (2021) evaluated the performance of a manganese-iron mixed oxide doped with titanium ((Mn66Fe)-Ti7) as an oxygen carrier in a 0.5 kWth CLC unit, achieving nearly 100% CO_2 capture efficiency. Optimized conditions reduced oxygen demand to about 10%, with magnetic properties aiding separation from biomass ashes. No NO_x emissions were detected, and tar content in the CO_2 stream was low, minimizing operational issues. Mei et al., (2022) examined the reaction rates of a manganese ore from Egypt with CH_4, CO, and H_2 in a batch fluidized bed reactor, comparing fresh and used samples from a 10 kWth pilot. The ore showed lower reactivity with CH_4 but higher reactivity with syngas than other manganese ores, outperforming the benchmark ilmenite. Analytical modeling indicated high char gasification efficiency (98%) and 90% contact efficiency with bed material in the 10 kWth unit, though volatile conversion was low, highlighting the need to improve volatile-bed material contact. Shen et al., (2009) evlauated the performance of 10 kW_{th} capacity CLC integrated biomass gasification plant with Fe_2O_3 as oxygen carrier. The temperature of the fuel reactor was varied from 740 ºC to 920 ºC. It was observed that increase in fuel reactor temperature caused an increase in CO production from gasification of biomass and a decrease in CO_2 production from oxidation of CO by the metal oxide. Mendiara et al., (2013) performed experimental investigation on 500 W_{th} capacity CLC plant with iron oxide as oxygen carrier and pine sawdust as biomass fuel. Further, high carbon capture efficiencies (>95%) were attained for the temperature range 880-915 ºC using steam and CO_2 as gasifying agents. Li et al., (2010) developed moving bed reactor model for both oxidizer and reducer in ASPEN PLUS

and studied the Biomass direct CLC configuration. The process simulation results showed that this configuration was more efficient than conventional biomass combustion. Hence, it can be attractive option for high efficiency power generation. Adánez-Rubio et al., (2014) analyzed performance of Chemical Looping with Oxygen Uncoupling (CLOU) process using pine wood biomass as fuel and CuO as oxygen carrier in a continuously operated 1.5 kW_{th} capacity unit. A complete combustion of biomass and 100% carbon capture efficiency were attained at 935ºC fuel reactor temperature. Mendiara et al., (2016) presented a comparison study of 1.5 kW_{th} capacity biomass fired power plants operated with in-situ Gasification-Chemical Looping Combustion (iG-CLC) technology and CLOU technology. The performance assessment was carried out by analysing the following process parameters: combustion efficiency, CO_2 capture efficiency and the tar emission. It was observed that the CLOU technology achieved 2% higher CO_2 capture efficiency than iG-CLC with zero tar emission. The char conversion rate in CLOU process was 3 to 4 times more than the iG-CLC process at the operating temperatures of 900 ºC. Further, less oxygen carrier was required in the CLOU process as compared to iG-CLC process. However, Cu-based oxygen carrier used in the CLOU process is more expensive than the iron ore used as oxygen carrier in the iG-CLC process. Kevat et al., (2016) presented the performance analysis of CLOU and CLC based sawdust biomass fired power plants using ASPEN Plus flow sheeting software. For the same biomass input, the difference in power output was found to be 43 W at the optimum oxygen carrier to fuel ratio of 66.4 in CLC and 75 in CLOU BFPP respectively. The performance of CLOU based BFPP was much better than CLC BFPP, but at the cost of more metal oxide circulating in the loop. It can be noticed that most of the studies reported in the literature on CLC integrated biomass-fired power plants (BFPP) mainly focused on integration of CLC technology with steam cycle for power production.

2.2. Biomass Direct Chemical Looping (BDCL) combustion for hydrogen and power cogeneration

Hydrogen is one of the most promising sources of renewable energy. It is an important feedstock to the ammonia synthesis and oil refining and is environmentally friendly fuel for the transportation and power generation in the future. To produce hydrogen from biomass, chemical looping hydrogen (CLH) production using three reactor configuration is considered to be a potential alternative to Chemical Looping Gasification (CLG), as CLH avoid the complexities associated with the gasification step and increase the efficiency. Zaini et al., (2017) combined microalgae gasification with syngas CLH to co-produce power and H2, maximizing heat recovery while minimizing exergy destruction in the system. Darmawan et

al., (2018) utilized black liquor waste as feedstock for H_2 production through gasification with syngas CLH, achieving a net energy efficiency of approximately 70% with nearly 100% carbon capture. The CLH configuration often integrated with power production cycles for achieving the simultaneous hydrogen and electricity production (Luo et al., 2018). Huang et al., (2013) investigated the cyclic performance of natural hematite as an oxygen carrier in BDCL conversion. The oxygen carrier significantly enhanced biomass conversion. BDCL achieved higher gas yield (1.06 Nm^3/kg) and carbon conversion (87.63%) compared to biomass pyrolysis (0.75 Nm^3/kg and 62.23%). However, gas yield and carbon conversion decreased after 20 cycles (0.93 Nm^3/kg and 77.18%) due to oxygen carrier attrition and structural changes.

The energy and exergy performance of the CLH process is significantly enhanced by integrating it with the different cogeneration schemes. The presented literature in Table 2.3 highlights review of important simulation studies for synthesis of polygenerational schemes focused on hydrogen generation.

Table 2.3. Summary of biomass based polygenerational schemes

Authors	Configuration	Products	Power cycle	Energy Efficiency / % of CO_2 capture
Kobayashi and Fan (2011)	BDCL scheme, which converts biomass into hydrogen/electricity with CO_2 capture	Electricity and Hydrogen	Steam Cycle	Energy - 38.1 % CO_2 capture – 99
Situmorang et al., (2021)	BDCL scheme at 30 bar operating pressure using benzene as working fluid	Electricity	ORC cycle	Electric energy – 19.1 %
Cormos (2015)	BDCL scheme for hydrogen and power cogeneration	Electricity and Hydrogen	Steam cycle, Brayton cycle	Energy – 49.26 CO_2 capture – >99

Li et al., (2010)	BDCL scheme with Fe_2O_3 metal oxides as oxygen carriers	Electricity and Hydrogen	Steam cycle	Energy – 67.15 CO_2 capture – >99
Sun and Aziz (2021a)	Biomass Chemical Looping Gasification (BCLG) and BDCL for methanol synthesis	Hydrogen and Methional	Not modelled	Exergy efficiency of BCLG - 75.61% and BDCL - 71.59%
Sun et al., (2022)	Integrated system consist of self heat recuperation, BDCL for hydrogen production, Haber-Bosch (H-B) process to produce ammonia and Brayton-Rankine combined cycle	Hydrogen, ammonia and electricity	Brayton-Rankine combined cycle	Exergy efficiency: ammonia 44.36% and net power 1.73%
Aghaie et al., (2016)	Combined cycle that integrates biomass gasification, solid oxide fuel cell (SOFC), and chemical looping hydrogen production. Used CaO as the oxygen carrier in the chemical looping unit	Electricity	Steam cycle and SOFC	Electric energy – 55.8 % CO_2 capture – 100
Oruc and Dincer (2020)	Fe_2O_3 metal oxide based chemical looping process using different biomasses to produce hydrogen.	Hydrogen production	Not modelled	Energy efficiency – 91% with bagasse

Sun and Aziz (2021b)	tri-gen system featuring a direct CLC section as the prime mover, two gas turbines (GTs), an organic Rankine cycle (ORC) for power generation, an absorption chiller (AC) for cooling, and two heat exchangers (HEs) for heat generation.	Electricity, heating and cooling	ORC Cycle, Brayton cycle	energy efficiency - 90.92% and exergy efficiency 33.82%

2.3. CLC in Practice: Operational issues and performance of oxygen carriers

The total heat emerged from a redox cycle in CLC is still the same as in normal combustion, which is consistent with Hess law. As a result, it is obvious that CLC has zero gain or loss in enthalpy and offers a better overall efficiency than traditional power production facilities that use alternative capture technologies. However, scalability of CLC depends on a number of factors such as plant configuration, economic aspects, exergy efficiency and oxygen carrier (OC) performance, etc (Alalwan and Alminshid 2021). Among these factors, the OC performance has been identified as a key factor as it effects the process viability on commercial scale to a larger extent. Hence, the experimental research is more focussed on meeting the following criteria while developing the OCs (Qasim et al., 2021): thermodynamically favourable, economically advantageous, resistive to agglomeration, high oxygen transport capacity, good mechanical strength, non-toxicity and low carbon deposition.

CLC research focus on solid fuels has been recent (for the last 15 years) compared to that on gaseous fuels. CLC of solids adds additional complications to CLC of gases such as solid-solid reactions, possible adverse interactions with the fuel ash, and the contacting pattern/ reactor configuration. In 1954, Lewis and Gilliland developed and patented a concept closely resembling chemical looping combustion. Their patent, titled "Production of Carbon Dioxide," described reducing oxygen carriers in two interconnected fluidized beds using various fuels. The process relies on oxygen derived from a metal oxide (MxOy) serving as the oxygen carrier (Lewis et al., 1954). Later, there were many developments and today there are a number of works reported on solid fuel conversion kinetics in lab scale to real pilot-scale continuous operation using coal and biomass as solid fuels (Lyngfelt, 2014; Coppola and Scala, 2021). The CLC of solid fuels can be conducted by (i) chemical looping gasification (CLG), (ii) in-

situ gasification CLC (iG-CLC) and (iii) ex-situ gasification followed by CLC of gasified combustible products. The first two methods require gasification agents such as steam or CO_2 and involve solid-solid reactions and interaction of solid fuel ash with the OCs. Different types of reactors for carrying out reduction (in fuel reactor) and oxidation (air reactor) are attempted by the researchers. Fixed bed, bubbling bed, spout fluidized bed, interconnected fluidized beds are some of the main types used for CLC of solids. Among these, circulating fluidized bed (CFB) reactor configuration is the most widely used and several CLC units using solid fuels in CFBs were build and operated by Chalmers University with thermal input from 0.3kW to 5 MW (Lyngfelt, 2023). Ohio State University demonstrated a 25 kW_{th} CLC units with solid fuels using moving bed as fuel reactor and entrained bed as air reactor (Song and Shen, 2018). Several studies were conducted using computational fluid dynamics and the possible design changes were made on these interconnected fluidized bed reactors (Adanez et al., 2012).

Based on the experience of using coal as solid fuel in some pilot-scale CLC facilities in the world, it is reported that a big challenge lies in accelerating gasification of char in the fuel reactor in order to achieve complete conversion in the fuel reactor (Song and Shen, 2018). Generally, the rate of OC particles circulation between the air and fuel reactors is high, whereas the char gasification is a slow process in the fuel reactor and is therefore the limiting step in the CLC process of solid fuels (Adanez et al., 2012; Song et al., 2013). As a result, there are high amounts of unreacted char in fuel reactor. Consequently, the entry of char particles in air reactor along with the circulating OC particles becomes unavoidable, and the CO_2 formed as a result of combustion of char with the air cannot be captured. Another major issue the unavoidable interaction between OC and solid fuel ash.

The majority of CLC experimental studies employed synthetic OCs for combustion of gaseous fuels such as CH_4, natural gas, syngas and CO. The most often used transition metal oxides are NiO, Fe_2O_3 and CuO (Lyngfelt, 2023). Usually, these transition metal oxides are supported on inert material (Al_2O_3, TiO_2, SiO_2, ZrO_2, CeO_2, MgO and $MgAl_2O_4$) to increase the surface area and mechanical strength (Qasim et al., 2021). Mattisson et al., (2006) investigated the performance of NiO oxygen carriers supported on $NiAl_2O_4$, $MgAl_2O_4$, and ZrO_2 in the CLC process. They observed high reduction rates and no tendencies toward sintering with $NiO/MgAl_2O_4$, NiO/ZrO_2, and $NiO/NiAl_2O_4$. However, NiO/TiO_2 exhibited sintering and agglomeration during the reduction. Ismaeil et al. (2016) examined the fluidization properties of iron-based oxygen carriers enhanced with calcium ferrites, finding no agglomeration and improved reactivity due to calcium addition. Ridha et al., (2016) observed agglomeration in Canadian ilmenite ore at 1050 °C during pressurized CLC cycles. Zhang et al., (2020) noted

severe sintering of iron ore oxygen carriers at a calcination temperature of 1150°C. Copper-based oxygen carriers are prone to agglomeration and sintering due to copper's low melting point (1085°C). Diego et al., (2005) found that calcination temperature, CuO content, and the reduction conversion of the OC influenced agglomeration, with CuO content below 20 wt% being crucial to prevent it. Wen et al., (2012) tested three natural Cu ores in the CLOU process and noted that high copper content led to agglomeration, while low copper content avoided significant agglomeration after 20 redox cycles at 980°C. CuO oxygen carriers with 60 wt% of various supports (TiO_2, SiO_2, ZrO_2, $MgAl_2O_4$) showed no significant agglomeration in a fixed bed reactor. The distribution of the transition metal oxide and the support material and their interactions, if any, will have significant effect on the OC's reactivity, mechanical strength and thermal stability. The preparation methods and metal oxide loadings of supported OCs significantly impact their physicochemical properties and redox performance in CLC applications (Abdalla et al., 2023). Well established preparation methods such as mechanical mixing (Liu et al., 2019), coprecipitation (Sun et al., 2029), impregnation (Maya et al., 2017), solgel (Hu et al., 2016) and spry drying (Siriwardane et al., 2016) have been employed to synthesize the composite metal oxides at a bulk scale and the performance of these OCs were tested from laboratory to pilot scale.

Numerous OCs were synthesized at macro to micro scale which generally have the following demerits: low porosity, less surface area (< 10 m^2/g) and low oxygen carrying capacity (De Vos et al., 2019; Akram et al., 2021). Nevertheless, these metal oxides generally offer high mechanical stability and reasonable resistance to sintering. Hence, these metal oxides have been explored further to use at commercial scale in-spite of the low oxygen carrying capacity. The attention of researchers has recently been drawn to the synthesis of nanoscale oxygen carriers, because of the high reactivity of the OCs at nanoscale due to their high surface area. However, these nanomaterials exhibit severe sintering problems at high temperatures. Hence, it is necessary to engineer the surface morphology and composition of nanomaterials to arrest the sintering at high temperatures, otherwise it may limit to low temperature CLC applications (Mishra and Li, 2018).

Recent review articles by Mishra and Li (2018) and Akram et al. (2021) provided an overview of the current developments in CLC at the nanoscale and challenges ahead. Alalwan et al. investigated the performance of Co_3O_4 nanoparticles (Alalwan et al., 2017) and α-Fe_2O_3 nanoparticles (Alalwan et al., 2018) for CLC of CH_4 in the temperature range of 600 to 800 °C and observed huge reduction in surface area after 10 redox cycles due to sintering. Ma et al. (2019) also observed that the main reason for deactivation of the nanoscale oxygen carriers is

sintering at high temperatures. These observations highlight the need for a binder or support material to prevent particle structure from being altered at high temperatures. Liu et al., (2015) synthesized porous nano-sized SiO_2 granulates impregnated with 30% CuO and performed CLC tests at 850 °C. The OC exhibited stable performance with high conversion rate up to 11 redox cycles due to favourable porous structure of the oxygen carrier. Chang et al., (2014) used bimetallic CuO-NiO (20%) nanoparticles impregnated onto chabazite mineral as an oxygen carrier for CLC of syngas at temperatures between 700 to 900 °C. The synthesized oxygen carrier showed stable performance with good conversion up to five redox cycles. Using nanoscale iron oxide particles embedded in SBA-15 mesoporous silica, Liu et al., (2019) achieved 100% CO selectivity in chemical looping methane partial oxidation. The morphology of Fe_2O_3@SBA-15 nanochannels was maintained even after 75 redox cycles carried out at 800 °C. However, obtaining the high cyclic stability can be attributed to the use of maximum support material (80 vol %). Hu et al., (2017) impregnated 6 wt.% of Fe_2O_3 nanoparticles into ZrO_2 shells and further coated the core-shell structure with ZrO_2. When tested over 100 cycles of chemical looping conversion of CO_2 to CO at 650°C, these nanostructured OCs showed better sintering resistance than the core-shell nanostructured OCs without coating. Even though the composite material has excellent sintering resistance, only 6 wt.% transition metal oxide loading was used in their study. Otto et al., (2019) synthesized $La_{0.5}Ca_{0.4}Ni_{0.2}Ti_{0.8}O_{2.95}$ perovskite using a modified solid-state method to get the smaller grains. The perovskite was then exsolubilized with Ni metal in a controlled environment to produce composite material with less than 10 mole % transition metal oxides concentration. Even after 50 redox cycles, the OC did not degrade in terms of particle position or size.

2.4. Research gaps identified from literature

From the review of the literature on the chosen field of study, following research gaps are identified to develop the chemical looping combustion of biomass based thermal power plants.

1. India, known for its agricultural strength and robust biomass production, holds significant potential for generating electricity in rural areas through the utilization of agricultural biomass like bagasse. Achieving sustainability and carbon negativity in this technology requires the integration of effective CO_2 capture mechanisms with biomass-fired power plants.
2. While the literature is somewhat limited, there's a gap in the analysis of thermodynamics in biomass-fired power plants. Although some studies have explored energy and exergy analyses in biomass-fired power plants with chemical looping combustion integrated into steam cycles, there's a notable absence of research on CLC combined with organic Rankine

cycles. This integration not only holds promise for carbon-negative power generation from biomass but also offers a sustainable solution for small-scale, off-grid power plants.

3. Currently, a comprehensive examination of CLC-based biomass-fired power plants, considering both power and H_2 co-generation along with energy, exergy, and environmental analyses, is conspicuously absent in existing literature. Such a thorough analysis is crucial for evaluating feasibility and making informed policy decisions regarding the future establishment of environmentally friendly co-generation power plants. Furthermore, no comprehensive study has investigated the energy, exergy, and environmental implications of combining CLC technology with CO_2 utilization.
4. The literature presents several oxygen carriers, each with its own merits and drawbacks. The selection of an appropriate oxygen carrier poses a notable challenge. Given India's substantial iron ore production (as reported by the U.S. Geological Survey, 2017), iron oxide emerges as a potential oxygen carrier for CLC applications in the country. While copper oxide boasts greater reactivity, it's costlier. Nonetheless, blending a fraction of copper oxide with iron oxide can potentially enhance reactivity without significantly inflating overall operational costs. Missing from the literature are analyses of energy, exergy, environmental, and economic factors related to CLC-based biomass-fired power plants employing such mixed oxygen carriers. Furthermore, there's a dearth of comparisons between these plants and conventional biomass-fired power plants.
5. Composite metal oxide particles consisting of Fe_2O_3-Al_2O_3 have been a popular choice for oxygen carriers in numerous CLC studies. These particles, varying in size from micro to nanoscale, offer improved reactivity, efficient heat transfer, and increased availability of lattice oxygen due to their favorable surface-to-volume ratio. However, it's noteworthy that nanoscale metal oxides can sinter during high-temperature CLC cycling, which affects their cyclic stability. While certain nanostructured oxygen carriers exhibit good cyclic stability through high support and low transition metal oxide loadings, achieving both high oxygen-carrying capacity and cyclic stability is essential for efficient CLC applications. Among the various techniques for synthesizing nanomaterials, electrospinning stands out as an efficient method capable of tailoring nanofiber composition and morphology. However, this synthesis approach has yet to be explored for oxygen carrier preparation.

Above research gaps lead to the formulation of the following objectives of the present work.

2.5. Aim and objectives of the research work

Aim: The primary purpose of this research is to explore the viability of merging chemical looping combustion and CO_2 utilization technologies into biomass-fired power plants through

theoretical analysis. Additionally, the study aims to synthesize innovative nanostructured oxygen carriers for CLC applied to biomass.

Objectives: Accordingly, the following objectives have been formulated to conduct the research work in achieving the above goal.

Objective 1: Perform energy, exergy, and environmental analyses of a unique CLC-integrated biomass-fired power plant combined with an Organic Rankine Cycle system. This hybrid configuration is aimed at power generation with inherent CO_2 capture.

Objective 2: Conduct energy, exergy, and environmental analyses of a CLC-based biomass-fired power plant designed for co-generation of hydrogen and power. Investigate its potential integration with diverse CO_2 utilization methods.

Objective 3: Undertake energy, exergy, and environmental assessments of a CLC-based biomass-fired power plant utilizing different oxygen carrier options.

Objective 4: Develop and synthesize novel Fe_2O_3/Al_2O_3 composite nanofibrous oxygen carriers using the electrospinning technique. These carriers are intended for CLC applications with syngas derived from biomass sources.

Chapter 3

Modelling and Simulation Methodology

Chapter 3

Modeling and Simulation Methodology

Having identified the research objectives of the study, the aim of this chapter is to discuss about the detailed methodology adopted to achieve the objectives. Section 3.1 details the methodology adopted for devising configurations of biomass-based power plants. These configurations encompass both standalone power generation and power generation coupled with hydrogen co-generation. Furthermore, integration with CO_2 capture and utilization processes is explored. The unit models essential for configuring the power plants are simulated and validated against existing literature findings. Through systematic integration of these unit models, a spectrum of power plant setups is synthesized. The primary focus is on investigating the benefits of CO_2 capture, CO_2 utilization, and cogeneration strategies. To provide context, conventional biomass power plant configurations from prior literature are replicated and taken as reference cases in the comparative analysis. Section 3.2 outlines the assumptions made and mathematical equations employed to assess the performance of the proposed configurations. This evaluation is grounded in energy, exergy, and environmental analyses.

3.1. System Description

This project's theoretical facet involves the creation of diverse flowsheet configurations tailored for biomass-fired power plants. The simulation tool employed is aspenONE v10.0. This platform aids in structuring the plant layout and computing pivotal operational conditions, encompassing temperature, pressure, flow rates, fuel composition, unit efficiency, and other significant parameters. The range of plant variations studied within this project falls into the subsequent four categories:

Category 1: Conventional BFPP without CO_2 capture.

Category 2: CLC based BFPP with power generation alone.

Category 3: CLC based BFPP with hydrogen and power co-generation.

Category 4: CLC based BFPP with hydrogen and power co-generation coupled with CO_2 utilization plant.

3.1.1. Category 1: Conventional BFPP without CO_2 capture

The BFPP configuration consists of three major modules, i.e., combustor, thermal oil tank, and ORC unit for power generation. The ORC unit is structured with several components: a pump, an evaporator, a turbine/expander, and a condenser. The pump's role involves the compression of the working (organic) fluid, transitioning it from low-pressure (2.4 bar) to high-pressure liquid (11.4 bar) state. Subsequently, the high-pressure liquid enters the evaporator, undergoing evaporation by harnessing the thermal energy from the thermal oil. This results in the formation of high-pressure vapor, which advances through the turbine, expanding isentropically to generate electricity in the process. Ultimately, the low-pressure vapor emanating from the turbine is cooled, condensed, and reintegrated into the cycle. The ORC process unit model, drawn from (Ozdil et al., 2015), provides the foundational framework for this intricate mechanism. The outcome of the ORC process configuration is simulated and presented for validation against source models, as illustrated in Table 3.1. Remarkably, all results exhibit deviations well within the range of ± 4%. Consequently, the simulated outcomes showcase a high level of concurrence with the configurations established in existing literature, affirming the accuracy of the synthesized model.

Table 3.1. Validation of ORC based on main stream parameters

	Source model	ASPEN model		Source model	ASPEN model		Source model	ASPEN model	
Stream ID	Mass flowrate (kg/s)	Mass flowrate (kg/s)	Error %	Temperature (K)	Temperature (K)	Error %	Pressure (bar)	Pressure (bar)	Error %
1	13.48	13.48	0	400	400.00	0.00	2.7	2.7	0
2	13.48	13.48	0	356.9	366.90	-2.80	2.2	2.2	0
3	10.63	10.63	0	368.4	368.40	0.00	11.4	11.4	0
4	10.63	10.63	0	326	324.75	0.38	2.4	2.4	0
5	10.63	10.63	0	303	303.00	0.00	2.4	2.4	0
6	10.63	10.63	0	303.17	304.07	-0.30	11.4	11.4	0
7	110	110	0	300.5	300.50	0.00	1.37	1.37	0
8	110	110	0	305.4	303.97	0.47	1.37	1.37	0

Integration of BFPP Configuration: The synthesis of the biomass fired power plant configuration involves the strategic integration of three key modules: the combustor, thermal

oil tank, and ORC unit, as visually depicted in Figure 3.1. Within this power plant setup, the combustor operates at a consistent temperature, upheld through a continuous feed of biomass, specifically sugarcane bagasse, and an additional 20% excess air. This excess air supply ensures the thorough combustion of fuel. To mitigate localized overheating and the potential chemical instability of the organic fluid (refrigerant), the hot flue gas resulting from combustion engages in heat exchange with thermal oil within a dedicated heat exchanger. This configuration, as highlighted by Algieri and Morrone (2019), prevents direct contact between the organic fluid and the high-temperature flue gases.

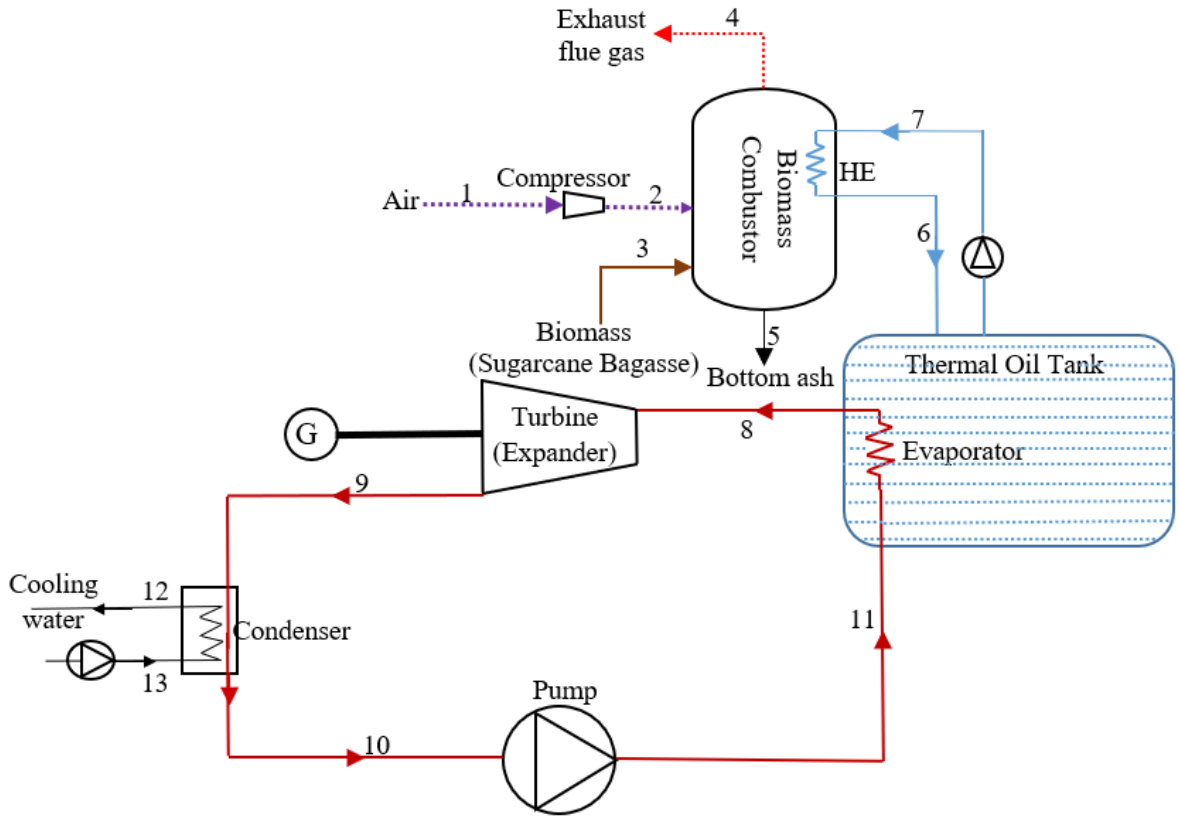

Legend

	Working fluid
	Thermal oil
	Fuel
	Air

	Heat exchanger
G	Generator
	Flue gas stream
	Bottom ash

Figure 3.1. Schematic layout of conventional ORC integrated BFPP

3.1.2. Category 2: CLC based BFPP with power generation alone

Figure 3.2 illustrates a simplified block diagram showcasing the operational architecture of a CLC-based BFPP. The core constituents driving this innovative system encompass several integral units, each playing a pivotal role in the overall process efficiency. The fundamental components within this advanced setup encompass a sizing and drying unit, a dual-reactor configuration utilizing CLC, intricate thermal oil and organic fluid loops, an Organic Rankine Cycle unit, gas turbine assembly, and a designated CO_2 compressor and storage unit. A noteworthy departure from conventional Coal-Fired Power Plants (CFPP) is the substitution of the standard combustor with distinct air and fuel reactors within the CLC-based framework. This alteration forms the foundation for enhanced efficiency and reduced emissions.

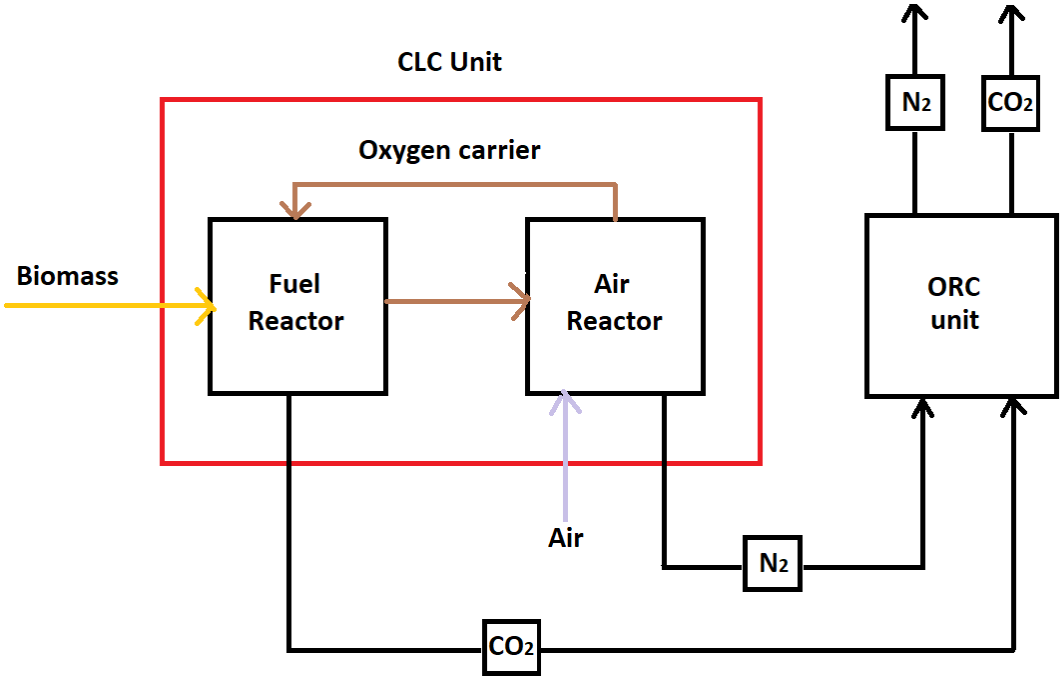

Figure 3.2. Simplified block diagram of a CLC-based BFPP

The initial phase involves the introduction of pulverized biomass from the sizing and drying unit, synergistically combined with an oxygen carrier. This composite mixture is then channelled into the adiabatic fuel reactor, where controlled combustion of the biomass takes place. This process, characterized by its adiabatic nature, ensures optimal utilization of resources while minimizing heat loss. A key aspect of this design is the utilization of a CLC unit that generates a nitrogen-rich stream. This stream undergoes a dual-phase utilization, first propelling a gas turbine for power generation before being directed into a heat exchanger. Within the heat exchanger, the thermal oil captures and harnesses the residual heat, optimizing energy recovery and overall system efficiency. Additionally, the energy-rich CO_2 stream, a

direct outcome of the CLC process, interacts with the thermal oil. This interaction enables effective heat exchange, subsequently directing the CO_2 stream towards a dedicated condenser unit. Within this condenser, water vapour is condensed, facilitating the isolation of pure CO_2. The isolated CO_2 is subsequently subjected to compression for efficient storage, setting the stage for potential future utilization or safe disposal.

The synergy of Chemical Looping Combustion, Organic Rankine Cycle, and gas turbine systems within the CLC-based BFPP configuration not only ensures sustainable energy production but also significantly reduces carbon emissions. This approach stands as a theoretical testament to the ongoing evolution of clean energy solutions and their potential to reshape the energy landscape.

3.1.3. Category 3: CLC based BFPP with hydrogen and power co-generation.

The schematic representation of a CLC-based BFPP also referred as BDCL facility is vividly depicted in Figure 3.3. This intricate arrangement comprises a trio of reactors, namely the air reactor, steam reactor, and fuel reactor, all seamlessly integrated within the CLC framework. Alongside these reactors, pivotal components such as the air compressor, gas turbine unit, CO_2 separator and compressor units, H_2 separator and compressor units, ORC turbine, and condenser collectively form the operational backbone of the plant.

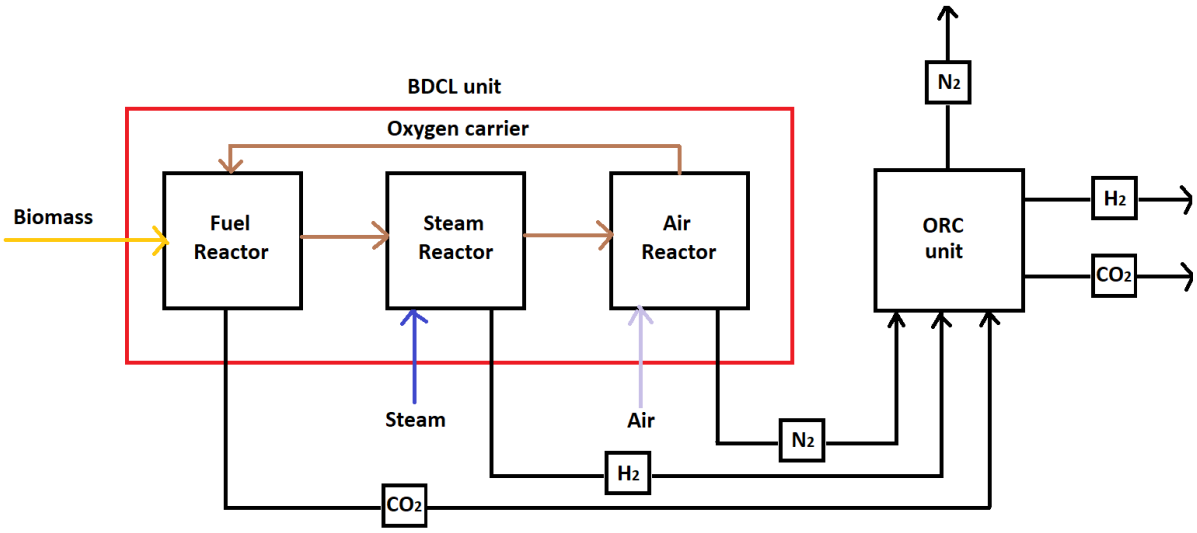

Figure 3.3. Simplified block diagram of a CLC-based BFPP with hydrogen and power co-generation

A key distinguishing feature of this plant, when compared with the standard CLC-based power generation plant, lies in the incorporation of an additional stream rich in hydrogen, derived from the steam reactor. This augmented H_2-rich stream, concomitantly with streams enriched

in carbon dioxide (CO_2) and the depleted air fraction, synergistically engages in a thermal integration with a thermal oil system, orchestrating the pinnacle of energy harnessing. The isolation of hydrogen from the steam takes place within a dedicated H_2 separator unit, where after it is channelled towards a specialized H_2 compressor unit, fine-tuning its thermodynamic state for subsequent utilization. Each distinct unit adeptly carries out its designated function, collectively culminating in the efficient generation of power and the co-production of hydrogen. The intricate chemistry within the air, fuel, and steam reactors is underpinned by a series of chemical reactions enumerated from Reaction (5.1) to (5.10). These reactions intricately dictate the intricate transformations transpiring within the reactors, further amplifying the multifaceted nature of the BDCL concept.

3.1.4. Category 4: CLC based BFPP with hydrogen and power co-generation coupled with CO_2 utilization plant.

Illustrated in Figure 3.4 is a simplified block diagram delineating the configuration of a BDCL system, exquisitely tailored to aide in a synergy of hydrogen and power co-generation, with the judicious utilization of carbon dioxide. By following the established trajectory outlined for the BDCL entailing power and hydrogen co-generation, this plant seamlessly adheres to a proven blueprint of operational efficacy. A noteworthy augmentation materializes in the form of an adjunctive CO_2 utilization module, underscoring the plant's versatility and commitment to sustainable practices. This distinctive configuration not only amplifies the plant's operational portfolio but also stands as a testament to its proactive role in mitigating carbon emissions and harnessing CO_2 as a valuable feedstock for productive ends. The resulting integration of hydrogen and power co-generation synergistically intertwined with innovative CO_2 utilization underscores the plant's embodiment of sustainability-driven innovation.

3.2. Flowsheeting details and simulation assumptions

The above presented configurations are simulated in Aspen Plus software using the appropriate models and necessary reference data from the literature. To enable the direct comparison between the conventional and CLC integrated BFPP configurations, similar unit models and common operating assumptions have been considered. The composition of sugarcane bagasse biomass is given in the Table 3.2. Table 3.3 highlights the process models, initial operating conditions and assumptions considered in the present study. Table 3.4 presents the unit models, property estimation methods, stream class, reference ambient conditions, simulation strategy, etc. considered in the simulations. The sugarcane biomass content 2.09% ash. It mainly contains the following component SiO_2 (60.9%), Al_2O_3 (14.83%) and FeO (12.8%).

The reactive silica and other component may corrode the internal part of the equipment. However, in this work while doing the simulations the ash in the biomass is considered as a non-conventional inert component. Further the present work is not focused on the separation of ash particles from the oxygen carrier particles and interaction of biomass-ash with the oxygen carriers.

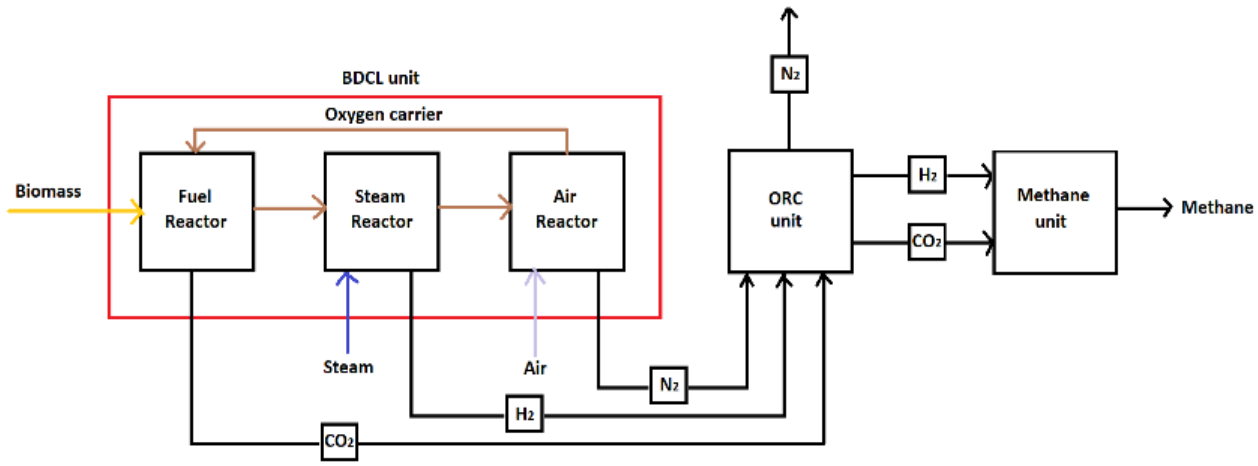

Figure 3.4. Simplified block diagram of CLC based BFPP with hydrogen and power co-generation coupled with CO_2 utilization plant.

Table 3.2. Composition of sugarcane bagasse biomass (Pillai et al., 2019).

Ultimate analysis (wt.%)	
Carbon	44.48
Oxygen	40.69
Hydrogen	6.057
Nitrogen	0.19
Sulfur	0.047
Moisture	6.44
Ash	2.09
H.H.V. (MJ/kg)	16.45

In this analysis, the stream class MIXED defines the conventional fluids and the stream class CIPSD and NCPSD defines the conventional and non-conventional solids, respectively. The HCOALGEN and DCOALIGT are used as enthalpy models to define non-conventional components (coal and ash). Peng Robinson and Boston Mathias (PR-BM), Soave Redlich Kwong (RKS), Electrolyte NRTL, Ideal gas, and STEAMNBS were used for the estimation of

properties of solid, electrolytes components in the CO_2 capture process, air, flue gases, steam and water.

Table 3.3. Process equipment operating conditions (Mukherjee et al., 2015; Cormos and Cormos, 2014; Erdem et al., 2009; Skorek-Osikowska et al., 2017; Diego et al., 2016; Wang et al., 2013; Suresh et al., 2010; Meyer et al., 2017)

Unit	**Operating conditions/assumptions**
Combustor	Modelled as: isothermal reactor At pressure and temperature:1.013 bar and 1610.3 ^{0}C Approach: Chemical and phase equilibrium Combustion efficiency: 100 %
Air Reactor	Modelled as : Isothermal reactor Pressure and temperature:10 bar and 1000 ^{0}C Approach: Chemical and phase equilibrium
Fuel Reactor	Modelled as : Adiabatic reactor Operating Pressure: 10 bar Approach: Chemical and phase equilibrium Oxygen carrier to support ratio: 70:30 (mass basis) Combustion efficiency: 100 %
Steam Reactor	Modelled as : Isothermal reactor Pressure and temperature: 10 bar and 750 0C Approach: Chemical and phase equilibrium Combustion efficiency: 100 %
Fan/Blower/Compressor	conventional BFPP: Fan/Blower: modelled as isentropic compressor Pressure: increased from 1.013 bar to 1.04 bar CLC-BFPP: Compressor: modelled as isentropic compressor Outlet pressure: 5% higher than the operating pressure of the air reactor.
CLC-BFPP Gas Turbine	Discharge pressure: 1.013 bar Isentropic efficiency: 85 %
ORC turbine	Discharge pressure: 2.4 bar Isentropic efficiency: 90 %

ORC Condenser	Condenser pressure: 2.4 bar Exit temperature: 33.5 ^{0}C No pressure drop
ORC Pump	Discharge pressure: 11.4 bar
ORC evaporator	Modelled as heat exchanger Minimum temperature approach: 5 ^{0}C Tube side pressure: 11.4 bar Shell side pressure: 2.2 bar Zero Pressure drop
CO_2 Compressor	Delivery pressure: 110 bar ---- for utilization Compressor efficiency: 85%

Table 3.4. Aspen plus steady state flow sheeting input data (Pillai et al., 2019; Surywanshi et al., 2019; Suresh et al., 2010; Mendiara et al., 2018; Aspen Tech Aspen Physical Property System, 2009)

Components / Methods	ASPEN Data
Non-conventional solid components- Coal and Ash	Defined using MCINCPSD stream
Conventional solid, liquid and gaseous components	Defined with molecular structure
Simulation strategy	Sequential modular approach
Property estimation methods used	PR-BM, STEAM-TA
Unit operations models	
BFPP combustor, CLC-BFPP air and fuel reactors	RGibbs
Ammonia synthesis reactor	RPlug
Methane synthesis reactor	RGibbs
Mixers/splitters	Mixer/Fsplit
Separators	Sep/Flash2
Pressure changers	Pumps/Compr/MCompr/Turbine
Heat exchangers	Heater/HeatX/MHeatX
Plant assumptions	
Ambient pressure and temperature	P = 1.013 bar and T = 33 ^{0}C.

Chemical composition of reference environment	75.62% N_2, 20.3% O_2, 3.12% H_2O, 0.03% SO_2, 0.92% others
Conventional BFPP - Excess air	20%
CLC-BFPP metal oxide circulation	Stoichiometric requirement
Condenser pressure	2.4 bar
Bottom to fly ash ratio	20:80
Minimum temperature approach in heat exchangers	≈ 10 ^{0}C
Auxiliary power consumption	5 % of gross turbine power output
Plant operation	7008 hours per year
Efficiency of pumps	85%
Presence of other pollutants	The presence of N_2 and S related compounds in the flue gases is not considered.

3.3 Data Analysis

The performance of the proposed configurations are systematically analysed by evaluating different parameters as presented in the following sub sections.

3.3.1 Energy Analysis

For steady flow processes, the mass and energy balances are shown in Equation 3.1 and 3.2 (Kanoğlu et al., 2012):

$$(\sum \dot{m}_n)_{in} = (\sum \dot{m}_n)_{out} \tag{3.1}$$

$$\left(\sum \dot{E}_n\right)_{in} = \left(\sum \dot{E}_n\right)_{out} \tag{3.2}$$

The plant net power ($\dot{W}_{net}$) was calculated by using Equation 3.3, where, $\dot{W}_{gross}$ is the gross power output of turbine, $\dot{W}_{comp}$ is the energy consumption by air compressor, $\dot{W}_{pump}$ is the energy consumption by centrifugal pump, $\dot{W}_{ASS}$ is the energy consumption by ASS and $\dot{W}_{aux}$ is the sum of all auxiliary power consumptions.

$$\dot{W}_{net} = \dot{W}_{gross} - \dot{W}_{comp} - \dot{W}_{pump} - \dot{W}_{ASS} - \dot{W}_{aux} \tag{3.3}$$

The net energy efficiency (η_{net}) of biomass fired power plants were determined by using Equation 3.4. The chemical energy of biomass ($\dot{E}_b$) was calculated by using Equation 3.5 and the Higher Heating Value of biomass (HHV_b) in kJ/kg was calculated empirically by using Equation 3.6 which was based on Dulong's and Petit law (Sahoo et al., 2016). In the HHV_b

calculation the carbon, H_2, oxygen and sulphur components weight percent are represented as C, H_2, O_2 and S, whereas m_b denotes the mass flow rate (kg/sec) of biomass in biomass fired power plants.

$$\eta_{bp} = \frac{(\dot{W}_{net})}{(\dot{E}_b)} \tag{3.4}$$

$$\dot{E}_b = \dot{m}_b \times HHV_b \tag{3.5}$$

$$HHV_b = 338.3 \times C + 1443 \times \left(H_2 - \frac{O_2}{8}\right) - 94.2 \times S \tag{3.6}$$

3.3.2 Exergy analysis

The exergy flow entering and leaving of individual stream is defined using the EXERGYFL property set in Aspen Plus V10.0. The individual unit exergy destruction and efficiency are calculated in terms of kW and % using the equations (3.7) and (3.8), respectively.

$$Ex_d = (\sum Ex_{in} - \sum Ex_{out}) \tag{3.7}$$

$$Ex_{eff,unit} = \left(1 - \frac{Ex_d}{\sum Ex_{in}}\right) \times 100 \tag{3.8}$$

The net exergy efficiency (ψ) of biomass fired power plants was calculated by using Equation 3.9. The specific exergy of the fuel ($SCEx_b$) for biomass fired power plants was calculated by using Equation 3.10, 3.11 and 3.12 (Sahoo et al., 2016). In these equations the LHV_b and $SCEx_b$ represent lower heating value and standard specific exergy of biomass. The *w* denote the mass fraction of moisture present in the biomass whereas λ represents latent heat of vaporization of H_2O at ambient temperature (T_0) i.e., 33 ^{0}C.

$$\psi = \frac{\dot{W}_{net}}{\dot{m}_b \times SCEx_b} \tag{3.9}$$

$$SCEx_b = (LHV_b + w \times \lambda).\varphi + 9417 \times S \tag{3.10}$$

$$\varphi = 0.1882\frac{H_2}{C} + 0.061\frac{O_2}{C} + 0.0404\frac{N_2}{C} + 1.0437 \tag{3.11}$$

$$LHV_b = HHV_b - (226.04 \times H_2) - 25.82 \times w \tag{3.12}$$

Net power output of the BDCL plant:

An electrochemical conversion device known as a solid oxide fuel cell (SOFC) directly generates energy by oxidizing a fuel instead of combustion. Significant losses in thermal

efficiency are caused by the combustor's high irreversibility. Due to this, SOFC has a better electrical efficiency than a traditional heat engine since the thermodynamic Carnot constraint is absent. The SOFC stack's anode receives the outlet H_2 stream from the steam reactor, while the cathode receives the reduced air from the air reactor. Following are the reactions (3.13 & 3.14) that take place in the SOFC unit's anode and cathode:

Anode: $$H_2 + O^{2-} \rightarrow H_2O + 2e^- \quad (3.13)$$

Cathode: $$O_2 + 4e^- \rightarrow 2O^{2-} \quad (3.14)$$

Cell voltage is typically a function of many SOFC stack factors such as temperature, pressure, and gas composition. In general, cell voltage is influenced by factors such as temperature, pressure, and gas composition. In lieu of a full examination of cell voltage loss owing to polarizations, cell voltage is considered to be in a reasonable range. For a nominal design condition, a reference cell voltage (V_{ref}) of 0.7 V is assumed, as stated in (Park et al., 2011). The cell voltage of a fuel cell with cell pressure adjustment and the power generation of a SOFC stack are characterized as given equation (3.15).

$$V_{cell} = V_{ref} + \left(\frac{RT}{4F}\right) \ln\left(P_{SOFC}/P_{ref}\right) \quad (3.15)$$

where, R is the universal gas constant, F denotes the Faraday constant, T denotes the stack temperature, P_{ref} denotes the reference pressure, and P_{SOFC} denotes the SOFC pressure. The SOFC stack's alternating current (AC) power output is determined using equation 3.16.

$$W_{SOFC} = \eta_{DC/AC} * V_{cell} * n_{H_2} * U_f * 2F \quad (3.16)$$

where, n_{H_2} is the inlet molar flow rate of H_2, U_f is the fuel utilization factor and $\eta_{DC/AC}$ is the DC/AC converter efficiency, which are assumed to be 0.8 and 95%, respectively. The SOFC unit's output streams are sent to the ORC unit at high temperatures. Outlet stream is then released heat at ORC thermal oil tank and sent to the compression unit.

The plant net power ($\dot{W}_{net}$) was calculated by using Equation 3.17, where, $\dot{W}_{SOFC}$ is the AC power output of SOFC, $\dot{W}_{gross}$ is the gross power output of turbine, $\dot{W}_{comp}$ is the energy consumption by air compressor, $\dot{W}_{pump}$ is the energy consumption by centrifugal pump and $\dot{W}_{aux}$ is the sum of all auxiliary power consumptions.

$$\dot{W}_{net} = \dot{W}_{SOFC} + \dot{W}_{gross} - \dot{W}_{comp} - \dot{W}_{pump} - \dot{W}_{aux} \quad (3.17)$$

3.3.3 Environmental Analysis

Specific CO_2 emission (E_{CO_2}) is assessed in terms of amount of CO_2 emission per *kWh* power production (*g/kWh*) using equation (3.18). The carbon capture efficiency η_{CO_2} of the CLC integrated BFPP plant is calculated using equation (3.19).

$$E_{CO_2} = \frac{\left(\dot{m}_{CO_2.emit}\right)}{\left(W_{net}\right)} \tag{3.18}$$

$$\eta_{CO_2} = \frac{\left(\dot{m}_{CO_2}\right)}{\left(\dot{m}_{CO_2.tot}\right)} \times 100 \tag{3.19}$$

Here, $\dot{m}_{CO_2.emit}$ is the mass flow rate of CO_2 emission to the atmosphere, $\dot{m}_{CO_2}$is the amount CO_2 sent for storage and utilization and $\dot{m}_{CO_2.tot}$ is the total CO_2 emitted from the combustion system.

The annual CO_2 emissions rate per unit of biomass ($\varepsilon_{af.CO_2}$) is determined using the equation (3.20), where $\dot{m}_{CO_2.a.emit}$ is the amount of CO_2 emitted into the atmosphere yearly from the power plant (*kg*) and $Ex_{a.ch.f}$ is the chemical energy of total biomass fed annually (*kWh*).

$$\varepsilon_{af.CO_2} = \frac{\left(\dot{m}_{CO_2.a.emit}\right)}{\left(3.6Ex_{a.ch.f}\right)} \tag{3.20}$$

3.4 Summary

This chapter details the methodology employed for constructing Aspen Plus flowsheet models encompassing the processes/plants explored in Chapters 4 to 6. It delves into the specifics of configuring process flowsheets using Aspen Plus and examines the characteristics and capabilities. These units are harnessed within the flowsheets to accurately emulate specific processes such as combustion, pumping, heat exchange, and compression. The discussion also encompasses the validation of conventional BFPP process, illustrating how simulation models were cross-referenced with data from established literature to ensure accuracy. The validation findings underscore the high degree of correspondence between the models developed within the aspenONE v10.0 simulation software and the outcomes documented in the literature. Furthermore, the chapter encapsulates the general techniques deployed for evaluating and comparing the performance of the developed flowsheet models. This includes the elucidation of definitions and equations associated with parameters like net electrical efficiency, CO_2 capture rate, net energy efficiency, and exergy efficiency. Finally, with the proposed models and thermodynamic equations, the chapter lays the foundation for subsequent analysis detailed in Chapters 4 to 6.

Chapter 4

CLC based biomass fired power plant integrated with Organic Rankine Cycle

Chapter 4

CLC based biomass fired power plant integrated with ORC cycle

The first objective of the present study is addressed in this chapter by conducting the performance evaluation and comparison of conventional and CLC based biomass fired power plants. The overall performance of these configurations are examined based on the energy, exergy, and environmental analyses. Various sensitivity analyses such as effects of operating temperature, pressure and OC-to-biomass ratio on the overall performance of CLC based BFPP are also presented in this chapter.

4.1. Motivation and Objective

From existing literature, it becomes evident that the utilization of CLC technology has undergone comprehensive investigation concerning its application to both coal and biomass combustion or gasification processes, predominantly involving heat recovery and the generation of steam cycles. It is worth noting that despite this extensive exploration, the integration of CLC technology within a BFPP through the incorporation of an ORC remains an uncharted area, as per our rigorous review of available literature sources.

This study aims to bridge this gap by introducing a highly efficient configuration that amalgamates CLC technology with an ORC. Notably, this innovative approach possesses the potential to render the power generation process not only carbon-negative but also remarkably sustainable. This attribute is especially crucial in the context of establishing grid-independent, small-capacity power plants. The proposed grid independent power plant configurations operates at low capacity by utilizing the biomass available at rural areas. The amount of heat energy generation with such low fuel feed rate in the biomass combustor is more suitable to drive an ORC rather than a steam turbine. Similar studies on integration of ORC with biomass combustion is available in the literature (Al-Sulaiman et al., 2012; Quoilin et al., 2013; Ahmadi et al., 2013). The primary objective of this research entails the formulation and development of an intricate yet efficient configuration for a CLC-integrated BFPP. The utilization of sugarcane bagasse biomass as the feedstock underscores the relevance of this investigation in

the context of sustainable energy generation from agricultural residues. Sugarcane is the second most-produced agricultural commodity after cereals and a key crop grown in tropical and subtropical regions. Brazil and India are the leading producers of sugarcane with annual production of 746.83 million tons and 376.9 million tons respectively (Khatri and Pandit, 2022). To facilitate a comprehensive understanding of this novel configuration, Section 4.2 elaborates on the methodology employed for the synthesis of the CLC-integrated BFPP design. Moving forward, Section 4.3 of the study embarks on a systematic and thorough thermodynamic analysis, the primary aim of which is to optimize the pivotal operational parameters. By doing so, the objective is to achieve two pivotal outcomes: maximizing the energy efficiency and exergy efficiency of the entire process. This optimization process is crucial not only for the overall performance enhancement but also for the validation of the feasibility and viability of the proposed configuration.

The conclusion of the study lies in the presentation of a comprehensive comparative analysis in the final section. This analysis serves as a critical point of reference for evaluating the proposed CLC-integrated BFPP configuration against the conventional BFPP. Such a comparative evaluation is essential for showcasing the advantages, limitations, and distinctive attributes of the innovative configuration, thereby providing a solid foundation for future developments in the field of sustainable and efficient power generation. The anticipated outcomes have the promise to reshape the energy landscape, offering a greener, more sustainable, and technologically advanced pathway towards grid-independent power generation.

4.2. Model description and approach

This section explores the synthesis of the CLC integrated BFPP configuration. To foster autonomous power generation, a novel approach is posited, involving the design of a modest-capacity power plant that employs an ORC instead of the conventional steam cycle.

Within the framework of the CLC integrated BFPP, intricate systems involving air and fuel reactors are harnessed to manage the combustion process of biomass. The underlying concept entails the introduction of biomass, in this case sugarcane bagasse, into the fuel reactor alongside oxygen carrier particles, with a composition primarily of Fe_2O_3 supported on 30% Al_2O_3. The combustion of biomass within the fuel reactor hinges on an direct interaction with oxygen, facilitated by the iron oxide particles. A crucial element of this scheme is the continuous circulation of the oxygen carrier particles between the air and fuel reactors, effectively forming a closed loop. Pertinently, the oxidation of the oxygen carrier within the

air reactor is an exothermic process, while the reduction of the oxygen carrier within the fuel reactor is an endothermic one. Consequently, temperature regulation is pivotal: isothermal conditions are maintained within the air reactor, facilitated by the dissipation of excess heat via air, while the fuel reactor is regarded as an adiabatic reactor, relying on the supplied heat from the circulating solid oxygen carrier particles, intertwined with the fluidizing medium (Mukherjee et al., 2015).

The chemical transformations transpiring within the fuel and air reactors are presented through Equations (4.1) to (4.5). Notably, the reactions within the fuel reactor exhibit an endothermic character, while the solid stream originating from the air reactor bears a high temperature profile. Contrarily, the reactions within the air reactor lean towards an exothermic nature, necessitating the removal of excess heat through the introduction of surplus air into the air reactor. This adjustment is achieved by employing a calculator block integrated into the aspenONE simulation software. The iron oxide compound displays various oxidation states. An interesting observation arises when anticipating diverse levels of reduction: the transition from Fe_2O_3 to Fe_3O_4 outpaces subsequent steps, namely the conversions from Fe_3O_4 to FeO and from FeO to Fe. The oxygen-carrying capacity inherent to iron oxide escalates with the extent of reduction in Fe_2O_3. In the context of the fluidized bed fuel reactor catering to solid fuels, the oxygen transport capability remains constrained to the Fe_2O_3 to Fe_3O_4 transformation. This limitation is attributed to the equilibrium constraints operating within the reaction ambiance, wherein CO_2 and/or H_2O not only serve as the fluidization medium but also emerge as the resultant products of combustion.

$C + H_2O \rightarrow CO + H_2$ ΔH = 131.3 kJ/mol at 298 ºC and 1 atm (4.1)

$C + CO_2 \rightarrow 2CO$ ΔH = 172.5 kJ/mol at 298 ºC and 1 atm (4.2)

$CO + 3Fe_2O_3 \rightarrow 2Fe_3O_4 + CO_2$ ΔH = -42 kJ/mol at 1000 ºC and 1 atm (4.3)

$H_2 + 3Fe_2O_3 \rightarrow 2Fe_3O_4 + H_2O$ ΔH = -9.9 kJ/mol at 1000 ºC and 1 atm (4.4)

$2Fe_3O_4 + {}^1/_2\, O_2 \rightarrow 3Fe_2O_3$ ΔH = -239.4 kJ/mol at 1000 ºC and 1 atm (4.5)

This integration of the CLC approach for biomass combustion is interfaced with the ORC cycle to harness power generation capabilities. Notably, a portion of the high-temperature stream, comprising CO_2 and steam, is employed as the fluidizing medium within the CLC fuel reactor, after undergoing heat exchange with thermal oil. Meanwhile, the heated, spent air stream emanating from the air reactor sends to a gas turbine for effective power generation. Subsequently, the residual low-pressure heat energy within this air stream is efficiently harvested via thermal oil. In parallel, the CO_2 segregated from the flue gas stream of the fuel

reactor is subjected to heat exchange with thermal oil followed by undergoes separation by condensing the steam. The isolated CO_2 is then subjected to compression, elevating its pressure to a level compatible with sequestration protocols, typically around 110 bar. For an illustrative overview, refer to Figure 4.1, which presents a schematic representation of the CLC integrated BFPP's intricate flow diagram.

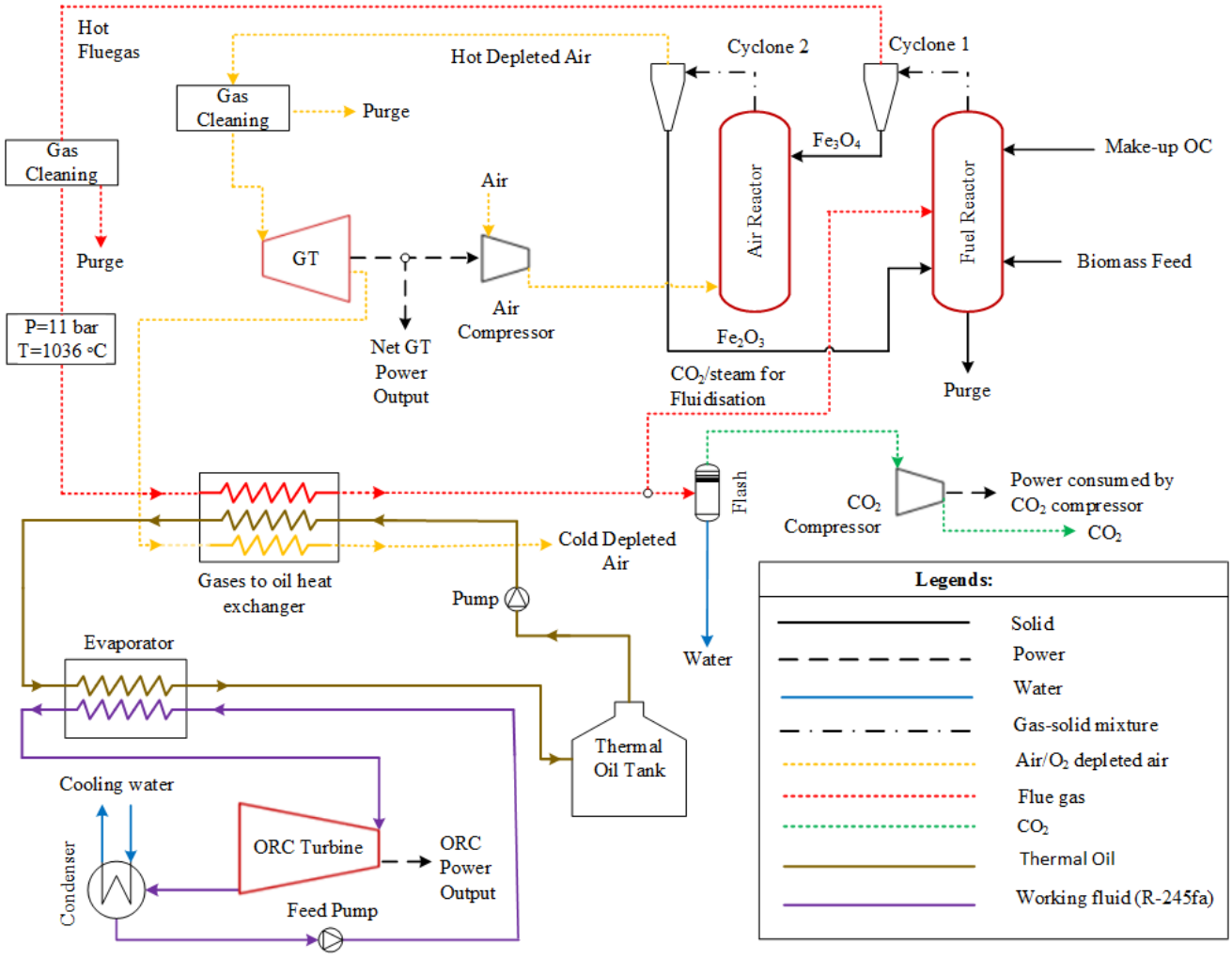

Figure 4.1. Schematic diagram of CLC integrated BFPP.

4.3. Results and Discussion

To evaluate the performance enhancements offered by the newly introduced CLC integrated BFPP configuration, a comprehensive comparison is established with the conventional BFPP model, which was detailed as a reference model in Section 3.1. Under stable operational circumstances, the conventional BFPP configuration is simulated for a consistent biomass flow rate of 0.139 kg/s.

Concurrently, the novel CLC integrated BFPP configuration, presented in Section 4.2, is subjected to analogous steady-state simulations, maintaining an identical biomass flow rate of 0.139 kg/s. Notably, these simulations encompass the examination of two distinct sets of CLC loop operating conditions, both sourced from the existing literature: a) In the first set, the air reactor is maintained at a pressure of 30 atm and a temperature of 1300 °C, harmoniously coupled with an adiabatic fuel reactor operating at a pressure of 30 atm (Mukherjee et al., 2015) . b) The second set involves the air reactor being held at a pressure of 10 atm and a temperature of 1000°C, synergistically with an adiabatic fuel reactor also operating at a pressure of 10 atm (Darmawan et al., 2018). The ensuing computational outcomes, systematically presented within Table 4.1, yield insightful revelations. It becomes evident that the CLC integrated plant, operating under the conditions outlined in case (b), surpasses its counterparts in terms of energy efficiency and exergy efficiency. These results collectively signify that the configuration grounded in case (b) serves as the optimal benchmark, thus warranting its selection as the base case for subsequent rounds of comprehensive analysis and evaluation. In both the cases the energy and exergy efficiencies are low as compared with the steam based Rankine cycle due to the low pressure and temperature operations in ORC cycle and existence of one more heat transfer loop with the thermal oil as a heat exchange fluid.

Table 4.1. Overall performance comparison of case studies

Parameter	Unit	Case (a)	Case (b)
Total energy input	kW	2280.3	2280.3
Gross turbine output	kW	441.35	493.51
Net power consumption	kW	28.61	53.35
Net power output	kW	412.74	440.16
Gross energy efficiency	%	19.36	21.65
Net energy efficiency	%	18.10	19.31
Gross exergy efficiency	%	16.65	18.61
Net exergy efficiency	%	15.57	16.60

4.3.1. Sensitivity Analysis

Within this particular section, a exploration of sensitivity has been undertaken, entailing the deliberate alteration of a singular variable to its maximum extent. The primary objective

centers around comprehensively scrutinizing the performance exhibited by the established base case, delving into the consequential impact induced by several pivotal process parameters. Specifically, the parameters under scrutiny encompass the oxygen carrier to biomass ratio, the operational pressure, and the operational temperature. This analytical study inherently seeks to reveal the interplay between these variables and the overall system performance. Extending the ambit of investigation, the study delves into the performance facets of the optimally configured process arrangement. This is further expanded through the incorporation of three distinct working fluids, each applied within the framework of the ORC. This strategic diversification facilitates a comprehensive grasp of how various working fluids influence the overall system performance. Furthermore, an innovative approach is introduced to amplify the output of the ORC cycle's power generation. This entails the strategic extraction of waste heat from a pair of intermediary process streams, employing specialized recuperators. By harnessing this latent waste heat, the efficiency and effectiveness of the ORC cycle are enhanced, thereby augmenting the overall power output.

As a culmination of this comprehensive analysis, the subsequent focus shifts towards Section 4.3.2, wherein a compelling comparation is established. This involves a rigorous comparison of the performance metrics exhibited by the optimal CLC integrated BFPP configuration against the conventional BFPP. This comparative analysis serves as the bedrock for affirming the advancements and superiority of the newly proposed configuration within the broader context of biomass-fired power generation.

4.3.1.1. Effect of oxygen carrier to biomass ratio

The effect of OC to biomass ratio on different performance indicators including net power consumption & generation, air feed flow rate and the overall energy and exergy efficiencies is evaluated by varying OC mass flow rate for constant biomass feed flow rate of 0.139 kg/s. In the present study, isothermal condition in the air reactor is maintained by varying the air flow rate. The sensitivity analysis results are presented in Figure 4.2, 4.3 & 4.4. As the flowrate of OC circulating in the loop is increased, the increase in gas turbine power output, ORC turbine power output and gross power output is observed as can be seen from Figure 4.2. This is because of the increased of fuel combustion rate in the fuel reactor, which further increased the temperature of fuel reactor (flue gas and metal oxide temperatures) as shown in Figure 4.3. As combustion rate increases with OC circulation rate, reduction rate of metal oxides and the flue gas flow rate from the fuel reactor increases. Hence, more amount of air is needed in air reactor (an isothermal reactor operating at 1000 ^{0}C) to oxidize the reduced metal oxide. As the amount of air and flue gas flow rates increase, energy flow to the thermal oil cycle (in energy

exchange loop between CLC and ORC cycle) increases. To extract this energy, the thermal oil flow is adjusted by keeping inlet and outlet temperatures of the thermal oil at 125 ^{o}C and 395 ^{o}C respectively (as shown in Figure 4.4). The flow of energy from thermal oil to ORC fluid is extracted by the constant flow rate ORC fluid, which results in increase in the temperature of ORC fluid. This eventual effect of OC circulation rate on the thermal oil flow rate and exit temperature of constant flow ORC fluid from the evaporator is shown in Figure 4.4. The above factors ultimately resulted in increase of gas and ORC turbine power outputs and energy and exergy efficiencies with increase in OC to biomass ratio. This increase is observed up to an OC to biomass ratio of 54.43 and the maximum net power output of 427.18 kW is noticed as shown in Figure 4.2. The corresponding net energy and exergy efficiencies are 18.73 % and 16.11 %. (Figure 4.3). This OC-to-biomass ratio meets the stoichiometric requirement for an OC flow rate of 7.56 kg/s, resulting in the complete combustion of biomass. The captured carbon dioxide has a purity of 99.69%, as shown in Figure 4.5. Further increase of OC to biomass ratio, results in unnecessary circulation of non-reduced OC in the CLC loop, which has negative effect on overall performance of the plant. The net gas turbine output is the difference between the total power output and the power consumed by the air compressor.

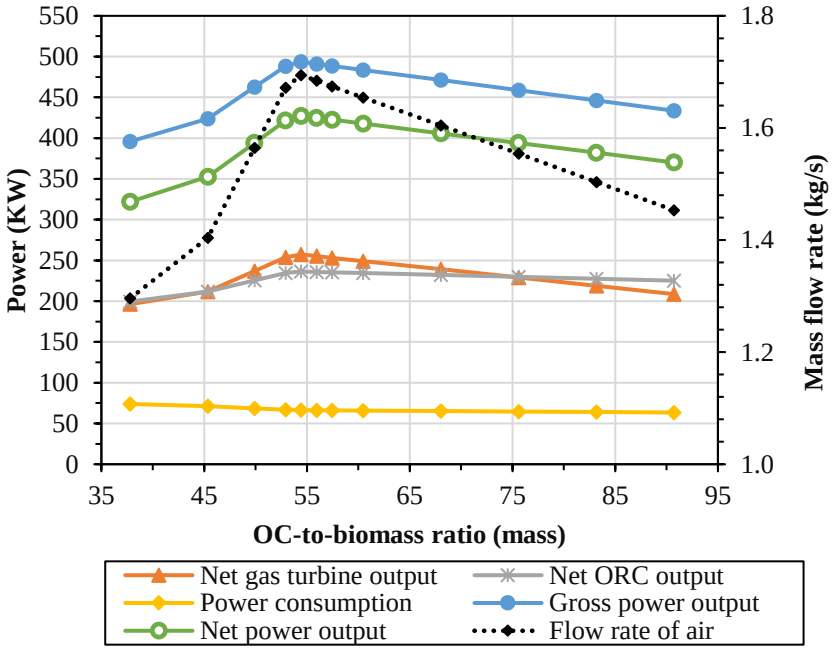

Figure 4.2. Effect of OC-to-biomass ratio on power consumption and generation.

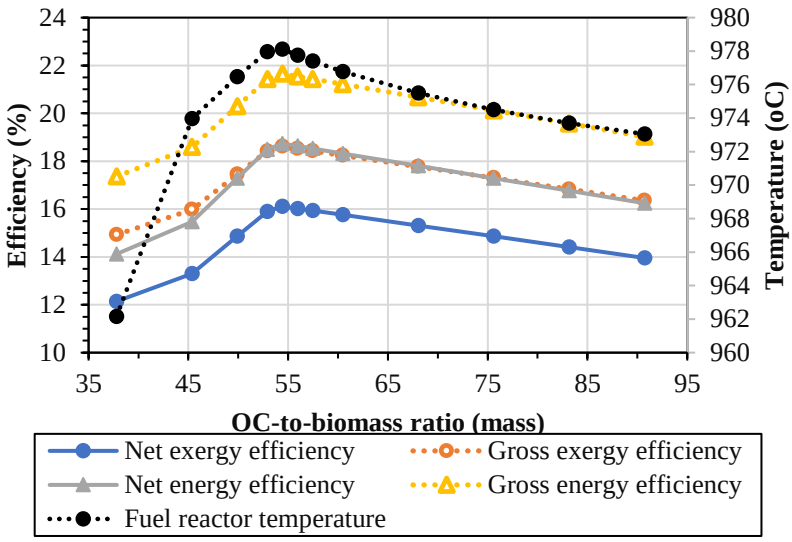

Figure 4.3. Effect of OC-to-biomass ratio on energy and exergy efficiency.

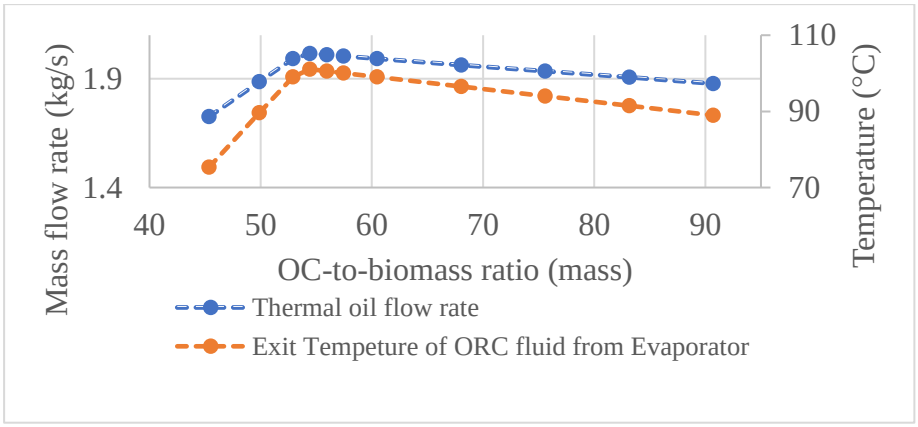

Figure 4.4. Effect of OC-to-biomass ratio on thermal oil flow rate and ORC fluid temperature

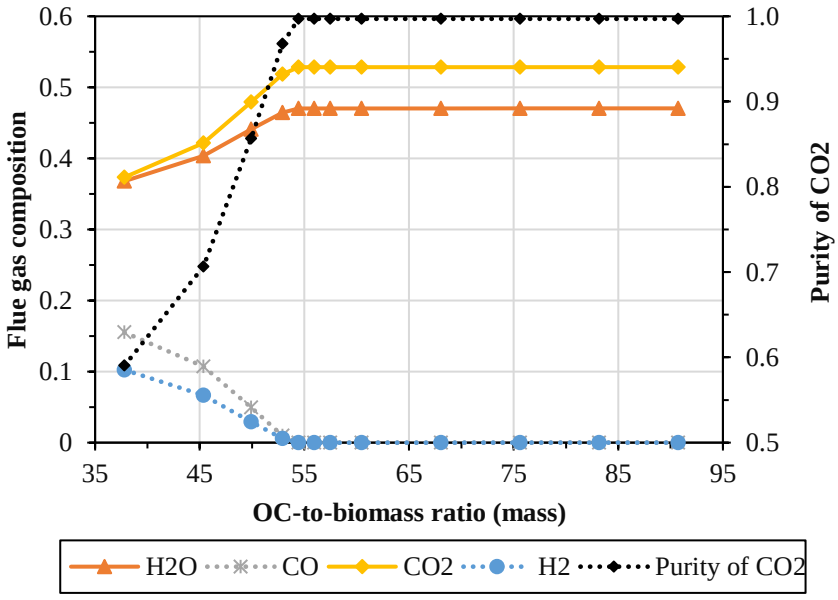

Figure 4.5. Effect of OC-to-biomass ratio on flue gas composition and purity of captured CO_2.

4.3.1.2. Effect of Air and Fuel Reactors Operating Pressure

The optimal OC-to-biomass ratio obtained from the above analysis is updated and the effect of CLC reactors operating pressure is evaluated. The effect of loop operating pressure variation from 1 bar to 18 bar on the overall process power consumption and generation is shown in Figure 4.6. As the reactor operating pressure increases, the gas turbine gross power output increases. With increase in the pressure from 1 bar to 10 bar, the net gas turbine power output (calculated as difference between gross turbine power output and air compressor power input) increases and at 10 bar pressure the net gas turbine power output is 257.19 kW. The net turbine power output decreases with further increase of pressure, because of the increased power consumption by the air compressor at the given operating conditions. With increase in air reactor pressure, the inlet depleted air stream pressure to the gas turbine increases and hence the power production by gas turbine increases and the temperature of the exit stream from the turbine decreases. This decrease in temperature of the air stream from the gas turbine affects the energy transfer with the thermal oil, which ultimately reduces the ORC turbine power output. CLC operating pressure range of 2 bar to 11 bar, increasing trend of gas turbine power output has more influence on the overall gross and net power outputs. The maximum net power output of 427.82 kW is observed at 11 bar pressure. Further, the process energy and exergy efficiencies are also evaluated at different CLC operating pressures and the maximum efficiencies are obtained at 11 bar pressure as shown in Figure 4.7.

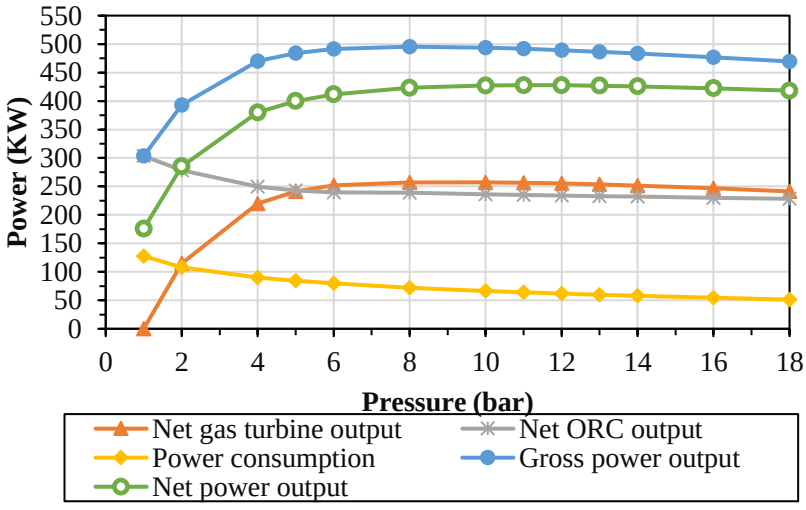

Figure 4.6. Effect of air and fuel reactor operating pressure on power consumption and generation.

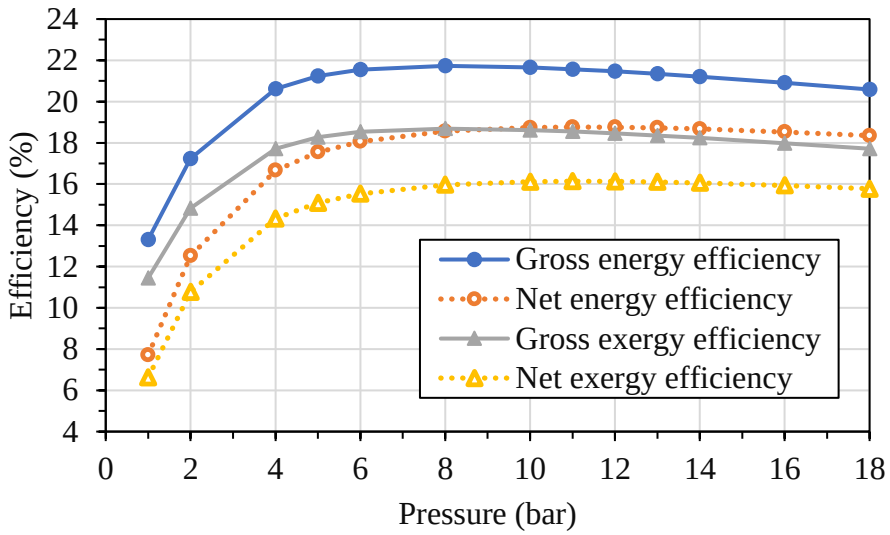

Figure 4.7. Effect of air and fuel reactors operating pressure on overall energy and exergy efficiency.

4.3.1.3. Effect of Air Reactor Operating Temperature

The effect of air reactor temperature on the plant performance is studied at optimal OC-to-biomass ratio and CLC operating pressure obtained from the above analysis. The optimal operating temperature for air reactor has been calculated from the suitable temperature range that is defined based on metal oxide properties. The effect of air reactor operating temperature on the air feed flow rate and power consumption and generation is shown in Figure 4.8. In order to maintain high temperature in the air reactor, minimum amount of heat needs to be removed, which further results in the reduction of air flow rate. Thus, the power consumed by the air compressor and gas turbine power output decreases with increase in air reactor temperature. The net gas turbine power output increases with increase in air reactor temperature up to 1050 ^{0}C and then shows a decreasing trend with air reactor temperature. This maximum is seen because of the fact that the rate of decrease in power consumption by air compressor is more than the rate of decrease in the gas turbine power output till 1050 ^{0}C. Beyond this air reactor temperature, the net gas turbine power output decreases. The net power generated follows the same trend and the maximum net power output is observed at air reactor temperature of 1050 ^{0}C as shown in Figure 4.8. The net power output decreases with further increase in the air reactor temperature even though the ORC turbine power output increases. The increase in ORC turbine power output is due to more energy flow to the thermal oil cycle from the flue gas. This increase in energy transfer from flue gas is due to increase in the fuel reactor temperature with increase in air reactor temperature. The fuel reactor temperature is increasing with the air reactor temperature, as the oxygen carrier transfers heat from the air

reactor to the fuel reactor. The effect of air reactor temperature on thermal oil circulation rate (at a constant pressure of 2.2 bar and exit temperature of 395 ^{0}C) and exit temperature of ORC fluid is presented in Figure 4.9. To extract this increased energy from the thermal oil, the ORC fluid outlet temperature is adjusted as shown in Figure 4.9. With increase in air reactor temperature, the amount of thermal energy extracted in ORC cycle increases, which results in the increase in ORC power output. The effect of air reactor temperature on fuel reactor temperature and overall energy and exergy efficiencies is shown in Figure 4.10. The step by step improvement in process efficiency by the above sensitivity analysis has been presented in Table 4.2.

Table 4.2: Step by step improvement of the process efficiencies from sensitivity analysis.

Case	Optimal Value	Net turbine work output (kW)	Net ORC work output (kW)	Net overall energy efficiency (%)	Net overall exergy efficiency (%)
Oxygen carrier (OC) to biomass ratio	54.43	257.19	236.39	18.73	16.11
Air and fuel reactor operating pressure (bar)	11	256.49	235.29	18.76	16.13
Air reactor operating temperature (^{o}C)	1050	256.46	239.64	18.94	16.29

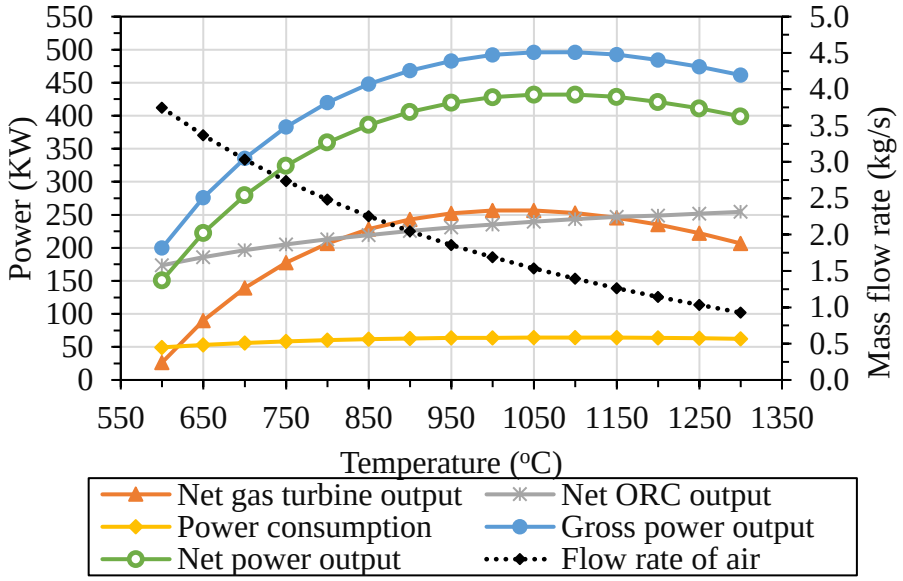

Figure 4.8. Effect of air reactor temperature on power consumption and generation.

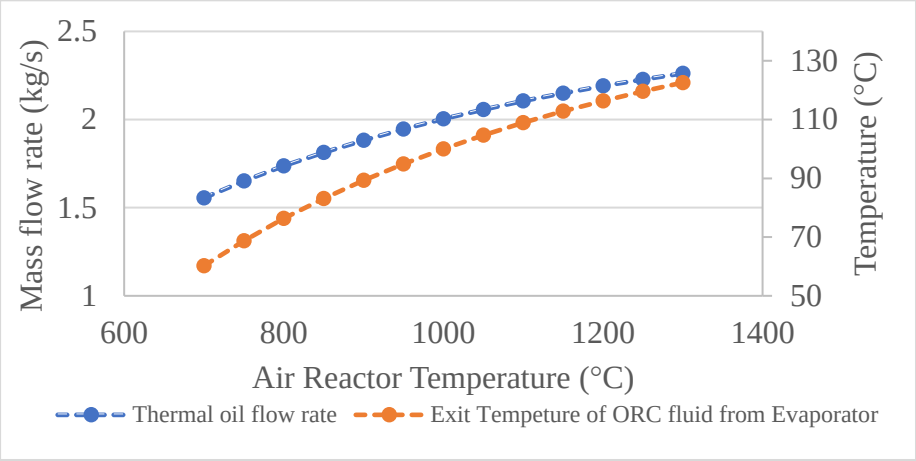

Figure 4.9. Effect of air reactor temperature on thermal oil flow rate and ORC fluid temperature

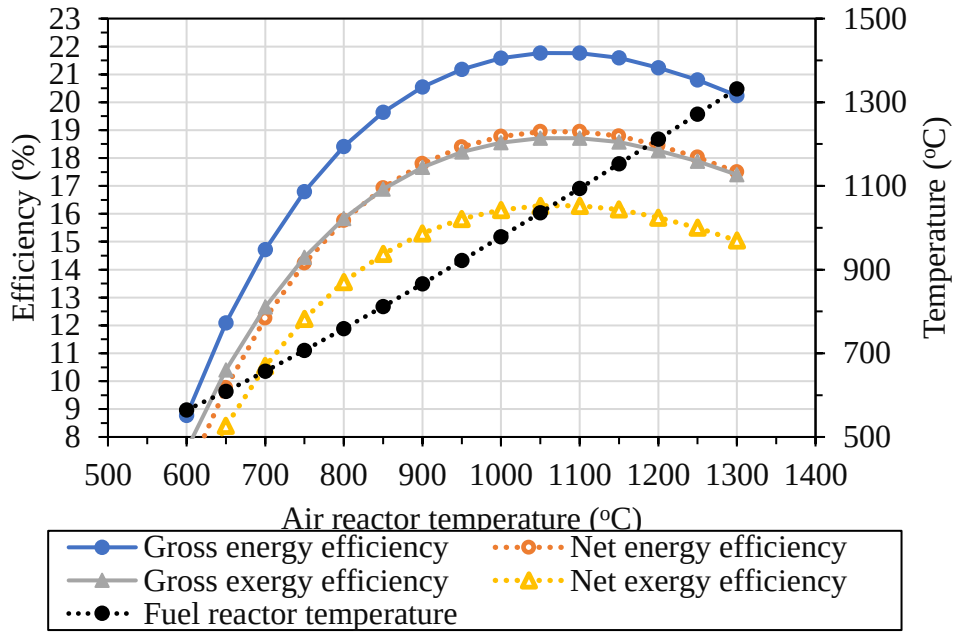

Figure 4.10. Effect of air reactor temperature on energy and exergy efficiency.

4.3.1.4. Effect of different ORC fluids and use of recuperators

Performance of the above optimal CLC-BFPP configuration is further analyzed using different ORC working fluids. In general, the ORC fluids are grouped into three categories based on the critical temperature, which limits the evaporation temperature - low temperature fluids with critical temperature less than 150 ^{0}C; medium temperature fluids with critical temperature in the range of 150 ^{0}C to 250 ^{0}C and high temperature fluids having critical temperature greater than 250 ^{0}C (Tchanche et al., 2011). In this section, the performance of ORC fluid - R245fa (critical pressure & temperature: 36.51 bar & 154 ^{0}C) is compared with three different fluids from the above categories: Iso-butane (R600a - critical pressure & temperature: 36.5 bar, 134.6 ^{0}C), R123 (critical pressure & temperature: 36.72 bar, 183 ^{0}C) and toluene (critical pressure &

temperature: 41.09 bar, 318.64 ^{0}C). The analysis has been carried out for the constant energy input (1682.34 kW) to the ORC evaporator from the thermal oil. Table 4.3 shows the ORC turbine gross and net power outputs for these fluids at the turbine inlet and outlet pressures of 11.4 bar and 2.4 bar. It can be observed that the maximum power output can be obtained by using low temperature fluids. Hence, R600a will be the most suitable working fluid with respect to high power output. However, it is highly flammable in nature and this attracts enough safety attention in operation (Bu et al., 2013). Therefore, in this work, the next suitable fluid i.e. R245fa has been selected as a working fluid in the ORC cycle. The health, safety, and operational pros and cons for the refrigerant liquids R600a, R245fa, R123, and Toluene are shown in Table 4.4 for further assessment.

Table 4.3. Performance of different ORC fluids

Fluid	Circulation rate (kg/s)	ORC turbine gross power output (KW)	ORC turbine net power output (KW)
R600a	4.3	253	240
R245fa	8.43	240	228
R123	7.34	190	181
Toluene	2.24	135	129

Table 4.4. Characteristics of different refrigerants

Fluid		R600a	R245fa	R123	Toluene
Health	Pros	Low toxicity.	Low toxicity.	Low acute toxicity.	
	Cons	Can cause dizziness	Can cause mild irritation to the respiratory system and eyes	Classified as a potential occupational carcinogen.	Highly toxic; exposure can cause severe health effects,
Safety Pros and Cons	Pros	Non-toxic. zero ozone depletion potential (ODP).	Low ozone depletion potential (ODP).	Non-flammable. Effective at low pressures, reducing the risk of leaks.	

	Cons	Highly flammable,	Moderate global warming potential (GWP).	Higher GWP.	Health hazards make it unsuitable for general refrigeration use.
Operational Pros and Cons	Pros	High energy efficiency.	Efficient for use in high-temperature heat pumps and Organic Rankine Cycle (ORC) systems.	Good efficiency in low-pressure systems.	Good thermodynamic properties.
	Cons	Requires safety measures due to flammability.	Higher GWP compared to some alternatives.	Being phased out due to environmental regulations	Not commonly used as a refrigerant due to significant health and safety risks.

The performance of ORC cycle in CLC-BFPP configuration is further improved by extracting the waste heat from the high pressure CO_2 stream and ORC fluid leaving from the turbine. Figure 4.11 shows the ORC cycle configuration integrated with two recuperators for waste heat recovery. This waste heat exploitation resulted in 20.8% increase in ORC gross power output.

4.3.2. Comparison of CLC Integrated Plant with the Conventional Plant

In this section, the overall CLC integrated BFPP is simulated using the optimal parameter values obtained from the above sensitivity analysis and the performance of the proposed final configuration is compared against the conventional BFPP using the thermodynamic and environmental parameters. Figure 4.12 shows the performance comparison of CLC integrated BFPP with the conventional BFPP based on power consumption and generation. It can be noticed from Figure 4.9 that the power consumption for CLC integrated BFPP is more than

conventional BFPP by 49.81 kW. The higher power consumption in CLC integrated BFPP configuration is due to the presence of high pressure loop and CO_2 capture unit, which are absent in the conventional BFPP as there is no CO_2 capture process involved and fuel combustion is only slightly above atmospheric pressure. In the absence of waste heat recovery using recuperators, the ORC turbine output is observed to be lower by 47.84 kW for CLC integrated BFPP configuration as compared to the conventional BFPP. On the other hand, the integration of recuperators for waste heat recovery resulted in the increase of ORC turbine output by 49.93 kW. The power produced by gas turbine is shown as zero in the conventional case as there is no gas turbine in the conventional BFPP,. In case of CLC integrated BFPP, the depleted air exiting the high pressure air reactor is at 11 bar and 1050 ^{0}C. Hence, this high energy stream is sent through the gas turbine and produced 256.46 kW of net power. This results in higher net power generation (492.19 kW) for CLC integrated BFPP compared to the conventional BFPP (273.12 kW). Figure 4.13 shows the performance comparison between conventional and CLC integrated BFPP based on overall energy and exergy efficiencies. It is noticed that the gross energy and exergy efficiencies are higher for CLC integrated BFPP by 11.34 % and 9.75 % respectively, as compared to the conventional BFPP.

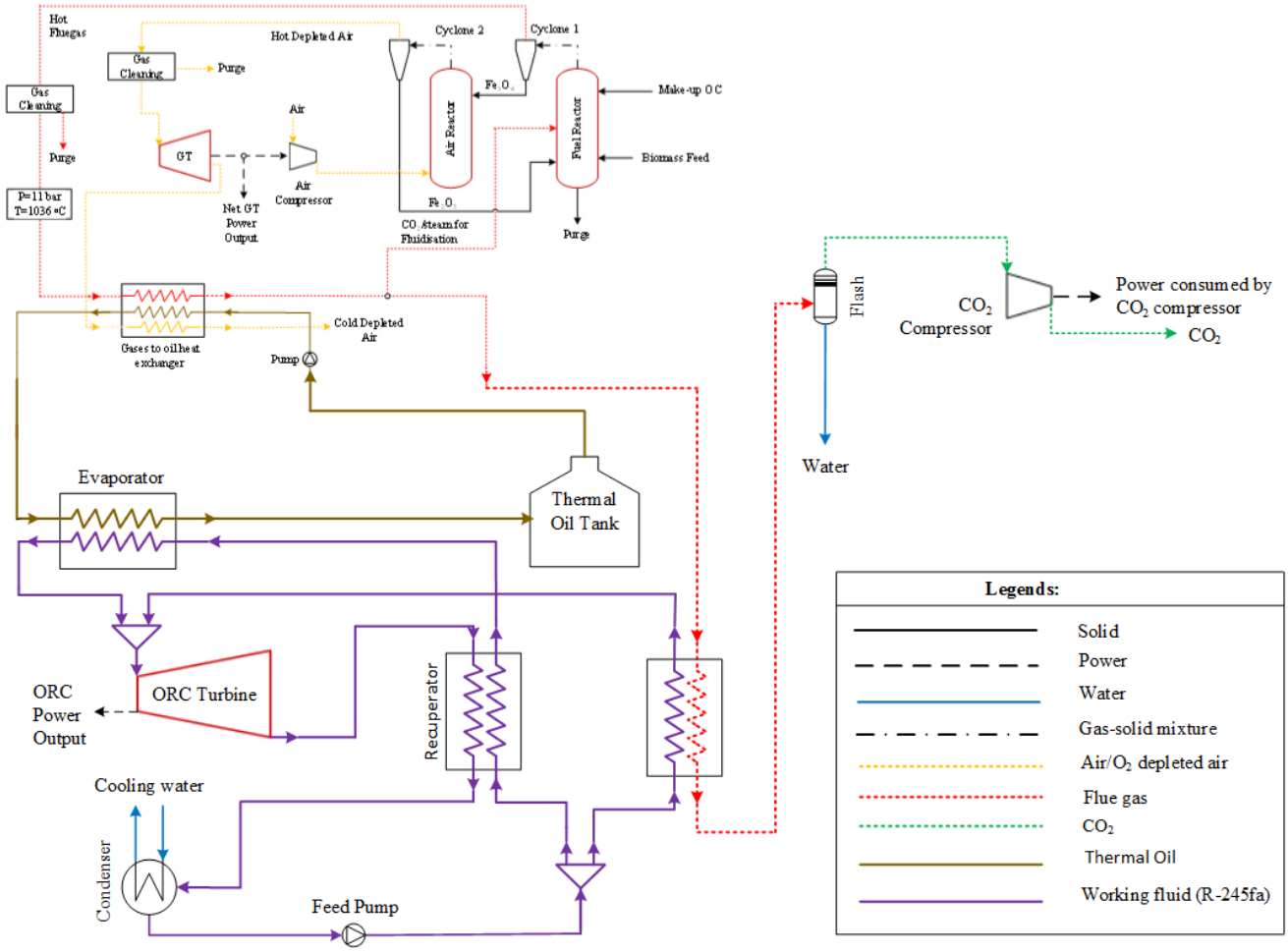

Figure 4.11. Schematic diagram of CLC integrated BFPP with recuperators

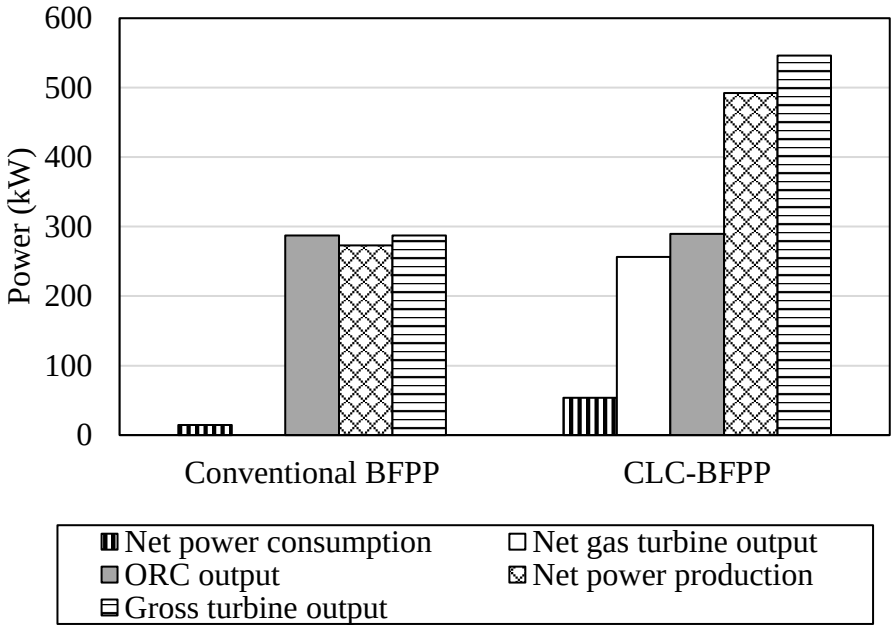

Figure 4.12. Performance comparison of CLC integrated BFPP with conventional BFPP based on power consumption and generation.

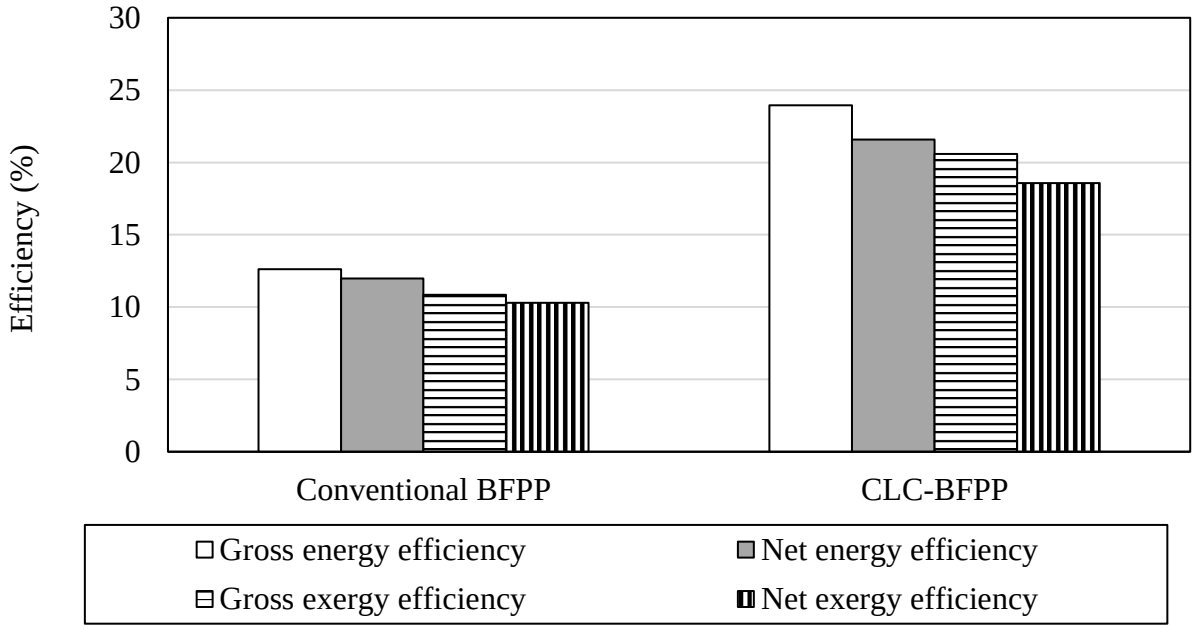

Figure 4.13. Performance comparison of CLC integrated BFPP with conventional BFPP based on overall energy and exergy efficiencies.

The key intention of integrating CLC with the BFPP is to reduce overall carbon emissions, hence the thermodynamic parameters alone cannot be the deciding criterion for the assessment. Further, the performance of the CLC integrated BFPP is also assessed in terms of environmental parameters as shown in Table 4.5.

For 7008 annual plant operation hours, the specific CO_2 emissions associated with the conventional BFPP is observed to be 2980.68 g/kWh and the same is zero in case of the CLC integrated BFPP. Hence, CLC integrated BFPP avoids an annual CO_2 emissions of 5.71×10^6 kg by capturing all the CO_2 generated from the plant. Thus, CLC integrated BFPP is shown to be an energy efficient and environmental friendly plant configuration.

Table 4.5. Environmental assessment of conventional and CLC integrated BFPP.

Parameter	Unit	Conventional BFPP	CLC integrated BFPP	CaL integrated BFPP (Sharif et al., 2021)
CO_2 emission	g/s	226.10	0.00	22.00
CO_2 captured	g/s	0.00	225.56	208.00
CO_2 capture efficiency	wt. %	0.00	100.00	90.43
Specific CO_2 emission	g/kWh	2980.68	0.00	376.62
Annual CO_2 emission	Kg	5.71×10^6	0.00	5.55×10^5
Average annual emission rate aggravating per unit of fuel	g.CO_2/GJ	139.00	0.00	13.50
Annual CO_2 avoided emission per unit fuel	g.CO_2/GJ	0.00	138.6	127.8

4.3.2.1. Exergy Analysis

In this section, a unit-wise exergy analysis is also carried out to assess the performance of individual plant units. Figure 4.14 shows the percentage of exergy efficiency in the major units of conventional and CLC integrated BFPP, respectively. The CLC loop consisting of Air Reactor and Fuel Reactor in CLC integrated BFPP is equivalent to the combustor of conventional BFPP. The combustor of the CLC integrated BFPP has the exergy efficiency 61.04% and the conventional BFPP combustor has 52.7% efficiency. Thus, the percentage exergy efficiency of CLC combustor is 8.34 % higher than the combustor of conventional BFPP. Figure 4.15 shows the percentage of exergy destruction in the major units of CLC integrated BFPP. The highest exergy destruction in air and fuel reactors is observed due to the

higher temperatures involved in the process. The exergy loss in the air and fuel reactors have been already minimized by performing the sensitivity analyses. The highest exergy destruction in the CLC integrated BFPP plant after the CLC reactors is observed in the evaporator (11.74%) and Air compressor (4.29%). The exergy efficiency of this plant can be further improved by operating the process under super-critical conditions.

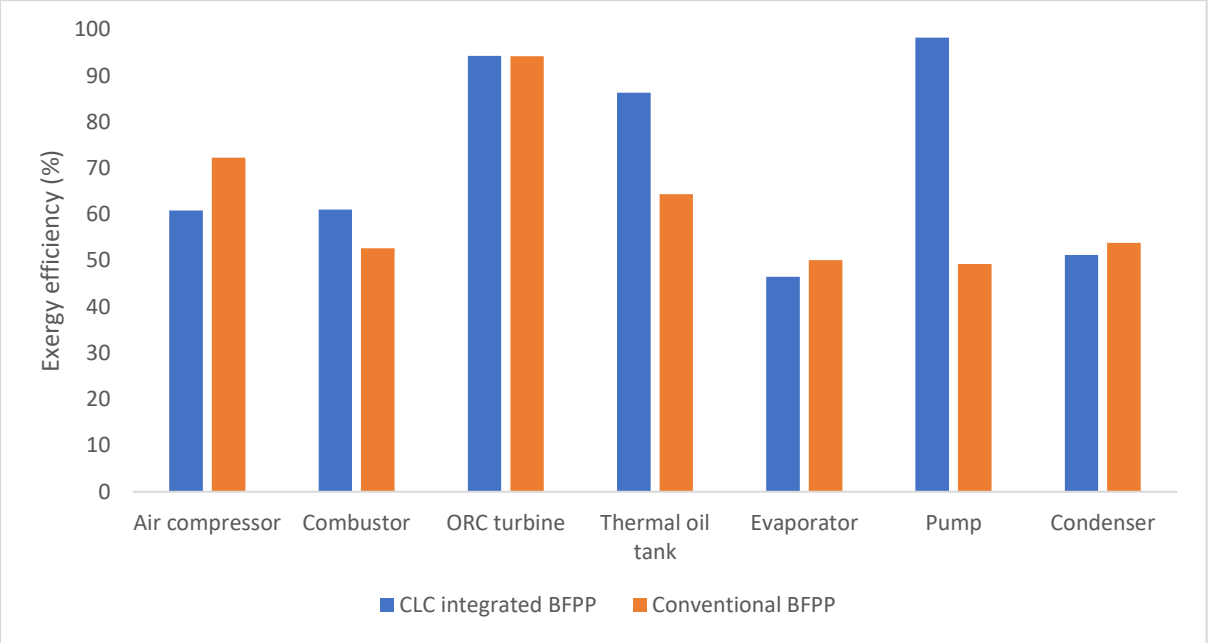

Figure 4.14. Comparison of Exergy efficiency of individual Plant units.

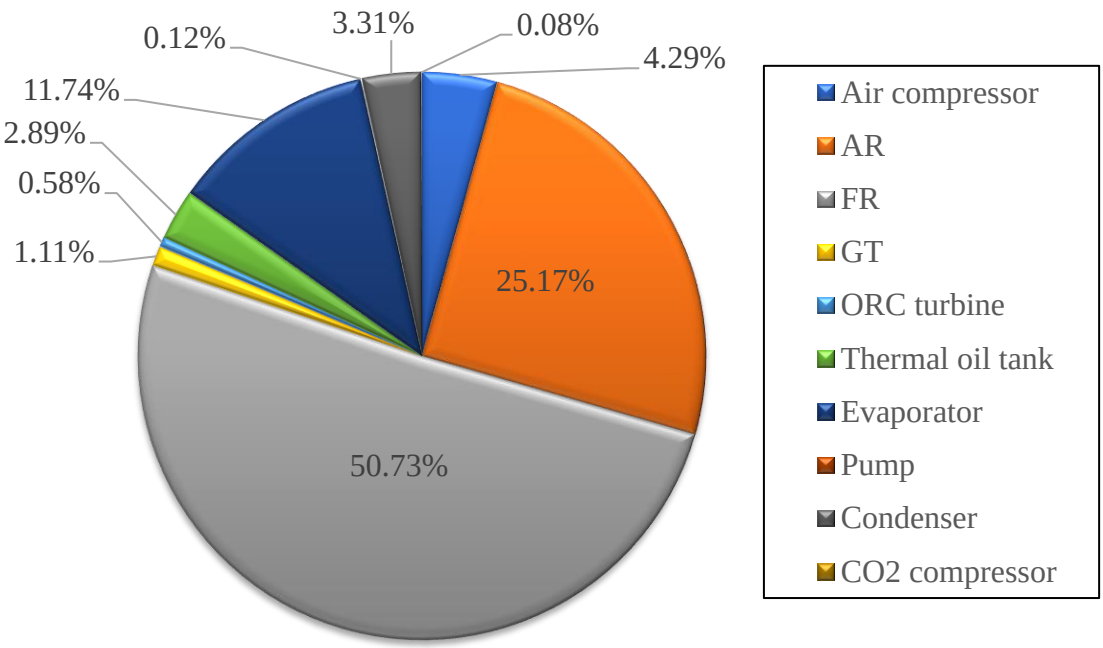

Figure 4.15. Unit-wise contribution of exergy destruction in CLC integrated BFPP.

4.4. Summary

This works introduces an innovative arrangement that combines chemical looping combustion with a biomass-fired power plant, seamlessly integrating them through an organic Rankine cycle to enhance power generation. This study conducts a comprehensive sensitivity analysis, strategically adjusting vital parameters including the oxygen carrier-to-biomass ratio, operational pressures of air and fuel reactors, and the operating temperature of the air reactor. The subsequent phase of the study involves the simulation of the CLC integrated BFPP using the optimized parameter set. This is followed by a comparison of its performance against the conventional biomass-fired power plant. This comprehensive evaluation explores various dimensions encompassing energy and exergy efficiency, as well as the environmental implications of the proposed system. Additionally, a meticulous analysis is carried out to identify the units within the system that contribute significantly to exergy losses.

The conclusions drawn from this exhaustive analysis can be summarized as follows:

- The optimization process reveals that the most favorable operational conditions for the CLC integrated BFPP consist of an oxygen carrier-to-biomass ratio of 54.43, air and fuel reactor pressures set at 11 bar, and an air reactor temperature of 1050°C.
- The strategic integration of waste heat recovery recuperators results in a remarkable 20.8% increase in the ORC turbine's output, thus enhancing overall system efficiency.
- The proposed CLC integrated BFPP, complemented by CO_2 capture, exhibits net energy and exergy efficiencies of 21.59% and 18.56%, respectively. These figures surpass the conventional BFPP by 9.61% and 8.26%, showcasing substantial enhancements.
- The intricate breakdown of unit-wise exergy analysis sheds light on the fuel reactor and the subsequent air reactor as the primary sources of exergy destruction. This observation suggests the potential for efficiency improvement through the implementation of supercritical conditions in this loop.
- On the environmental front, the assessment affirms the environmentally favorable characteristics of the CLC integrated BFPP.

The study culminates in a compelling demonstration of the capabilities of the proposed CLC integrated BFPP configuration. Its prowess extends across the domains of energy, exergy, and environmental considerations, marking a significant advancement beyond the conventional biomass-fired power plant paradigm.

Chapter 5

CLC based BFPP with hydrogen and power co-generation coupled with CO_2 utilization

Chapter 5

CLC based BFPP with hydrogen and power co-generation coupled with CO_2 utilization

The second objective of the present study is addressed in this chapter by conducting the performance evaluation of CLC-integrated biomass-fired power plant for co-generation of hydrogen and power. The overall assessment of the developed configurations is carried out on the basis of energy, exergy and environmental parameters and compared with conventional and CLC based biomass fired power plant configuration. Various sensitivity analyses such as effects of operating temperatures of the reactors, pressure and OC-flow rate on the overall performance of CLC based BFPP with hydrogen and power co-generation are also presented in this chapter. Furthermore, the utilization of the produced hydrogen and carbon dioxide for the synthesis of ammonia and methane is also explored.

5.1. Motivation and Objective

Hydrogen is extensively used in petrochemical industry for upgrading of fossil fuels and synthesis of ammonia and methanol. It is also used in semiconductor industry, cryogenic research, welding, rocket propulsion etc. It is also a potential environmentally beneficial energy source for transportation and electricity generating. The three reactor BDCL system is a very efficient option when aiming for co-production of power and hydrogen using CLC technology (Cormos, 2015). This study aims at synthesis of novel BDCL configuration by integrating three reactors CLC unit and ORC unit for power and hydrogen co-generation as mentioned in Chapter 3.

There are limited studies available CLC-based Biomass fired power plants and very few studies are available for hydrogen co-generation using these types of power plants. Most of the available studies lack detailed thermodynamic analysis and mainly focused on determining electrical efficiency. Till date, no studies were found in the literature based on the BDCL integrated with Organic Rankine Cycle configuration for power and hydrogen co-generation. Therefore, the objective of this research is to develop a novel energy efficient three reactor BDCL integrated with Organic Rankine Cycle configuration for power and hydrogen co-

generation from sugarcane bagasse biomass. The simulation methodology and key assumptions for synthesis of novel BDCL integrated with Organic Rankine Cycle configuration and formulations used for performance analysis are presented in Chapter 3. Further, sensitivity analysis is carried out to optimize the key operating parameters and maximize the energy and exergy efficiency of the configuration. Finally, performance of the proposed configuration is compared with conventional and CLC integrated biomass fired power plant configurations. Moreover, the captured hydrogen and carbon dioxide can be utilized to synthesize many valuable products such as methane, ammonia, formic acid, methanol etc. In this research, the methane and ammonia synthesis are considered as utilization product case studies.

5.2. Model description and approach

In this study, four plant configurations: 1) CLC integrated BFPP (see Chapter 4), 2) BDCL plant for H_2 and power co-production, 3) BDCL plant with Methane synthesis and 4) BDCL plant with Ammonia synthesis; are considered. The simplified block diagrams of these plants are shown in Figure 3.1, 3.2, 3.3 and 5.2, respectively. Steady state simulations and thermodynamic analyses of the above mentioned plants are performed in Aspen Plus V10. All of these plant configurations are simulated for sugarcane bagasse, whose properties are given in Table 3.2 of Chapter 3. Fe_2O_3 with 30 wt.% Al_2O_3 support is used as oxygen carrier in all cases. Operating parameters, suitable models, reference environment conditions and key assumptions considered in this study are summarised in Table 3.3 and Table 3.4 of Chapter 3.

5.2.1 Description of CLC integrated BFPP for power production

In this study, CLC integrated BFPP is considered as a reference case. The detailed analysis of the plant flowsheet can be found in Chapter 4. This plant is composed of two reactors (air and fuel reactors) which are simulated as single-stage RGibbs reactor while the plant studied in this chapter i.e. BDCL plant for H_2 and power co-production; is composed of three reactors (air, steam and fuel reactors).

5.2.2 Description of BDCL plant for H_2 and power co-production

Figure 5.1 depicts the schematic flow diagram of BDCL plant for H_2 and power co-production. The proposed BDCL process utilizes three reactors (air, steam and fuel reactors) instead of two reactors used in CLC integrated BFPP. In this case, both fuel and steam reactors are simulated as moving bed reactor (multi-stage RGibbs reactor) while air reactor is simulated as single-stage RGibbs reactor. Multi-stage RGibbs reactor is used because it helps in emulating the

moving bed conditions. The biomass is combusted in fuel reactor using the oxygen carrier (Fe_2O_3 with 30 wt.% Al_2O_3 support) where Fe_2O_3 is reduced to FeO/Fe. Then, reduced FeO/Fe is partially oxidized to Fe_3O_4/FeO using steam in steam reactor. Partially oxidized Fe_3O_4/FeO is fully oxidized to Fe_2O_3 in air reactor and sent back to fuel reactor thus forming a loop. Equations (5.1) to (5.10) shows the chemical reactions involved in all three reactors (Li et al., 2010):

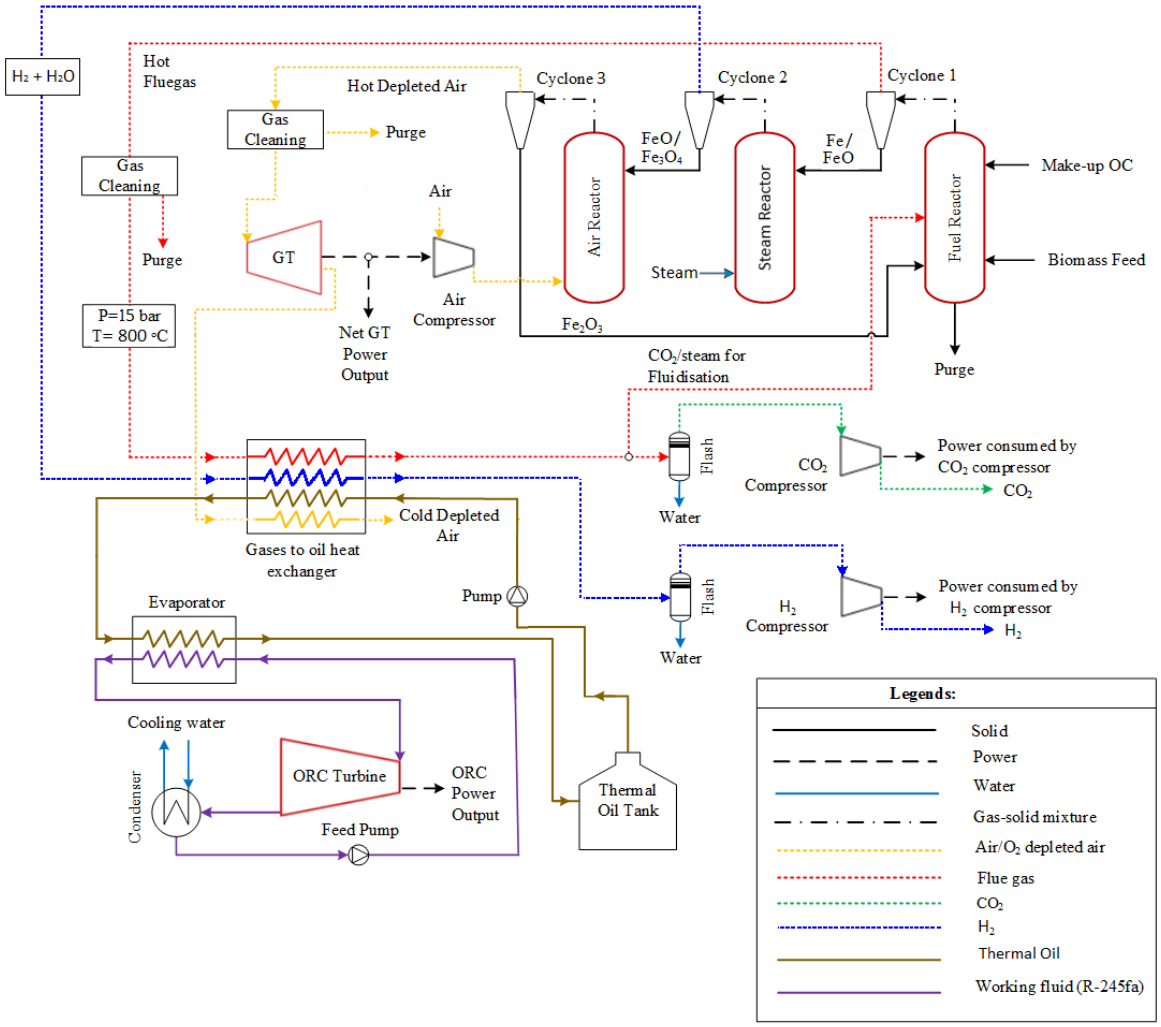

Figure 5.1. Schematic flow diagram of BDCL plant

Fuel reactor:

$$\text{Biomass} \rightarrow C + CO_2 + H_2O + CO + H_2 + CH_4 \quad (5.1)$$

$$C + CO_2 \rightarrow 2CO \quad (5.2)$$

$$C + H_2O \rightarrow CO + H_2 \quad (5.3)$$

$$CO/H_2 + Fe_2O_3 \rightarrow CO_2/H_2O + 2FeO \quad (5.4)$$

$$CO/H_2 + FeO \rightarrow CO_2/H_2O + Fe \quad (5.5)$$

$$CH_4 + 4Fe_2O_3 \rightarrow CO_2 + 2H_2O + 8FeO \quad (5.6)$$

Steam reactor:

$$Fe + H_2O \rightarrow H_2 + FeO \quad (5.7)$$

$$3FeO + H_2O \rightarrow H_2 + Fe_3O_4 \quad (5.8)$$

Air reactor:

$$4FeO + O_2 \rightarrow 2Fe_2O_3 \quad (5.9)$$

$$4Fe_3O_4 + O_2 \rightarrow 6Fe_2O_3 \quad (5.10)$$

As shown in Figure 5.1, hot gaseous streams of CO_2-rich flue gas produced from fuel reactor and H_2-rich gas produced from steam rector, are sent directly to ORC unit to extract their heat. After extracting heat from CO_2-rich flue gas and H_2-rich gas, they are sent to water separation and compression unit where pure CO_2 and H_2 gases are compressed to sequestration-ready pressures. Water separated from CO_2-rich flue gas and H_2-rich gas streams, is converted to steam using extra heat available from these two streams. This steam is recycled back to steam reactor for H_2 production.

5.2.3 Description of BDCL plant with Methane synthesis

Simplified block diagram of BDCL plant with Methane synthesis is presented in Figure 3.4. Apart from the units existed in BDCL plant, this plant has additional unit of methanation. In methanation unit, CO_2 and H_2 produced from BDCL plant are sent to methanation reactor. In the reactor, CO_2 and H_2 at 30 bar pressure and 50 °C temperature in the presence of Ni-catalyst, react to produce Methane through Sabatier reaction. Methanation reactor is simulated as single-stage RGibbs reactor where following Sabatier reaction (Eq. 5.11) takes place at 385 °C :

$$CO_2 + 4H_2 \rightarrow CH_4 + 2H_2O \ (\Delta H_{298K} = -164\ \text{kJ/mol}) \quad (5.11)$$

Sabatier reaction is exothermic which supplies the heat required to maintain high temperature in methanation reactor without any external heat source. The product stream of methane along with steam is sent to a separator to separate the steam and to produce pure methane.

5.2.4 Description of BDCL plant with Ammonia synthesis

Simplified block diagram of BDCL plant with Ammonia synthesis is presented in Figure 5.2. In addition to the units present in the BDCL plant, this process contains an extra ammonia synthesis unit. N_2 and H_2 generated by the BDCL plant are delivered to the ammonia synthesis

converter beds in the ammonia synthesis unit. The ammonia synthesis converter beds are modelled as a plug flow reactor by RPlug.

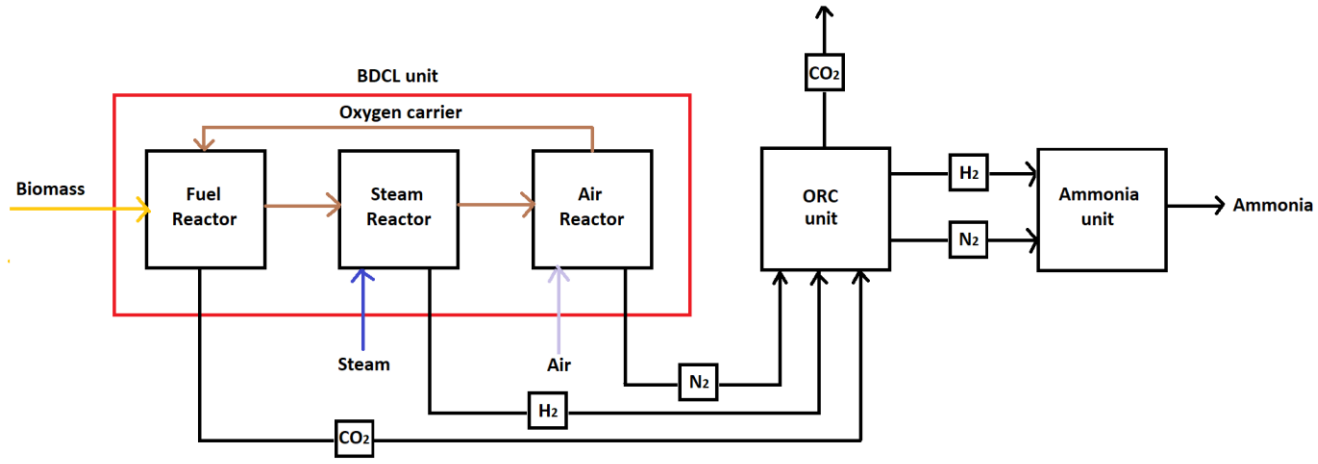

Figure 5.2. Simplified block diagram of BDCL plant with ammonia synthesis

The kinetics expression given in Equation (5.12) is used to model the reaction rate (Nielsen., 1968). The parameters A_c, k_{eq}, AK and K_a represents the catalyst activity, quilibrium constant, the specific rate constant, and the adsorption equilibrium constant respectively. The constants a_N, a_H, a_A, are the activities of nitrogen, hydrogen and ammonia. The reaction kinetics has been implemented by a user kinetics Fortran subroutine of RPlug model named SYNKIN. Subroutine SYNKIN calls RNH3, the Fortran kinetics subroutine developed by Mok (Mok, 1982). Subroutine KFORMC is used to find the component integer variables from the Aspen Plus system.

$$R = A_c \left[\frac{AK\left(a_N k_{eq}^2 - \frac{a_A^2}{a_H^3}\right)}{\left(1 + K_a \frac{a_A}{a_H^W}\right)^2 \alpha} \right] \frac{kgmole}{m^3 hr} \qquad (5.12)$$

5.3. Results and Discussion

5.3.1 Sensitivity analysis

Sensitivity study for the primary operational parameters of the BDCL plant's three reactor system for H_2 and power co-production, such as operational temperatures and operating pressure of the reactors have been carried out. This is done by adjusting one of these parameters at a time while holding the other parameters constant, evaluating the impact on the plant's overall energy and energy efficiency. For this sensitivity research, the values of the parameters given by (Surywanshi et al., 2019) are used as the base values. Also, to make the plant self-sufficient, a proper heat integration scheme is applied to the three reactor system such that

extra available heat from a reactor is distributed to other reactors and no additional heat is required from outside source. These analyses yielded the optimal values for these delicate parameters, which were then utilized in subsequent studies.

5.3.1.1. Effect of oxygen carrier flow rate

By adjusting the Oxygen Carrier mass flow rate for a fixed biomass feed flow rate of 0.139 kg/s, the impact of the OC flow rate on various performance indicators such as net energy and exergy efficiency and purity of captured CO_2 is examined. When the flow rate of OC circulating in the loop is raised, the gas turbine power output and ORC turbine power output rise. However, amount of H_2 produced decreases with increase in OC flow rate due to low conversion of Fe/FeO to FeO/Fe_3O_4. Overall, net energy and exergy efficiencies decrease continuously with increase in OC flow rate as shown in Figure 5.3. On the other hand, at lower OC flow rates, Carbon present in biomass is partially converted to CO_2 and purity of captured CO_2 is less than 100%. Nevertheless, purity of captured CO_2 is found to be almost 100% at OC flow rates more than equal to 1.6 kg/s as shown in Figure 5.3. The simulation results also confirm the stoichiometric requirement of OC flowrate as 1.6 kg/s for the given biomass flowrate of 0.139 kg/s. At this OC flow rate 100% conversion of fuels to CO_2 is achieved. Keeping that in mind, OC flow rate of 1.6 kg/s is found to be the best choice which is considered for further studies in this work.

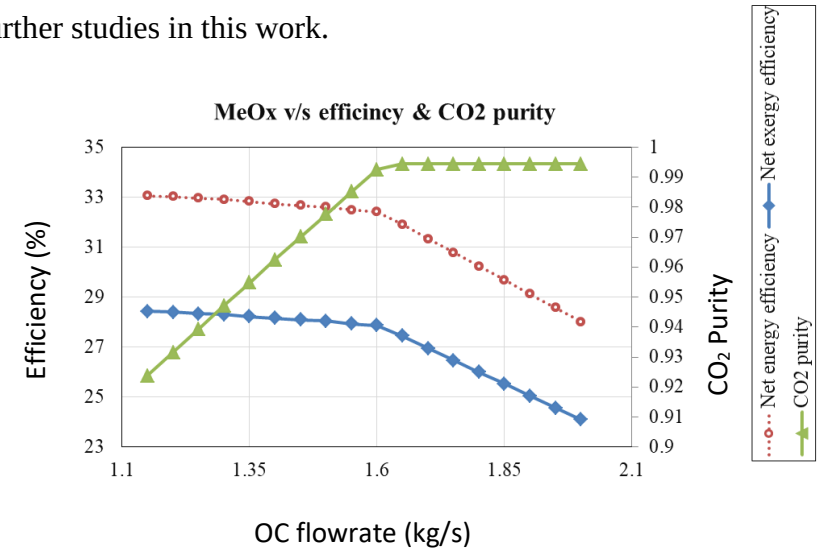

Figure 5.3. Effect of oxygen carrier flow rate on net energy and exergy efficiencies and purity of captured CO_2

5.3.1.2 Effect of operating pressure

The optimal oxygen carrier flow rate determined above is updated, and the impact of BDCL reactors operating pressure is assessed. In the BDCL process, metal oxides partially oxidize to Fe_3O_4/FeO in the steam reactor using steam, and ultimately completes its cycle by converting

to Fe_2O_3 in the air reactor, in the presence of air. This partial oxidation in the steam reactor reduces the amount of air needed, thereby lowering the power required by the air compressor. Unlike in the two-reactor CLC system, the power required by the air compressor does not dominate the overall efficiency. Consequently, as the pressure increases up to 15 bar, the efficiency increases exponentially. The operating temperatures of the air, steam, and fuel reactors are fixed at 1000 °C, 750 °C, and 900 °C, respectively, as described in (Surywanshi et al., 2019), to evaluate the impact of operating pressure of the three reactors system on the H_2 and power co-production plant efficiency. Figure 5.4 depicts the effect of changing the BDCL operating pressure from 1.013 bar to 40 bar on net energy and exergy efficiencies.

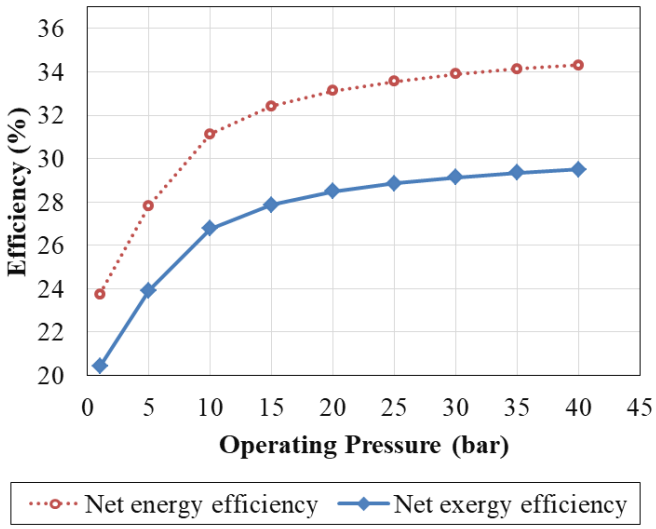

Figure 5.4. Effect of operating pressure on net energy and exergy efficiencies.

Both efficiencies are found to be lowest at 1.013 bar and increased with increase in operating pressure. The improvement in these efficiencies is very limited above 15 bar pressure, as seen by the minor change in the efficiencies. It happens because although gas turbine power production increases as the operating pressure increases but ORC turbine power production decreases. Similar trends were observed for CLC integrated BFPP with power generation only in our previous study (Sikarwar et al., 2020). As a result, operating air, steam, and fuel reactors over 15 bar pressure is not very energy efficient.

5.3.1.3 Effect of operating temperatures of the reactors

The effect of air, steam and fuel reactor temperature on plant performance is investigated at optimal oxygen carrier flow rate and BDCL operating pressure as determined by the preceding analysis. The operational temperatures of three reactors are investigated separately by altering one reactor temperature while maintaining the temperatures of the other two reactors constant.

The impact of air reactor temperature is investigated for constant fuel reactor and steam reactor temperatures of 900 °C and 750 °C, respectively. The effect of air reactor operating temperature on net energy and exergy efficiencies is shown in Figure 5.5.

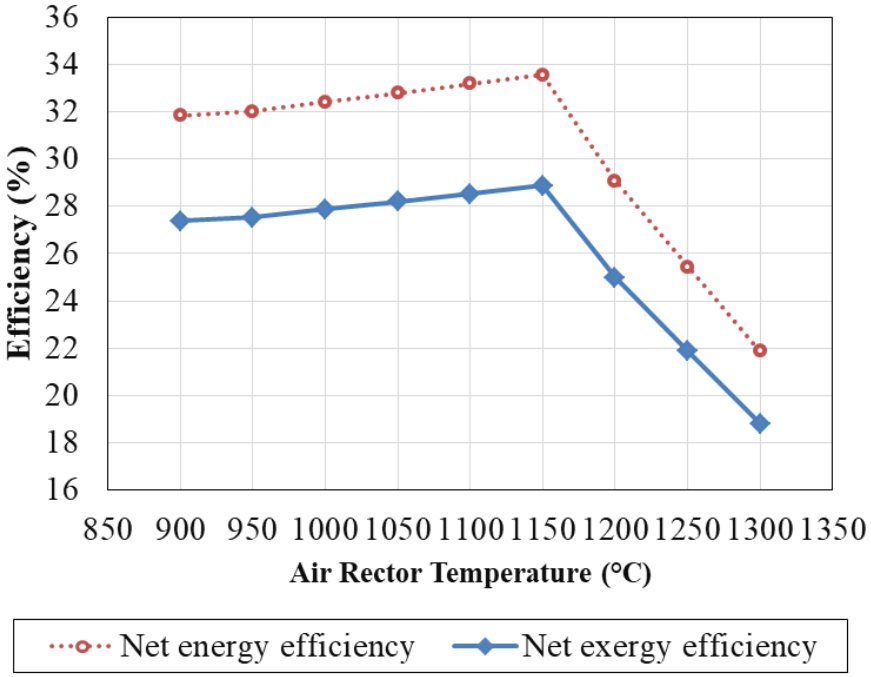

Figure 5.5. Effect of air reactor temperature on net energy and exergy efficiencies.

At lower temperatures, the air reactor is an exothermic reactor that produces some extra heat. The highest energy and exergy efficiency are observed when the reactor temperature reaches 1150 °C, however beyond this more heat is necessary to maintain the temperature which can not be supplied from steam and fuel reactors due to their lower operating temperature. As a result, the maximum net energy and exergy efficiencies are recorded at 1150 °C.

To investigate the impact of steam reactor temperature on the plant performance, the optimal value of air reactor temperature of 1150 °C and fuel reactor temperature of 900 °C are used. The effect of steam reactor temperature on net energy and exergy efficiencies is depicted in Figure 5.6. Since the reactions in steam reactor are endothermic, more amount of heat need to be supplied from air and fuel reactors to maintain its temperature. Further, to maintain the different operating temperatures in these reactors the flow rates of fluidizing mediums are also needs to be adjusted simultaneously as follows: (i) air flow rate to the air reactor, (ii) steam flow rate to the steam reactor, and (iii) CO_2 flow rate to the fuel reactor. The impact of air flow rate on the reactor temperature is discussed in detail in Section 4.3.1.3. On the other hand, decreasing the temperatures below 750 °C results in low hydrogen production. As a result, maximum net energy and exergy efficiencies are found at 750 °C. as shown in Figure 5.6.

To investigate the impact of fuel reactor temperature on the performance of the BDCL plant, the optimal values of both air and steam reactor temperatures, 1150 °C and 750 °C, are used. Figure 5.7 depicts the impact of fuel reactor temperature on net energy and exergy efficiency. The net energy and exergy efficiencies are observed to increase when the fuel reactor temperature rises up to 800 °C. After this, more amount of heat needs to be supplied from air reactor to maintain its temperature which caused decrease in efficiencies. However, lowering the temperatures below 800 °C resulted in poor hydrogen generation. Hence, maximum net energy and exergy efficiencies are found at 800 °C. as shown in Figure 5.7.

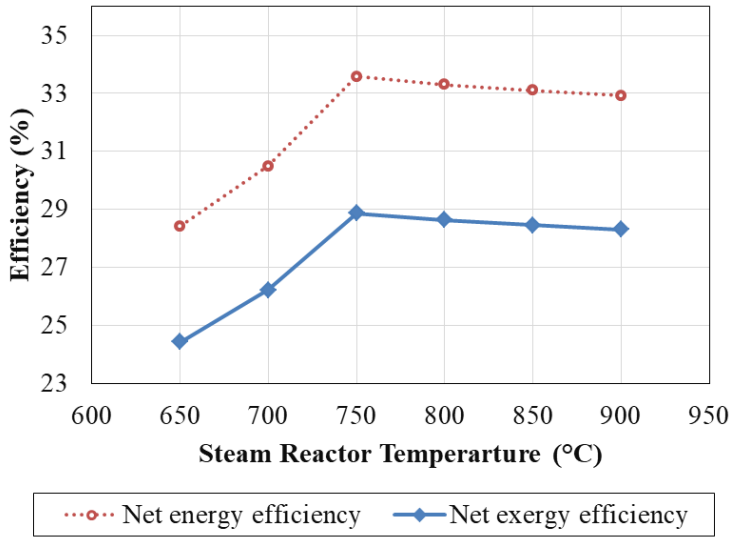

Figure 5.6. Effect of steam reactor temperature on net energy and exergy efficiencies.

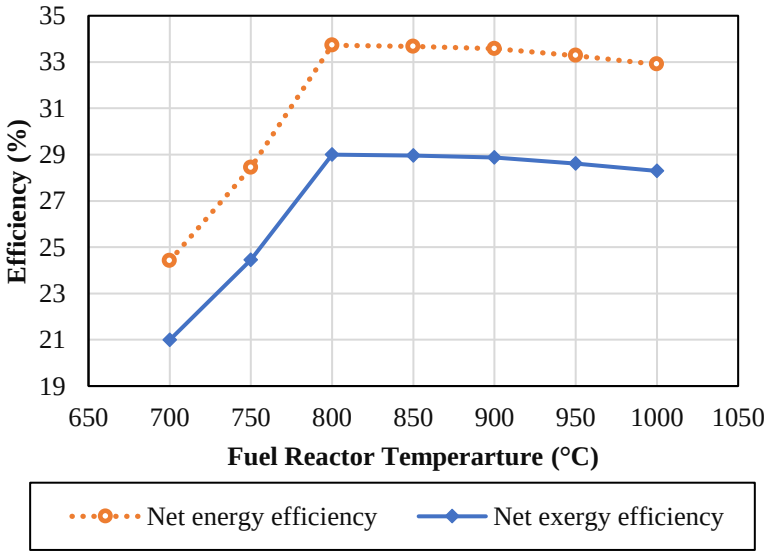

Figure 5.7. Effect of fuel reactor temperature on net energy and exergy efficiencies.

The optimal conditions for operating BDCL found from the sensitivity analysis are: Oxygen carrier flow rate: 1.6 kg/s, operating pressure of air, steam and fuel reactors: 15 bar, air reactor operating temperature: 1150 °C, steam reactor operating temperature: 750 °C and fuel reactor operating temperature: 800 °C. Table 5.1 shows the step-by-step improvement in process efficiency achieved by the aforementioned sensitivity analysis. As a result, these conditions were used in the subsequent studies, as shown below.

Table 5.1: Step by step improvement of net energy and exergy efficiencies from sensitivity analysis.

Case	Optimal Value	Net energy efficiency (%)	Net exergy efficiency (%)
Oxygen carrier (OC) flow rate (kg/s)	1.6	32.41	27.87
Air, steam and fuel reactor operating pressure (bar)	15	32.41	27.87
Air reactor operating temperature (^{o}C)	1150	33.58	28.87
Steam reactor operating temperature (^{o}C)	750	33.58	28.87
Fuel reactor operating temperature (^{o}C)	800	33.72	29.00

Subsequently, the performance of BDCL plant has been compared with conventional and CLC integrated BFPP configurations. From the results presented in Table 5.2, it is observed that the proposed BDCL plant has high energy and exergy efficiencies.

In the following sections, the use of CO_2, N_2 and H_2 from the BDCL power plant to create various chemical compounds is being investigated.

5.3.2 BDCL plant with Methane and ammonia synthesis

The use of all of the hydrogen generated by the BDCL plant results in electrical energy loss during methane and ammonia synthesis as shown in Table 5.3.

Table 5.2: Performance comparison based on energy and exergy efficiencies.

Case	Net overall energy efficiency (%)	Net overall exergy efficiency (%)
Conventional-BFPP	11.98	10.30
CLC integrated BFPP	21.59	18.56
BDCL plant	33.72	28.99

Table 5.3: Energy and exergy efficiencies with CO_2 and H_2 utilization

Case	Production rate (kg/hr)	Net energy efficiency (electrical) (%)	Net exergy efficiency (electrical) (%)	Net energy efficiency (overall) (%)	Net exergy efficiency (overall) (%)
Methane	62.08	13.65	11.74	55.63	47.84
Ammonia	181.9	1.84	1.58	51.70	44.46

The aforementioned BDCL plant produces 62.08 kg/hr of methane, with net overall energy and exergy efficiencies of 13.65% and 11.74%, respectively. The BDCL plant with methane synthesis has the same gas and ORC turbine power outputs as that of BDCL plant. The reason behind this is that there are no auxiliary units which require energy. For methane production, the stoichiometric ratio of H_2 to CO_2 is 4:1. As a result, the methane synthesis plant consumes 21% of the CO_2 and 100% of the H_2 generated by the BDCL plant.

When all of the hydrogen produced by the BDCL plant is used, energy is lost during ammonia synthesis. The BDCL plant indicated above generates 181.9 kg/hr of ammonia with net energy and exergy efficiencies of 1.84% and 1.58%, respectively. This is because gas turbine is removed and power output is coming from only ORC. To use high pressure N_2-rich depleted air stream in ammonia synthesis reactor, gas turbine is removed. For ammonia synthesis, the stoichiometric ratio of H_2 to N_2 is 3:1. As a consequence, the methane synthesis plant utilizes 18% of the N_2 and 100% of the H_2 produced by the BDCL plant.

5.3.3. Environmental analysis

The purpose of CLC technology is to reduce carbon dioxide emissions. The performance of the three plants (conventional BFPP, CLC based BFPP and CLC based BFPP with hydrogen and power co-generation) is evaluated in terms of CO_2 emissions and CO_2 captured. The environmental assessment is performed in terms of environmental parameters given in Table 5.4. For 7008 annual plant operation hours, both CLC based BFPP and CLC based BFPP with hydrogen and power co-generation avoid an annual CO_2 emissions of 5.71×10^6 kg by capturing nearly all the CO_2 generated from the plants. However, net power output per unit CO_2 captured is found to be higher for the co-generation plant due to its high power output.

Table 5.4. Environmental assessment of the three plants.

Parameter	Unit	Conventional BFPP	CLC based BFPP	CLC based BFPP with hydrogen and power co-generation
CO_2 emission	g/s	226.10	0.00	0.00
CO_2 captured	g/s	0.00	225.56	225.56
CO_2 capture efficiency	wt. %	0.00	100.00	100.00
Specific CO_2 emission	g/kWh	2980.68	0.00	0.00
Annual CO_2 emission	Kg	5.71×10^6	0.00	0.00
Average annual emission rate aggravating per unit of fuel	$g.CO_2/GJ$	139.00	0.00	0.00
Annual CO_2 avoided emission per unit fuel	$g.CO_2/GJ$	0.00	138.6	138.6
Net power output per unit CO_2 captured	kW/g	-	1.97	3.41

5.4. Summary

In this chapter, a new configuration of chemical looping combustion based biomass-fired power plant for power and hydrogen co-generation using sugarcane bagasse biomass and iron based oxygen carrier has been proposed. CLC based BFPP for power and hydrogen co-generation was simulated with the optimal parameters and the performance was compared against conventional BFPP and CLC based BFPP in terms of energy & exergy efficiency and environmental impacts. Following are the key observations from the study:

- The optimal conditions for operating the co-generation plant from the sensitivity analysis are: oxygen carrier flow rate of 1.6 kg/s, operating pressure of air, steam and fuel reactors of 15 bar, air reactor operating temperature of 1150 ^{o}C, steam reactor operating temperature of 750 ^{o}C and fuel reactor operating temperature of 800 ^{o}C.
- The net energy and exergy efficiencies of the co-generation plant are found to be 33.72% and 28.99%, respectively. These efficiencies are greater by 12.13% and 10.43% compared to CLC based BFPP.
- While utilizing all of the produced hydrogen for synthesis of other useful products, the co-generation plant produces 62.08 kg/hr of methane and 181.9 kg/hr of ammonia, with net overall energy efficiencies of 13.65% and 1.84%, respectively.
- CLC based BFPPs are more environment friendly than conventional BFPP. The study also demonstrated that the proposed co-generation plant configuration is energetically, exergetically and environmentally efficient.

Chapter 6

CLC based biomass fired power plant with different oxygen carriers

Chapter 6

CLC based biomass fired power plant with different oxygen carriers

The third objective of the present study is addressed in this chapter by conducting the performance evaluation and comparison of CLC based biomass fired power plants with different oxygen carriers. The overall performances of these configurations are examined based on the energy and exergy analyses. Various sensitivity analyses such as effects of operating temperature, pressure and OC-to-biomass ratio on the overall performances of these CLC based BFPPs are also presented in this chapter. The thermodynamic performance of the different oxygen carriers along with environmental and economical parameters are considered while deriving the conclusions.

6.1. Motivation and Objective

The study presented in Chapter 4 demonstrates that the CLC based BFPP configuration is energetically, exergetically and environmentally efficient compared to the conventional BFPP. Therefore, CLC based BFPP is being subjected to further exploration in this chapter. As mentioned in Chapter 2, CLC operations have been conducted using wide range of oxygen carriers. Performance of oxygen carrier was found to be an important factor for an efficient CLC operation. Most often used oxygen carriers are: 1) Fe-based, 2) Ni-based, 3) Cu-based, 4) Co-based and 5) Mn-based (Lyngfelt et al., 2019). Given India's substantial iron ore production (as reported by the U.S. Geological Survey in 2017), Fe_2O_3 is considered to be the main oxygen carrier in this study. Apart from Fe_2O_3, NiO is considered which shows high reactivity and CO_2 capture efficiency but it is expensive and toxic in nature and hazardous to the environment. Next, Co_3O_4 is considered which is even more toxic and costlier than NiO, but it exhibits CLOU properties which enhances the reactivity of oxygen carrier with the fuel. At last, CuO is considered which has significant advantages over Fe_2O_3 such as higher reactivity, exothermic reaction in fuel reactor and CLOU properties. It could be a better option than NiO and Co_3O_4 due to its non-toxic nature and lower cost. However, CuO is expensive than Fe_2O_3 and will still be a major hurdle from economic point of view. Therefore, mixing a

small fraction of CuO with Fe_2O_3 can potentially enhance reactivity of the oxygen carrier without considerably inflating overall operational costs.

In this study, the following tasks are completed:

1. Development of CLC based BFPP configurations using different oxygen carriers.
2. Sensitivity analysis to optimize operational parameters such as operating temperature, pressure and OC-to-biomass ratio for each case.
3. Comparative analysis of these cases based on the energy and exergy analyses.

The findings of this study would be useful in understanding the potential viability of CLC based BFPP employing different oxygen carriers that provide relatively adequate plant performance.

6.2. Model description and approach

CLC based BFPP considered in this chapter are simulated with the assumptions and performance evaluation given in Chapter 3. The shematic diagram of the CLC based BFPP integrated with ORC cycle is shown in Figure 4.1. In addition to Fe_2O_3, four more oxygen carriers – NiO, Co_3O_4, CuO and mixture of 10% CuO in Fe_2O_3 are used. Equations (4.1) to (4.5) show the general redox reactions associated with Fe_2O_3 oxygen carriers. The following equations (6.1) to (6.5) represent the probable redox reactions of biomass with NiO in the fuel reactor and air reactor.

$C + H_2O \rightarrow CO + H_2$ ΔH = 131.3 kJ/mol at 298 °C and 1 atm (6.1)

$C + CO_2 \rightarrow 2CO$ ΔH = 172.5 kJ/mol at 298 °C and 1 atm (6.2)

$CO + NiO \rightarrow Ni + CO_2$ ΔH = -47.2 kJ/mol at 1000 °C and 1 atm (6.3)

$H_2 + NiO \rightarrow Ni + H_2O$ ΔH = -15 kJ/mol at 1000 °C and 1 atm (6.4)

$Ni + {}^1/_2\, O_2 \rightarrow NiO$ ΔH = -234.2 kJ/mol at 1000K and 1 atm (6.5)

For Co_3O_4, the following equations represent the probable redox reactions of biomass with Co O_4 in the fuel reactor (Equations (6.1), (6.2), (6.6) and (6.7)) and air reactor (Equation (6.8)).

$CO + Co_3O_4 \rightarrow 3CoO + CO_2$ ΔH = -88.2 kJ/mol at 1000 °C and 1 atm (6.6)

$H_2 + Co_3O_4 \rightarrow 3CoO + H_2O$ ΔH = -56 kJ/mol at 1000 °C and 1 atm (6.7)

$3CoO + {}^1/_2\, O_2 \rightarrow Co_3O_4$ ΔH = -297 kJ/mol at 298 K and 1 atm (6.8)

For CuO, the following equations represent the probable redox reactions of biomass with CuO in the fuel reactor (Equations (6.9) and (6.10)) and air reactor (Equation (6.11)).

$4CuO + C \rightarrow 2Cu_2O + CO_2$ ΔH = -135.1 kJ/mol at 1000 °C and 1 atm (6.9)

$C + O_2 \rightarrow CO_2$ ΔH = -395.1 kJ/mol at 1000 K and 1 atm (6.10)

$2Cu_2O + O_2 \rightarrow 4CuO$ ΔH = -292 kJ/mol at 298 K and 1 atm (6.11)

6.3. Results and Discussion

As mentioned in Chapter 4, CLC based BFPP for constant biomass flow rate of 0.139 kg/s under steady state with the operating pressure of 10 atm and air reactor temperature of 1000 °C is considered as base case for further analysis.

6.3.1. Sensitivity Analysis for CLC based BFPP using NiO

The sensitivity analysis in this section is carried out by varying one parameter while keeping other parameters constant. The influence of various essential process parameters such as oxygen carrier to biomass ratio, operating pressure, and air reactor operating temperature on the performance of the plant is investigated.

6.3.1.1. Effect of oxygen carrier to biomass ratio

By altering the oxygen carrier mass flow rate, the influence of oxygen carrier to biomass ratio on several performance indicators such as net power consumption and generation, air feed flow rate, and overall energy and exergy efficiency is investigated. Figures 6.1 and 6.2 show the findings of the sensitivity analysis. As the oxygen carrier to biomass ratio increases, so does the biomass combustion rate and power outputs, as seen in Figure 6.1. This is due to increased flow rate of flue gas from fuel reactor. Also, amount of air required to re-oxidize the reduced metal oxides increases. With an increase in the oxygen carrier to biomass ratio, the aforementioned parameters resulted in an improvement in gas and ORC turbine power outputs, as well as energy and exergy efficiency. This rise is observed up to an OC/biomass ratio of 9.07 with the net energy and exergy efficiencies of 23.29% and 20.03%. The complete combustion of biomass is observed at this oxygen carrier to biomass ratio. Further increasing the oxygen carrier to biomass ratio leads in the wasteful circulation of non-reduced oxygen carrier in the CLC loop, which has a detrimental impact on the plant's overall performance.

6.3.1.2. Effect of Air and Fuel Reactors Operating Pressure

The ideal oxygen carrier to biomass ratio determined by the preceding study is updated, and the impact of CLC reactors operating pressure is assessed. Figure 6.3 depicts the effect of changing the loop operating pressure from 1 bar to 20 bar on overall process power consumption and generation. The net gas turbine power output increases with pressure from 1 bar to 11 bar, and at 11 bar pressure, the net gas turbine power output is 345.27 kW. The net turbine power output falls after 11 bar as pressure increases due to higher power consumption by the air compressor under the given operating conditions. Furthermore, the process energy

and exergy efficiencies are investigated at various CLC working pressures, with the highest efficiencies obtained at 12 bar pressure, as presented in Figure 6.4.

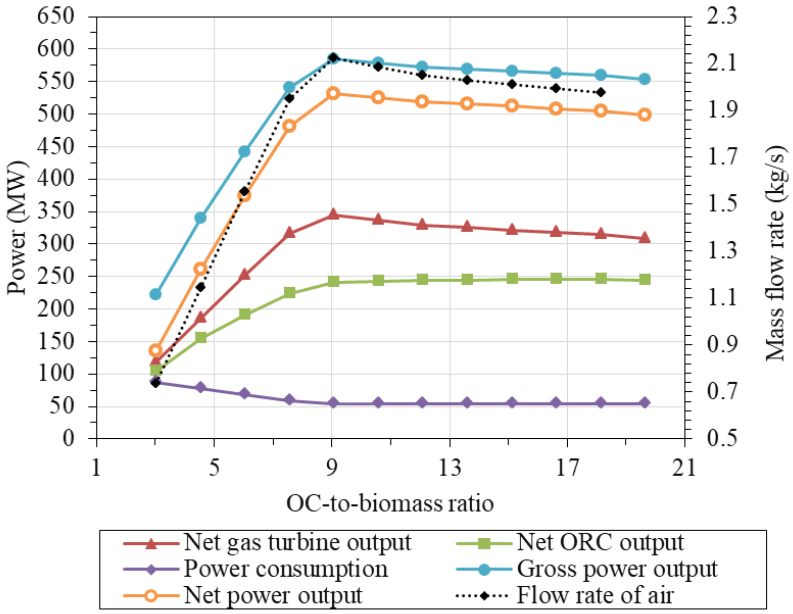

Figure 6.1. Effect of OC-to-biomass ratio on power consumption and generation for NiO

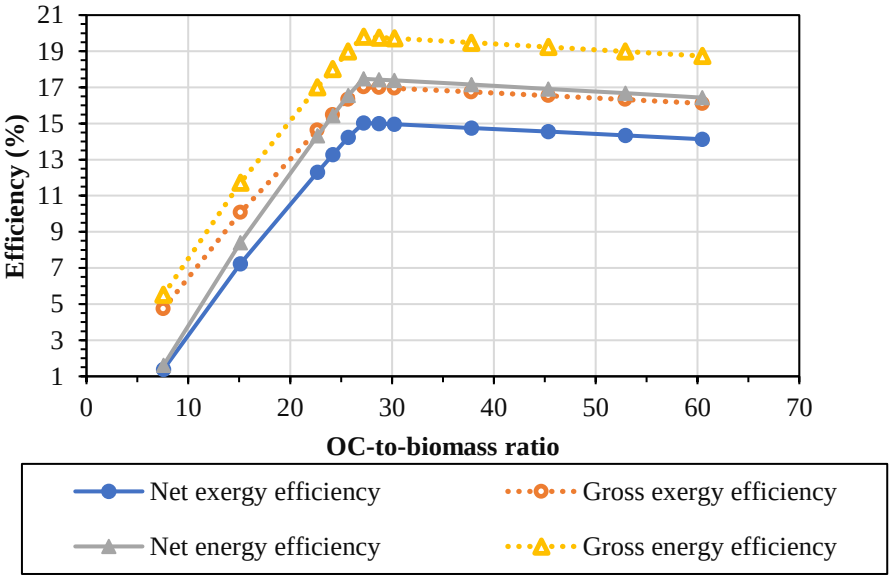

Figure 6.2. Effect of OC-to-biomass ratio on energy and exergy efficiency for NiO

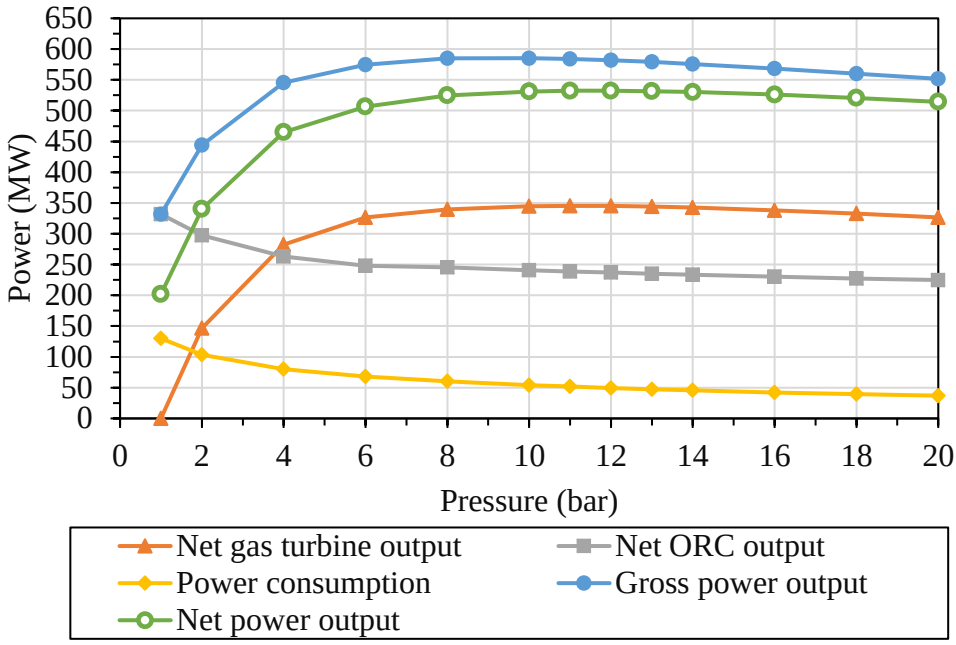

Figure 6.3. Effect of reactors operating pressure on power consumption and generation for NiO

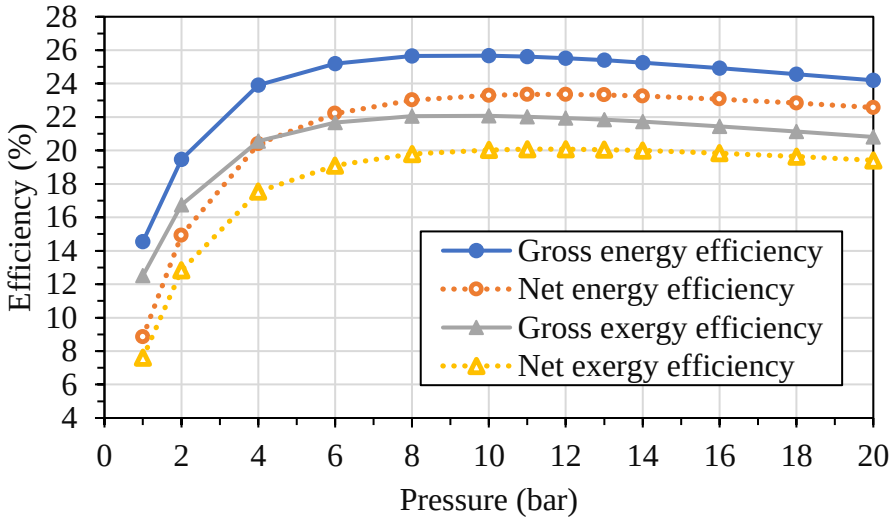

Figure 6.4. Effect of reactors operating pressure on overall energy and exergy efficiency for NiO

6.3.1.3. Effect of Air Reactor Operating Temperature

The influence of air reactor temperature on plant performance is investigated at optimal oxygen carrier to biomass ratio and CLC operating pressure determined by the preceding analysis. Figure 6.5 depicts the influence of air reactor operating temperature on air flow rate, power consumption, and generation. The net gas turbine power production increases with increasing air reactor temperature up to 1100 °C, then decreases with increasing air reactor temperature. This maximum is evident because the rate of decrease in power consumption by the air compressor is greater than the rate of decrease in gas turbine power output until 1100 °C. The

net gas turbine power production diminishes when the air reactor temperature rises over this point. Figure 6.6 depicts the influence of air reactor temperature on energy and exergy efficiency.

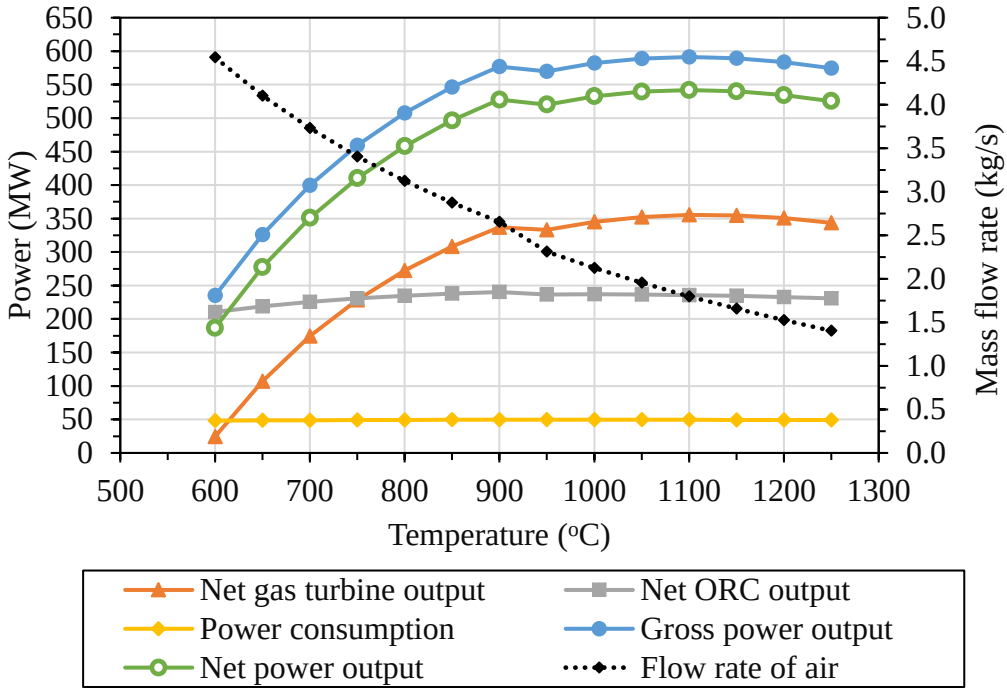

Figure 6.5. Effect of air reactor temperature on power consumption and generation for NiO

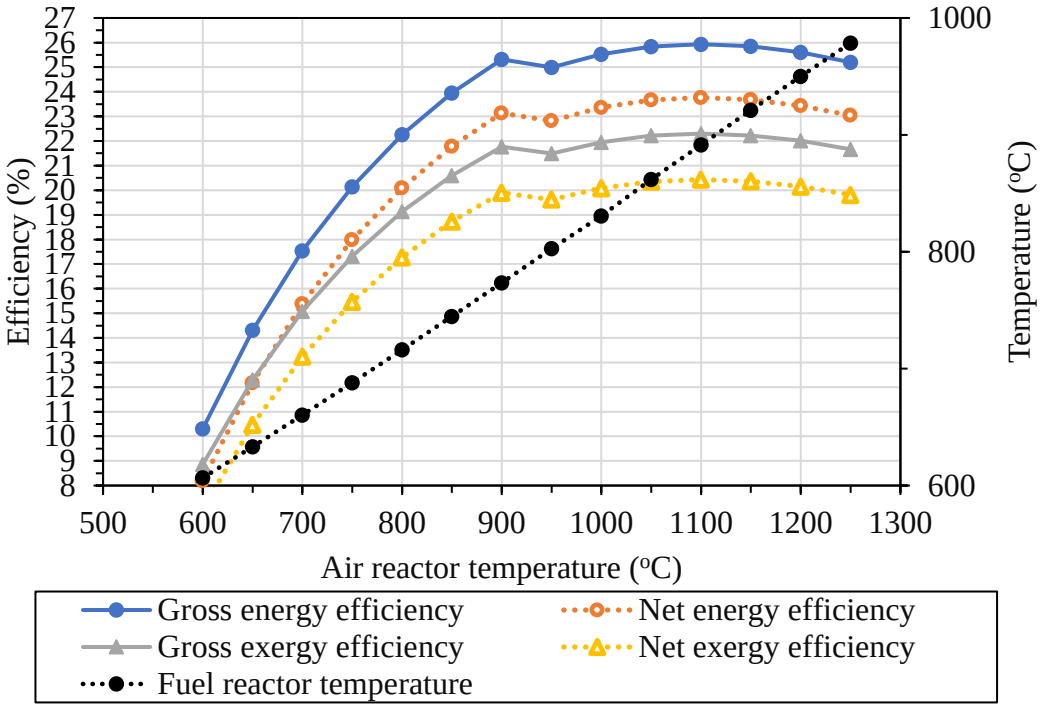

Figure 6.6. Effect of air reactor temperature on energy and exergy efficiency for NiO

Table 6.1 shows the step-by-step improvement in process efficiency achieved by the sensitivity analysis described above.

Table 6.1. Step by step improvement of the process efficiencies from sensitivity analysis for NiO

Case	Optimal Value	Net turbine work output (kW)	Net ORC work output (kW)	Net overall energy efficiency (%)	Net overall exergy efficiency (%)
Oxygen carrier (OC) to biomass ratio	9.07	344.58	240.69	23.29	20.03
Air and fuel reactor operating pressure (bar)	12	345.01	236.88	23.35	20.08
Air reactor operating temperature (^{o}C)	1100	355.52	235.76	23.77	20.44

6.3.2. Sensitivity Analysis for CLC based BFPP using Co_3O_4

Similar to preceding analysis, the sensitivity analysis is performed here by altering one parameter while holding the other values constant. The impact of key process factors such as oxygen carrier to biomass ratio, operating pressure, and air reactor operating temperature on plant performance is explored.

6.3.2.1. Effect of oxygen carrier to biomass ratio

Similar to NiO, as the oxygen carrier to biomass ratio increases, so does the biomass combustion rate and power outputs which can be seen in Figure 6.7. This rise is observed up to an OC/biomass ratio of 27.22 with the net energy and exergy efficiencies of 17.75% and 15.37%. Increasing the oxygen carrier to biomass ratio above this point causes the CLC loop to wastefully circulate non-reduced oxygen carrier, which has a negative influence on the plant's overall performance.

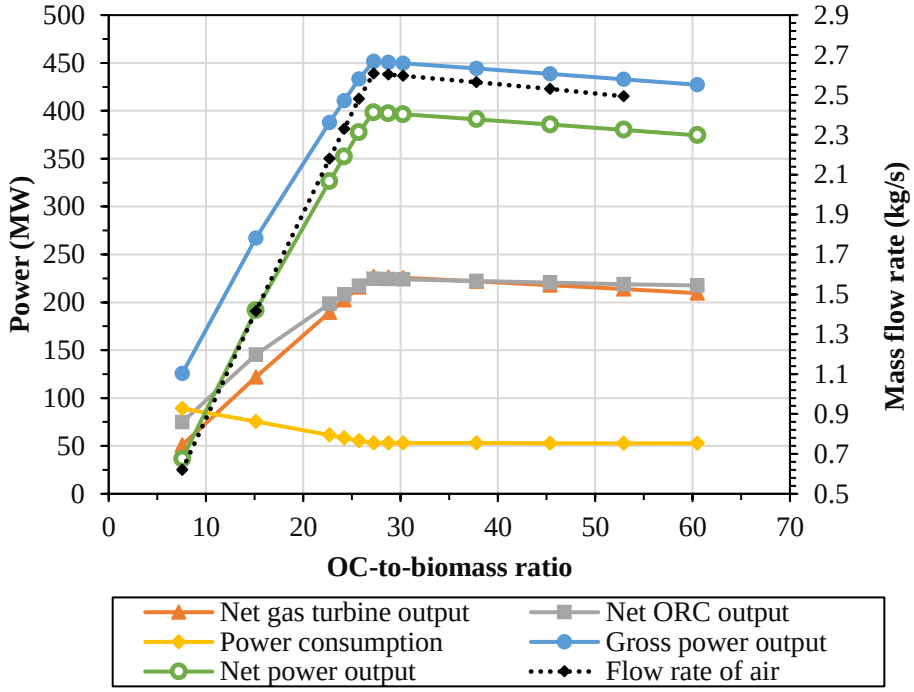

Figure 6.7. Effect of OC-to-biomass ratio on power consumption and generation for Co_3O_4

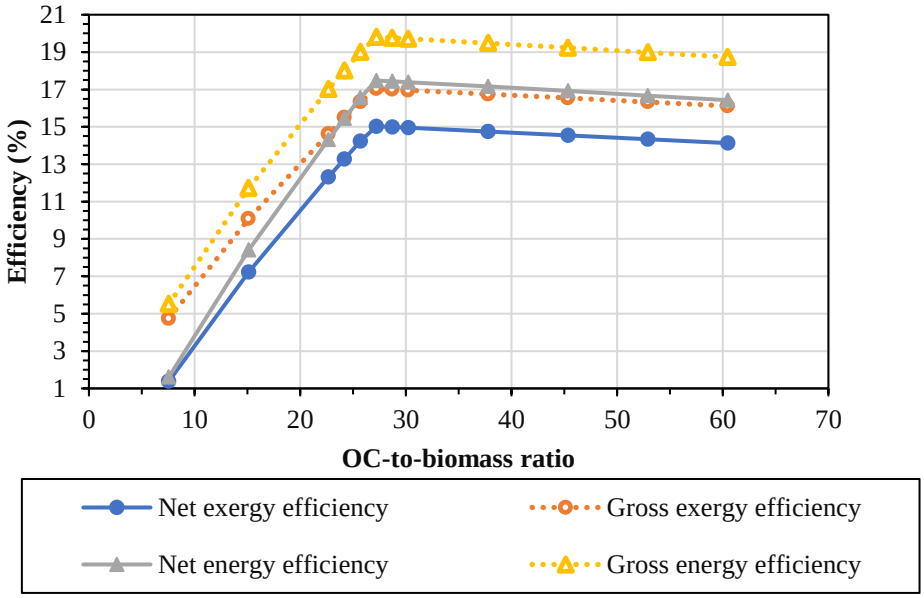

Figure 6.8. Effect of OC-to-biomass ratio on energy and exergy efficiency for Co_3O_4

6.3.2.2. Effect of Air and Fuel Reactors Operating Pressure

Figure 6.9 depicts the effect of changing the loop operating pressure from 1 bar to 20 bar on overall process power consumption and generation. From 1 bar to 6 bar pressure, the net gas turbine power output rises, and at 6 bar pressure, the net gas turbine power output is 239.88 kW. Under the stated operating circumstances, the net turbine power output decreases after 6 bar as pressure rises due to increased power consumption by the air compressor. Furthermore,

the process energy and exergy efficiencies at various CLC operating pressures are examined, with the maximum efficiencies obtained at 7 bar pressure, as shown in Figure 6.10.

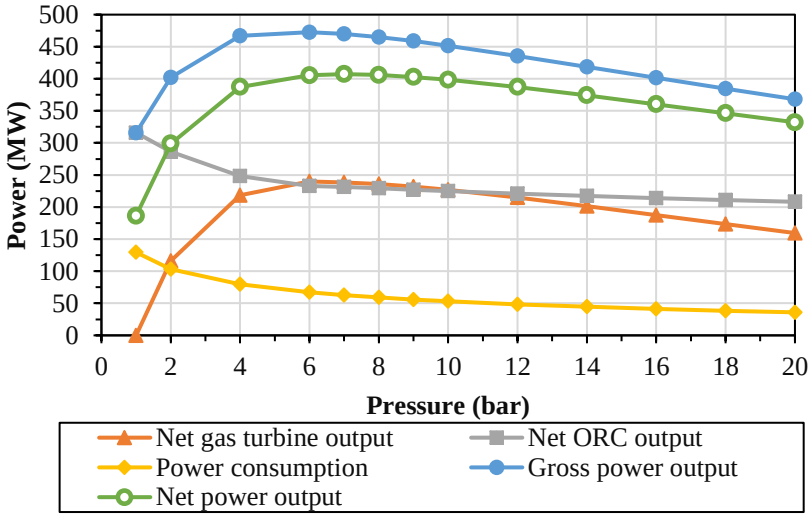

Figure 6.9. Effect of air and fuel reactor operating pressure on power consumption and generation for Co_3O_4

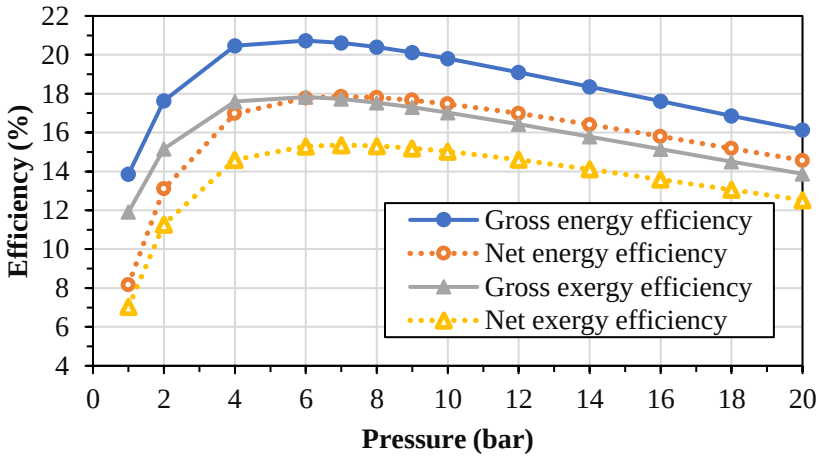

Figure 6.10. Effect of air and fuel reactors operating pressure on overall energy and exergy efficiency for Co_3O_4

6.3.2.3. Effect of Air Reactor Operating Temperature

The effect of air reactor operating temperature on air flow rate, power consumption, and generation is depicted in Figure 6.11. The net gas turbine power generation grows with rising air reactor temperature until it reaches 750 °C, then drops. This maximum is visible because the rate of decline in air compressor power consumption is faster than the rate of decrease in gas turbine power output till 750 °C. When the air reactor temperature exceeds this level, the net gas turbine power generation decreases. The effect of air reactor temperature on energy and exergy efficiency is depicted in Figure 6.12.

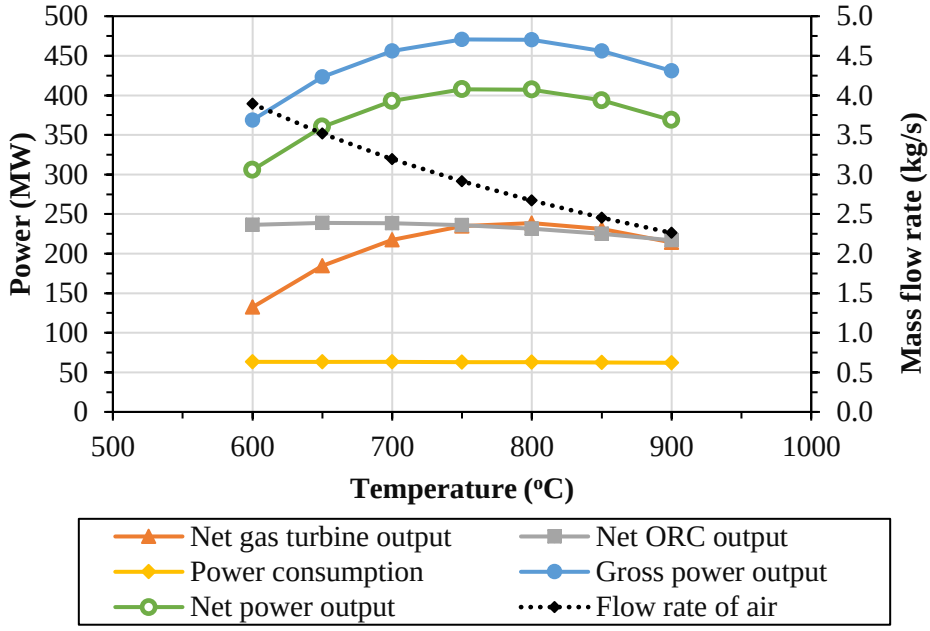

Figure 6.11. Effect of air reactor temperature on power consumption and generation for Co_3O_4

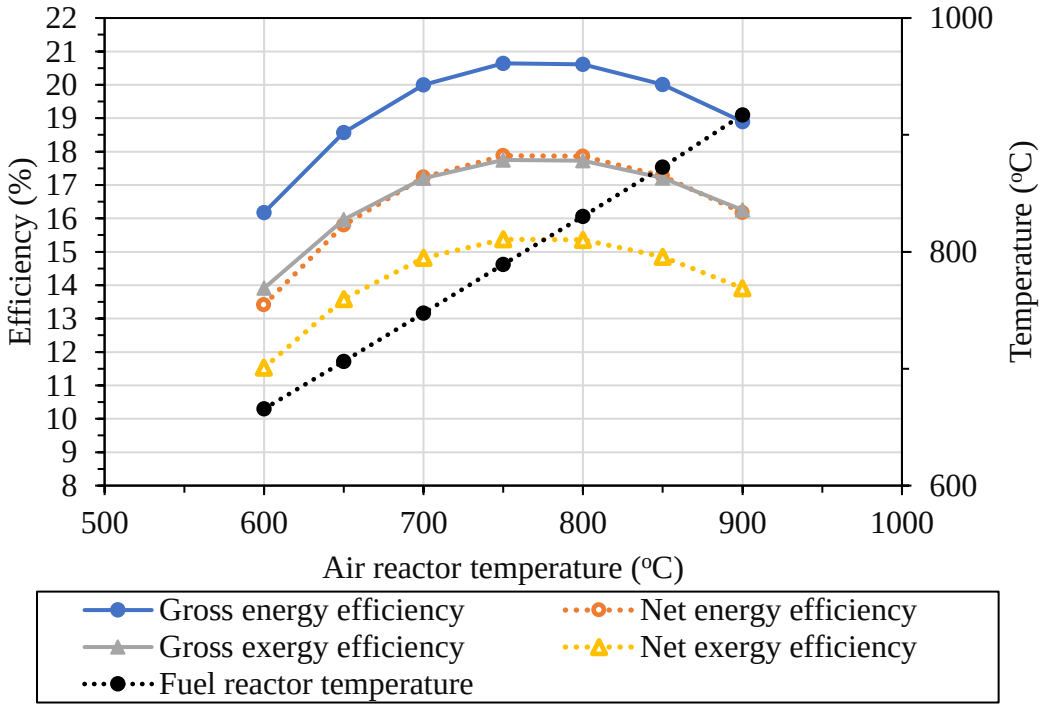

Figure 6.12. Effect of air reactor temperature on energy and exergy efficiency for Co_3O_4

The step by step improvement in process efficiency by the above sensitivity analysis has been presented in Table 6.2.

Table 6.2. Step by step improvement of the process efficiencies from sensitivity analysis for Co_3O_4

Case	Optimal Value	Net turbine work output (kW)	Net ORC work output (kW)	Net overall energy efficiency (%)	Net overall exergy efficiency (%)
Oxygen carrier (OC) to biomass ratio	27.22	226.81	224.74	17.48	15.03
Air and fuel reactor operating pressure (bar)	7	238.59	231.43	17.86	15.36
Air reactor operating temperature (°C)	750	234.69	235.98	17.88	15.37

6.3.3. Sensitivity Analysis for CLC based BFPP using CuO

6.3.3.1. Effect of oxygen carrier to biomass ratio

Similar to the previous cases, as the oxygen carrier to biomass ratio increases, so does the biomass combustion rate and power outputs which can be seen in Figure 6.13. This rise is observed up to an OC/biomass ratio of 19.66 with the net energy and exergy efficiencies of 20.80% and 17.88% as sown in Figure 6.14.

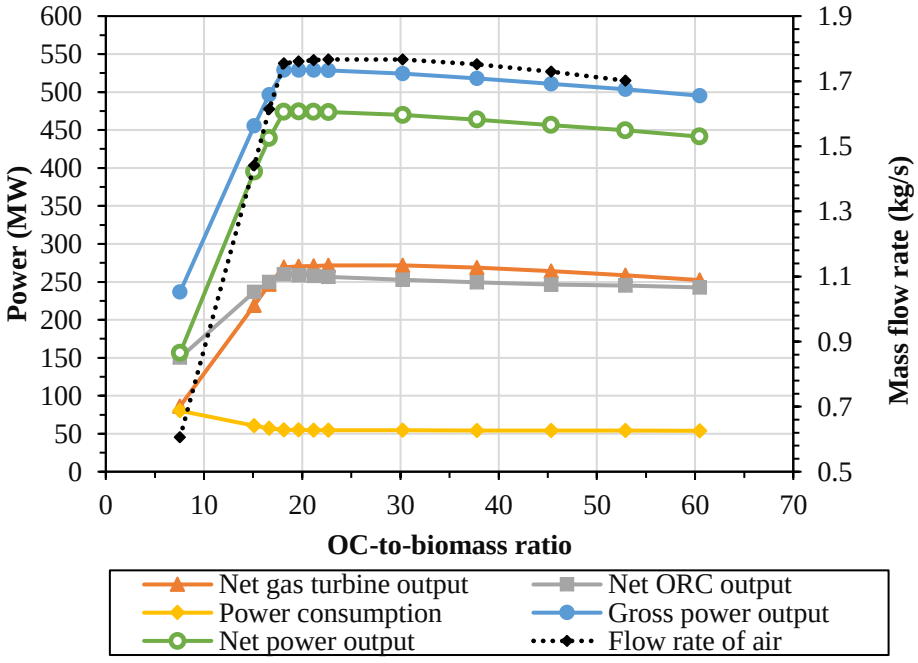

Figure 6.13. Effect of OC-to-biomass ratio on power consumption and generation for CuO

6.3.3.2. Effect of Air and Fuel Reactors Operating Pressure

Figure 6.15 depicts the effect of changing the loop operating pressure from 1 bar to 20 bar on overall process power consumption and generation. Furthermore, the process energy and exergy efficiencies at various CLC operating pressures are examined, with the maximum efficiencies obtained at 12 bar pressure, as shown in Figure 6.16.

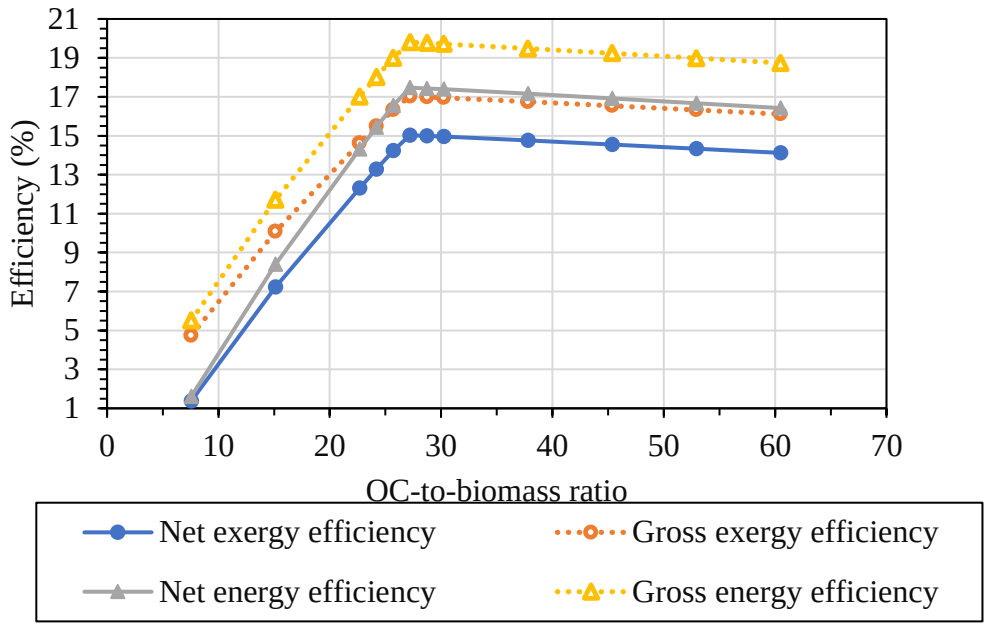

Figure 6.14. Effect of OC-to-biomass ratio on energy and exergy efficiency for CuO

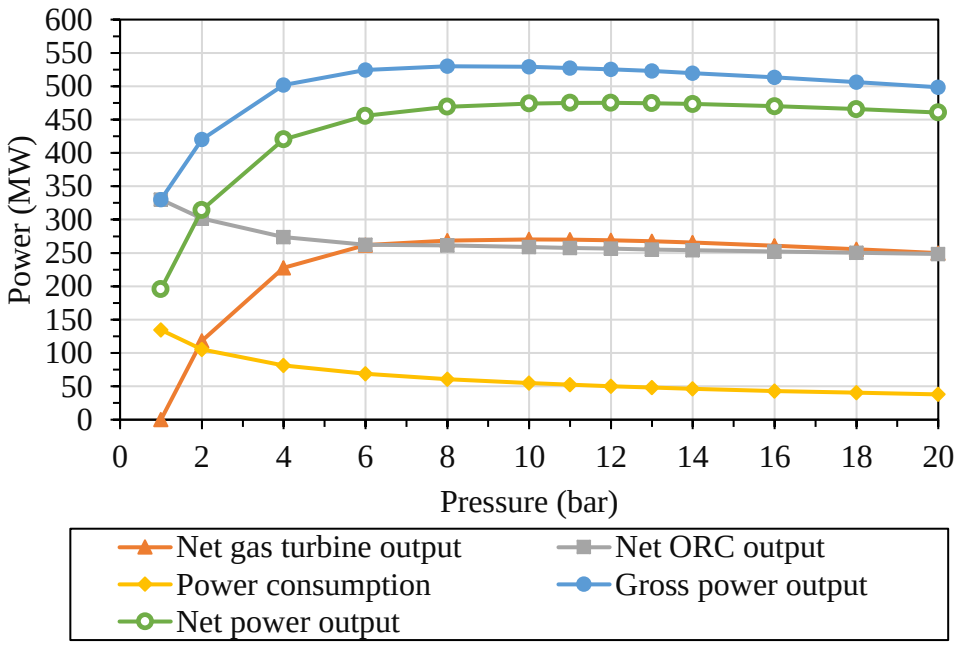

Figure 6.15. Effect of air and fuel reactor operating pressure on power consumption and generation for CuO

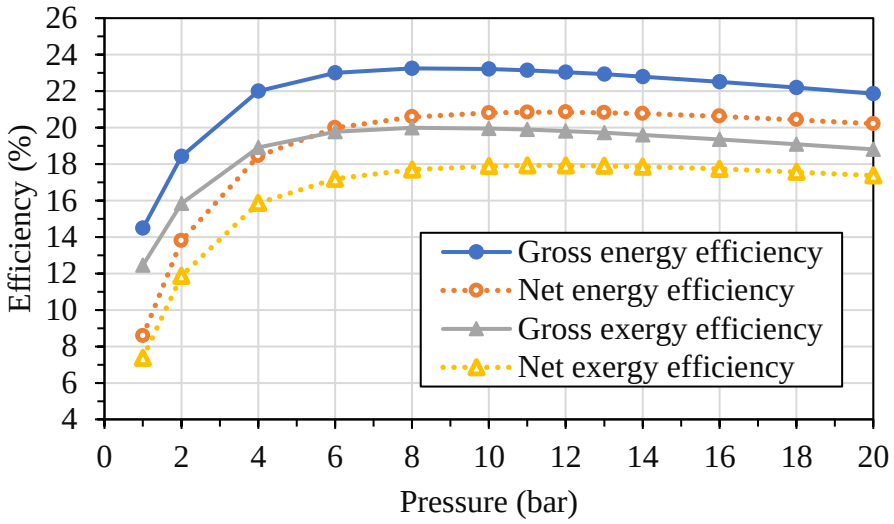

Figure 6.16. Effect of air and fuel reactors operating pressure on overall energy and exergy efficiency for CuO

6.3.3.3. Effect of Air Reactor Operating Temperature

The effect of air reactor operating temperature on air flow rate, power consumption, and generation is depicted in Figure 6.17. The effect of air reactor temperature on energy and exergy efficiency is depicted in Figure 6.18.

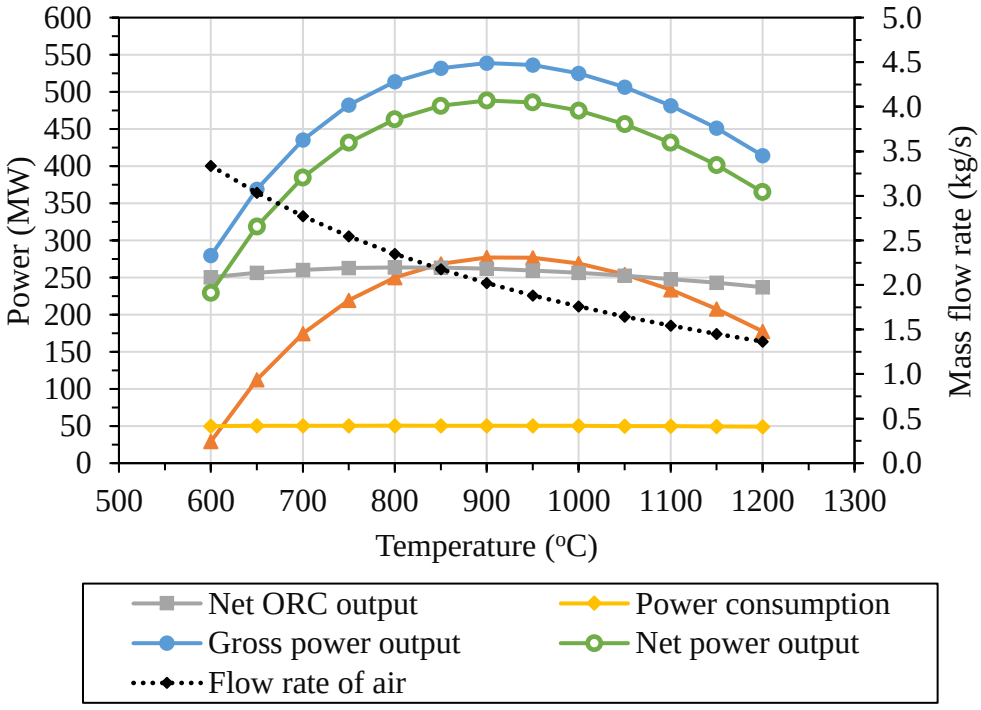

Figure 6.17. Effect of air reactor temperature on power consumption and generation for CuO

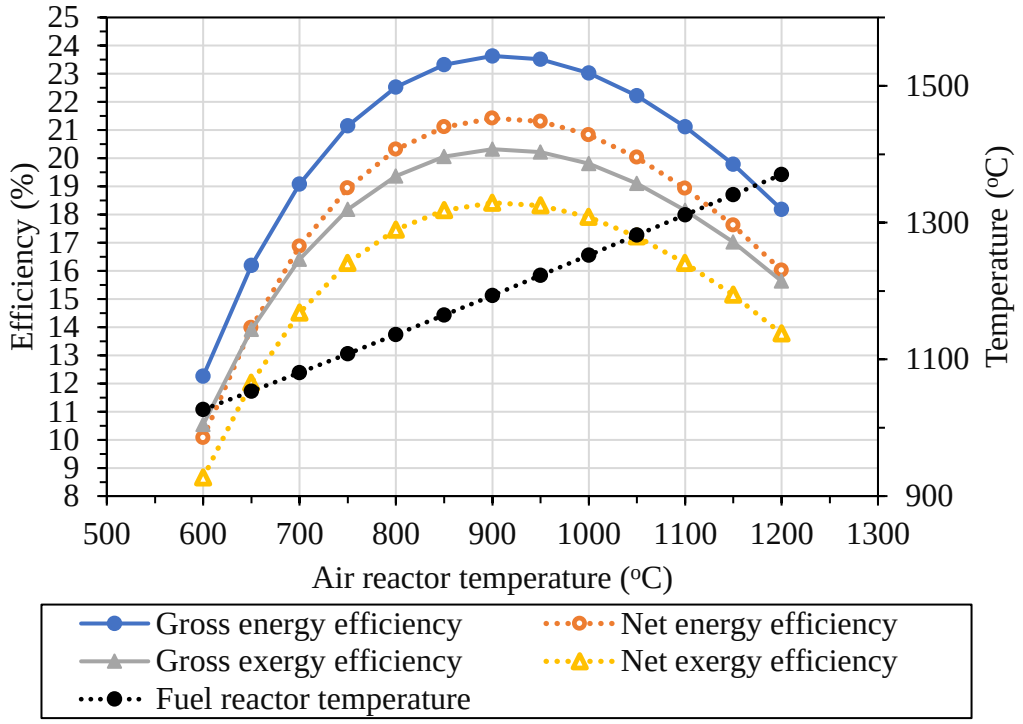

Figure 6.18. Effect of air reactor temperature on energy and exergy efficiency for CuO

The step by step improvement in process efficiency by the above sensitivity analysis has been presented in Table 6.3.

Table 6.3. Step by step improvement of the process efficiencies from sensitivity analysis for CuO.

Case	Optimal Value	Net turbine work output (kW)	Net ORC work output (kW)	Net overall energy efficiency (%)	Net overall exergy efficiency (%)
Oxygen carrier (OC) to biomass ratio	19.66	270.27	258.76	20.80	17.88
Air and fuel reactor operating pressure (bar)	12	268.95	256.42	20.84	17.92
Air reactor operating temperature (°C)	900	276.96	261.84	21.42	18.42

6.3.4. Sensitivity Analysis for CLC based BFPP using 10% CuO + 90% Fe_2O_3

6.3.4.1. Effect of oxygen carrier to biomass ratio

As in prior cases, increasing the oxygen carrier to biomass ratio enhances the biomass combustion rate and power outputs, as shown in Figure 6.19. This increase is shown up to an OC/biomass ratio of 45.36, with net energy and exergy efficiencies of 19.88% and 17.09%, respectively.

6.3.4.2. Effect of Air and Fuel Reactors Operating Pressure

Figure 6.21 depicts the effect of changing the loop operating pressure from 1 bar to 20 bar on overall process power consumption and generation. Furthermore, the process energy and exergy efficiencies at various CLC operating pressures are examined, with the maximum efficiencies obtained at 11 bar pressure, as shown in Figure 6.22.

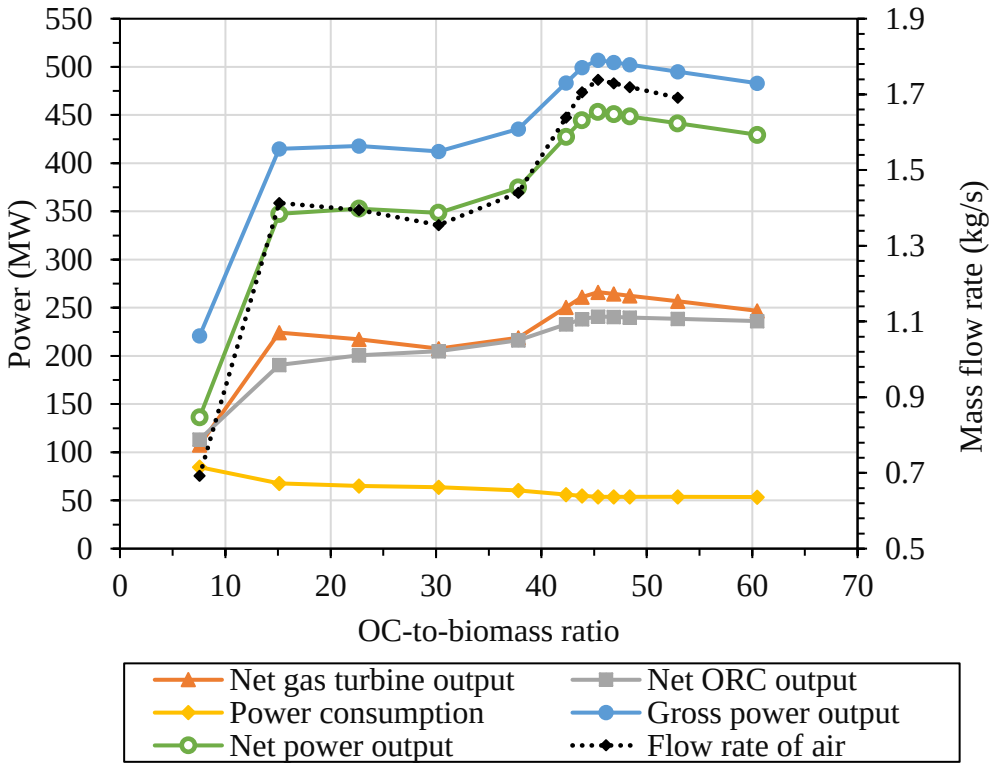

Figure 6.19. Effect of OC-to-biomass ratio on power consumption and generation for 10% CuO + 90% Fe_2O_3

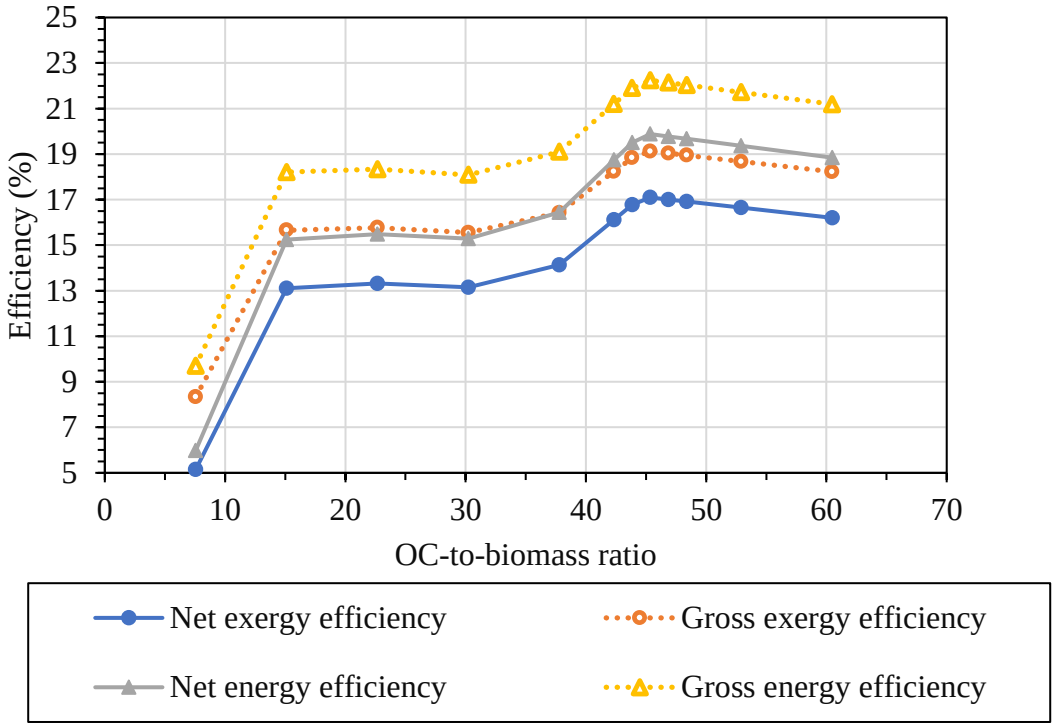

Figure 6.20. Effect of OC-to-biomass ratio on energy and exergy efficiency for 10% CuO + 90% Fe_2O_3

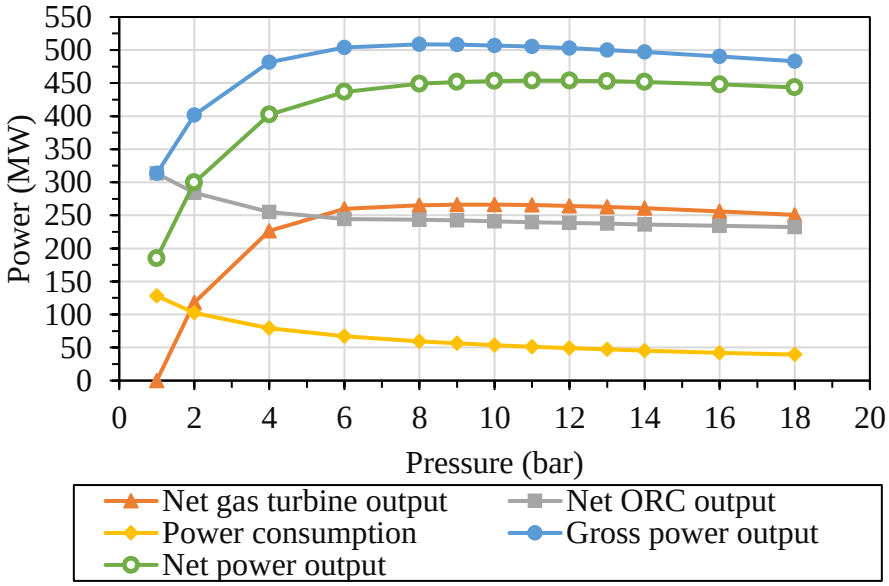

Figure 6.21. Effect of air and fuel reactor operating pressure on power consumption and generation for 10% CuO + 90% Fe_2O_3

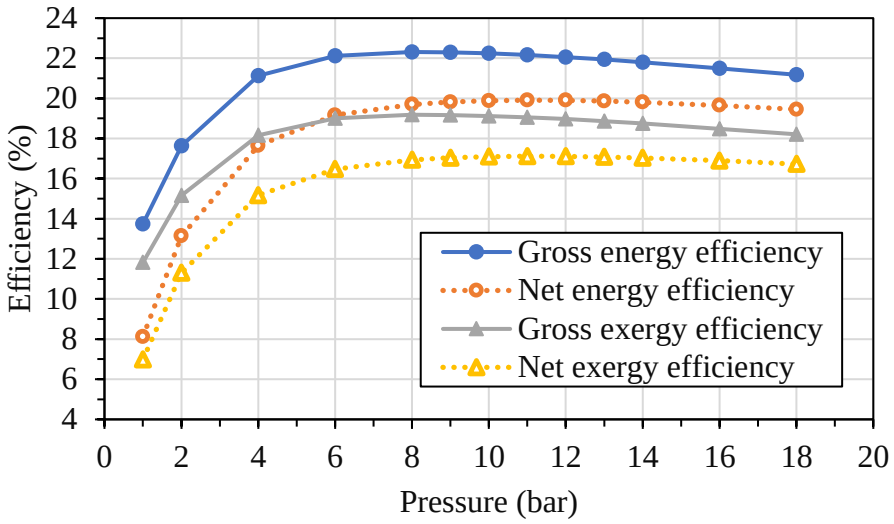

Figure 6.22. Effect of air and fuel reactors operating pressure on overall energy and exergy efficiency for 10% CuO + 90% Fe_2O_3

6.3.4.3. Effect of Air Reactor Operating Temperature

The effect of air reactor operating temperature on air flow rate, power consumption, and generation is depicted in Figure 6.23 The effect of air reactor temperature on energy and exergy efficiency is depicted in Figure 6.24.

The step by step improvement in process efficiency by the above sensitivity analysis has been presented in Table 6.4.

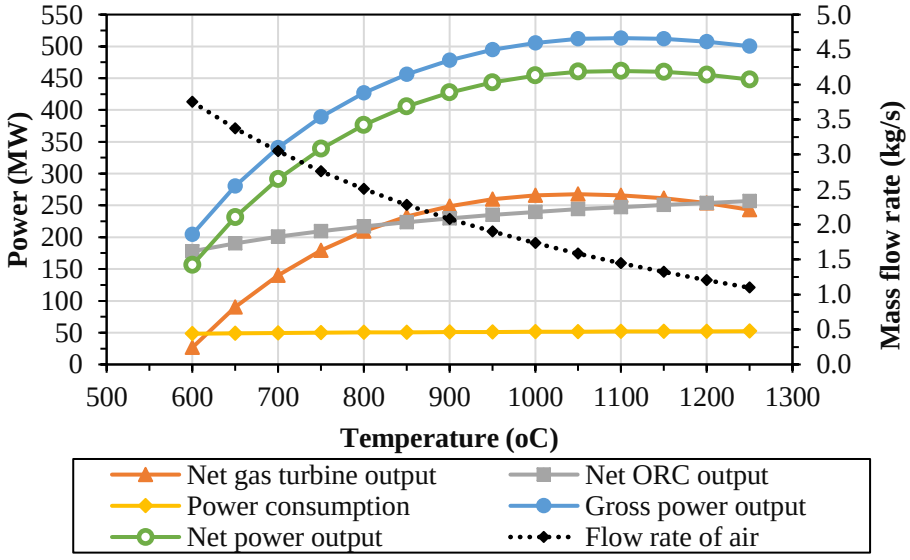

Figure 6.23. Effect of air reactor temperature on power consumption and generation for for 10% CuO + 90% Fe_2O_3

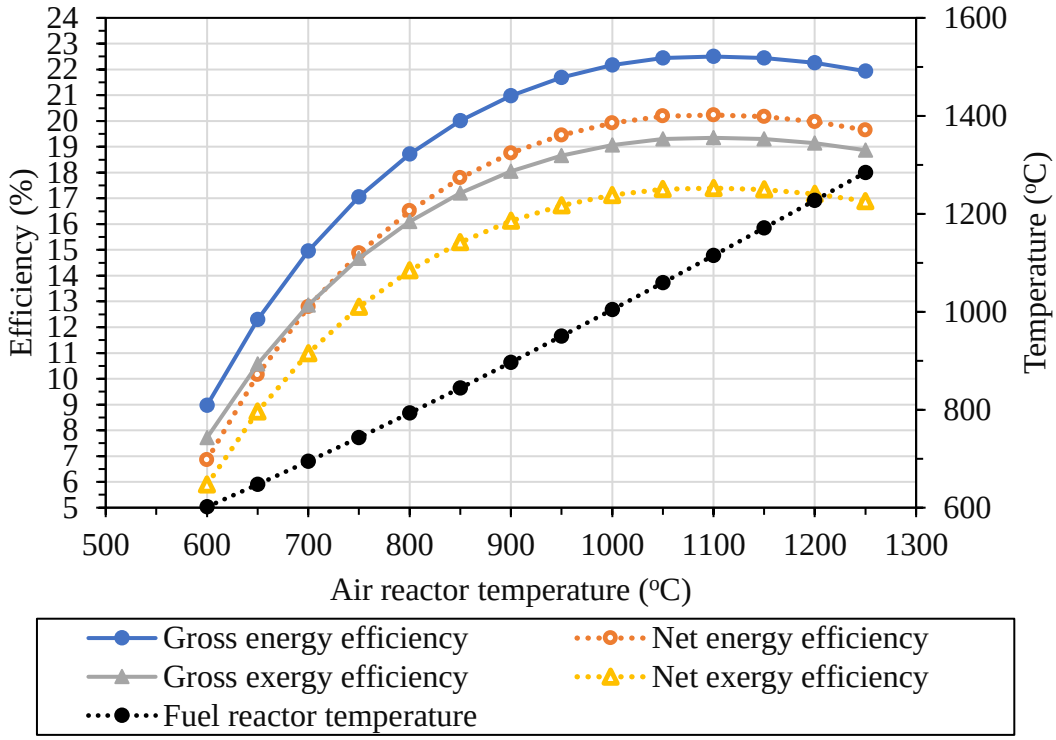

Figure 6.24. Effect of air reactor temperature on energy and exergy efficiency for 10% CuO + 90% Fe_2O_3

Table 6.4. Step by step improvement of the process efficiencies from sensitivity analysis for 10% CuO + 90% Fe_2O_3

Case	Optimal Value	Net turbine work output (kW)	Net ORC work output (kW)	Net overall energy efficiency (%)	Net overall exergy efficiency (%)
Oxygen carrier (OC) to biomass ratio	45.36	266.17	240.88	19.88	17.09
Air and fuel reactor operating pressure (bar)	11	265.59	239.71	19.91	17.12
Air reactor operating temperature (°C)	1100	266.01	247.00	20.23	17.40

6.3.5 Comparative analysis based on the energy and exergy analyses.

Table 6.5 presents energy and exergy efficiencies of CLC-based BFPP for different oxygen carriers. Nickel-based oxygen carriers showed maximum efficiencies followed by Cu-based and Co-based OCs. Ni-based oxygen carriers exhibit higher reactivity in redox environments, allowing them to be fully reduced to a zero-oxidation state and release more oxygen. Consequently, these metal oxides require a lower circulation rate in the loop, leading to higher efficiency compared to other metal oxides. However, they exhibit a low oxidation rate in the air reactor, and furthermore, these metal oxides are toxic and expensive. Hence, Ni-based OCs might not be a good choice for oxygen carrier. Cu-based metal oxides have high oxygen transfer capacity and reaction rates with no thermodynamic restrictions to achieve 100% fuel conversion to H_2O and CO_2. The capability of CuO and Co_3O_4 based oxygen carriers to release gaseous O_2 can be utilized in the conversion of solid fuels, effectively overcoming the extremely low kinetics associated with solid-solid reactions between fuels and oxygen carriers. However, care must be taken regarding their low melting points to ensure they are used within appropriate temperature ranges for optimal performance. Although these oxygen carriers exhibit oxygen uncoupling behaviour, their overall efficiency is lower than that of Ni-based oxygen carriers due to their lower operating temperature. Further, the Cu based oxygen carriers are costlier than iron-based, bauxite, perovskite and pyrite cinder but, they are cheaper than cobalt and nickel based oxygen carrier. Ni and Co based oxides are not being effectively utilized in CLC studies due to they are toxic in nature. This makes Cu-based oxygen carriers more suitable for CLC applications than Fe-based oxygen carriers. Hence, addition of some fraction of Cu-based oxygen carrier in Fe-based oxygen carrier could improve carbon conversion, redox characteristics and overall performance of the plant. As an instance, the performance of a 10% Cu and 90% Fe_2O_3 blended oxygen carrier is investigated. It is observed that even a small addition of Cu significantly improved the energy efficiency of the overall process. This improvement can be attributed to the enhanced oxygen uncoupling behavior and catalytic activity provided by the Cu component, which facilitates more efficient oxidation reactions. However, while increasing the Cu content in the blend would likely result in further performance enhancements, it would also lead to higher costs for the oxygen carrier. The higher cost is due to the relatively higher price of Cu compared to Fe_2O_3, which can make the overall process more expensive. Therefore, a balance must be struck between the performance benefits and the economic feasibility of increasing Cu content.

Table 6.5. Energy and exergy efficiencies of CLC-based BFPP for different oxygen carriers

Oxygen carrier	Gross energy efficiency (%)	Net energy efficiency (%)	Gross exergy efficiency (%)	Net exergy efficiency (%)
Fe_2O_3	21.18	18.94	18.21	16.29
NiO	25.93	23.77	22.30	20.44
Co3O4	20.64	17.88	17.75	15.37
CuO	23.63	21.42	20.32	18.42
10% CuO + 90% Fe_2O_3	22.50	20.23	19.35	17.40

6.4 Summary

In this chapter, chemical looping combustion based biomass-fired power plant using different oxygen carriers has been proposed. CLC based BFPP was simulated with the optimal parameters for each case and their performance was compared in terms of energy & exergy efficiency. Following are the outcomes from the study:

- The optimal conditions for oxygen carrier to biomass ratio, operating pressure of air and fuel reactors, and air reactor operating temperature using different oxygen carriers are as follows: (a) NiO: 9.07, 12 bar and 1150 ^oC, (b) Co_3O_4: 27.22, 7 bar and 750 ^oC, (c) CuO: 19.66, 12 bar and 900 ^oC, (d) 10% CuO + 90% Fe_2O_3: 45.36, 11 bar and 1100 ^oC.
- The net energy and exergy efficiencies of the process with different oxygen carriers at optimal operating conditions are as follows: (a) NiO : 23.77% and 20.44%, (b) Co3O4: 17.88% and 15.37%, (c) CuO: 21.42% and 18.42%, (d)10% CuO + 90% Fe_2O_3: 20.23% and 17.40%.

The study demonstrates that the bimetallic oxygen carrier (10% CuO + 90% Fe_2O_3) is a better option for achieving high process efficiency without considerably inflating overall operational costs.

Chapter 7

Development of novel Fe_2O_3/Al_2O_3 nanofiber-based oxygen carriers for CLC of syngas

Chapter 7

Development of novel Fe_2O_3/Al_2O_3 nanofiber based oxygen carriers for CLC of syngas

This chapter of the study embarks on fulfilling the fourth outlined objective, focusing on the synthesis of pioneering nanofibrous oxygen carriers through the utilization of the electrospinning technique. This innovation holds relevance within the context of chemical looping combustion integrated syngas-fired power plants. The narrative here delineates the synthesis and thermodynamic assessment of CLC of syngas derived from the biomass and comprehensive methodology employed in the synthesis of electrospun nanofibrous oxygen carriers. Furthermore, a comparative exploration is undertaken, pitting these advanced nanofibrous carriers against their conventional counterparts crafted through nanoparticle-based methods, specifically utilizing physical mixing.

Central to this endeavor is the assessment of the thermal stability and redox stability exhibited by the synthesized nanofibrous oxygen carriers. A rigorous comparison is drawn, aligning these attributes with those of the nanoparticle-based oxygen carriers. This evaluation serves as a crucible for gauging the prowess and utility of the newly synthesized nanofibrous carriers within the unique context of CLC-based biomass-fired power plants.

To illuminate the intricate characteristics of these oxygen carriers, the study delves into the microscopic world. The morphology of both pristine and utilized oxygen carriers is subjected to meticulous scrutiny, realized through an array of characterization techniques. These methods encompass SEM, XRD, and EDAX. Through this multifaceted exploration, a comprehensive understanding of the nanofibrous oxygen carriers' structural evolution, elemental composition, and performance dynamics is revealed.

7.1. Motivation and Objective

During the reduction process in CLC, the interaction between ash and oxygen carriers plays a pivotal role in dictating the efficiency and stability of the entire system. This intricate interplay, however, can also lead to a challenging issue – the rapid deactivation of oxygen carriers, consequently giving rise to a noticeable decline in cyclic stability within the CLC process (Staničić et al., 2020). The phenomenon of ash and oxygen carriers interaction deserves

particular attention due to its significant influence on the overall performance of CLC. Ash, which is a natural component of solid fuels, can potentially impede the function of oxygen carriers during their reduction phase (Keller et al., 2014). This interaction results in the formation of compounds that hinder the oxygen transfer between the fuel and the carrier material. As a consequence, the ability of the oxygen carrier to repeatedly participate in the redox reactions required for CLC diminishes, ultimately leading to a decrease in cyclic stability. Further, high ash coal needs low-cost oxygen carriers for the CLC operation due to the problem associated with the separation of metal particles from ash content (Wang et al., 2015; Mendiara et al., 2012).

To counteract this challenge, certain metal oxide sources have emerged as viable solutions. Crude metal oxides, such as those found in various ores, steel slag, and waste materials containing transition metal oxides discarded by industries, have gained prominence as effective alternatives. These materials possess inherent characteristics that make them suitable for CLC of solid fuels (Bhui and Vairakannu, 2019).

Despite the positive features, there is still a great deal of research needed to get the technology to a commercial stage. The key technological challenges to be addressed include the performance of oxygen carrier, possible adverse interactions with the coal/biomass ash components, and the contacting pattern/ reactor configuration. These specific challenges, which are particularly pertinent in the case of chemical looping combustion processes involving solid fuels, can overcome by ex-situ gasification of solid fuel followed by CLC of gasified combustible products.

On a different trajectory, the scenario shifts when dealing with gaseous fuels in the CLC process. In this context, synthetic oxygen carriers come to the forefront. These artificially engineered materials are designed with a focus on achieving optimal performance and durability in the presence of gaseous fuels. Through meticulous formulation and engineering, synthetic oxygen carriers display enhanced resistance to deactivation caused by sintering, thereby maintaining their cyclic stability over an extended operational period (Daneshmand-Jahromi et al., 2023).

In conclusion, the complex interaction between ash and oxygen carriers during the reduction process can profoundly impact the cyclic stability of CLC systems. While ash-induced deactivation remains a concern, the utilization of diverse metal oxide sources, including crude metal oxides and waste materials, has proven effective and economical for CLC of solid fuels (Bhui and Vairakannu, 2019). Conversely, synthetic oxygen carriers, carefully crafted to

withstand the challenges posed by gaseous fuels, stand as the preferred choice for ensuring consistent performance and longevity in the CLC of such fuels (De Vos et al., 2020). Through the strategic selection of oxygen carriers based on fuel type and careful consideration of the intricate interplay between ash and carrier materials, the prospects for advancing the efficiency and reliability of chemical looping combustion continue to evolve.

Further, the literature encompassed in Section 2.3 offers compelling evidence that the integration of nanostructured oxygen carriers (OCs) within the framework of chemical looping combustion for gaseous fuels is gaining considerable traction. A particularly promising facet emerges from investigations into nanostructured OCs with heightened support and diminished transition metal oxide loadings, showcasing commendable cyclic stability. However, the crux of efficient CLC applications demands an efficient OC composites boasting both substantial transition metal oxide loadings, translating to impressive oxygen carrying capacities, and the crucial attribute of cyclic stability.

In the landscape of diverse nanomaterial synthesis techniques, electrospinning rises as an efficacious route. This methodology exhibits the unique ability to meticulously tailor the composition and morphology of nanofibers, making it a formidable candidate for crafting nanostructured OCs. What's intriguing, though, is the relatively uncharted territory when it comes to leveraging electrospinning for OC preparation. Consequently, the present study embarks on unearthing the latent potential within this facile synthesis route, strategically applying it to synthesize nanostructured oxygen carriers. The subsequent stage unfurls an intricate comparison, assessing the performance of these novel nanofibrous oxygen carriers against their counterparts crafted through nanoparticle-based methods.

In this work, the focus is directed toward a dual assessment encompassing two vital aspects: (i) synthesis of process configuration for ex-situ gasification of solid fuel followed by CLC of gasified combustible products (ii) synthesis of novel nanostructured oxygen carriers for CLC of gaseous fuels. The investigation transcends the realms of mere theoretical contemplation and delves into practical application, thereby positioning the study to yield not only insights but also actionable data. Section 7.2 explores the simulation of biomass gasification followed by CLC of gasified combustible products process configuration. In section 7.3, synthesis, characterization and performance assessment of nanostructured oxygen carriers are presented.

7.2. simulation of ex-situ gasification and CLC combustion configuration

In Chapter 4, we delve into a comprehensive examination of the integration of CLC and ORC technologies within a BFPP configuration. This strategic integration represents a significant advancement in the realm of sustainable energy solutions. The conceptual foundation of this study is depicted in Figure 4.1, where the configuration is conceptualized with biomass serving as the primary fuel in the CLC fuel reactor. However, the research explored in this particular section takes the core configuration a step further by incorporating a steam gasification process. This augmentation introduces an advantage in terms of oxygen carrier's utilization and their performance enhancement.

In this envisioned configuration extension, the gasification process emerges as a pivotal component. It engenders the production of syngas, a mixture primarily composed of hydrogen (H_2), carbon monoxide (CO), and traces of other gases. This syngas, a potent energy carrier, takes on the role of the primary fuel source for the fuel reactor within the CLC system. This scheme avoids the ash and oxygen carrier interaction and separation problems.

It is noteworthy that despite this strategic augmentation, the fundamental architecture of the proposed configuration, as illustrated in Figure 4.1, remains largely intact. The integral processes, aside from the incorporation of the gasification unit and the utilization of syngas, retain their essential characteristics, thus ensuring a seamless integration of the novel aspects.

In summation, this section serves as a pivotal exploration into the enhanced potential of the CLC integrated BFPP configuration through the integration of a steam gasification system. By harnessing the power of syngas generated from the gasification process and its interplay with the CLC system, this configuration embodies a holistic approach to sustainable energy production. The amalgamation of these innovative components promises reduced environmental impact, effective utilization of oxygen carriers and a promising trajectory toward a more sustainable energy future. However, it's important to note that the addition of a gasification step introduces an energy penalty. Figure 7.1 illustrates the performance comparison among conventional BFPP, CLC integrated BFPP, and CLC integrated syngas-fired power plants based on overall energy and exergy efficiencies. Notably, the CLC integrated syngas-fired power plant exhibits significantly higher net energy and exergy efficiencies compared to the conventional BFPP. Due to the gasification step, the CLC integrated syngas-fired power plant experiences an energy penalty of 4.1% and an exergy penalty of 3.5% when compared to the CLC integrated BFPP.

The above thermodynamic analysis demonstrates that electricity generation through the use of CLC of syngas yields superior energy and exergy efficiency. As a result, this configuration is chosen for further investigation. During the simulations of the proposed configurations, we initially assumed the utilization of ideal Gibbs reactors for both the air and fuel reactors. However, it is crucial to acknowledge that, in practical applications, challenges such as solid-fluid contact, sintering of metal oxides, and agglomeration can hinder process performance. Section 7.3 offers a comprehensive exploration of the synthesis of highly effective nanostructured oxygen carriers and their subsequent evaluation, particularly in terms of their resistance to sintering.

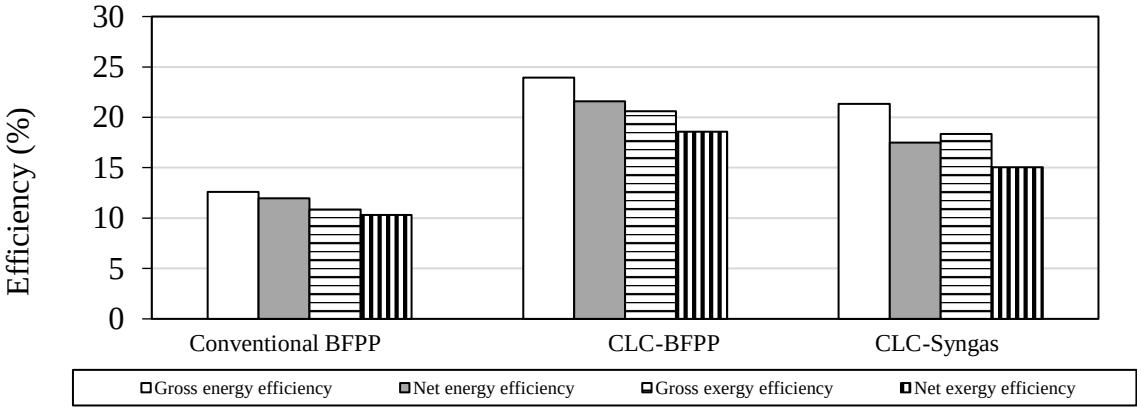

Figure 7.1. Thermodynamic performance of different power pants

7.3. Synthesis of nanostructured OCs

The chemicals used to prepare different precursors are listed in Section 7.3.1. A detailed step by step methodology used to synthesize the nanofibrous OCs from precursors using electrospinning technique is presented in section 7.3.2. In Section 7.3.3, the preparation of metal oxide nanoparticle composite using physical mixing is presented. The performance assessment using CLC experimentation is presented in Section 7.3.4.

7.3.1. Materials

Iron acetylacetonate (purity: 97%) and Aluminium acetylacetonate (purity: 99%) are purchased from Sigma–Aldrich, India. Ethanol (purity: 99.9%) is procured from Honyon International, Inc., China. Fe_2O_3 nanoparticles (Purity: 98%) of size 30 to 50 nm and Polyvinyl pyrrolidone (PVP; Mn = 1,300,000) are obtained from Alfa-aesar, India. Al_2O_3 nanoparticles (Purity: 99.9%) of size 20 to 30 nm and Acetone (purity: 99%) are purchased from Sisco Research Laboratories Pvt. Ltd. India. All the chemicals are used as received without any further modification.

7.3.2. Synthesis of Fe_2O_3-Al_2O_3 composite nanofibrous OCs

Fe_2O_3-Al_2O_3 composite nanofibrous OCs are synthesized using electrospinning setup (Espin-Nano-V1-VH, Physics Equipments Co., India). Initially, a polymer solution is prepared by mixing 12 wt.% of PVP in ethanol by stirring it for 5 hours to get a homogeneous solution. In the same way, Fe_2O_3-Al_2O_3 metal oxide solution is prepared by mixing 12 wt.% of combined iron acetylacetonate and aluminium acetylacetonate in acetone. Iron acetylacetonate and aluminium acetylacetonate are suitably proportioned to get the Fe_2O_3 and Al_2O_3 composite in the weight ratio of 60:40 after calcination of the fibers. The prepared polymer and metal oxide solutions are mixed together in 1:1 ratio and stirred for 12 hours at room temperature to obtain uniform solution. Then, the resulting solution is used as precursor for synthesis of composite nanofibers using electrospinning.

The electrospinning apparatus, the schematic of which is shown in Figure 7.2, is used for preparation of nanofibers. The prepared precursor is loaded in a 10 ml syringe and pumped through the 18 gauge needle. The flow rate and distance between the collector and needle are optimized as 0.5 ml/h and 11 cm. The solution is made to get charged by applying a high voltage of 14 kV between the needle tip and the grounded collector. A jet in straight line form is ejected from the tip of the needle due to opposing electrostatic force and surface tension on the droplet. Further, ejected fiber stretches and forms an unstable whip of jet before it reaches the collector to produce fibers in the size range of few hundred nanometers. The electrospun polymer composite fiber mat is calcined in a muffle furnace at 900 °C for 2 hours to obtain the crystalline Fe_2O_3-Al_2O_3 composite nanofibrous OCs. During calcination of the mat at high temperatures, the polymers present in the fibers get decomposed leaving behind the nanofibers containing only metal oxides. In the same way, pure Fe_2O_3 nanofibers were also prepared.

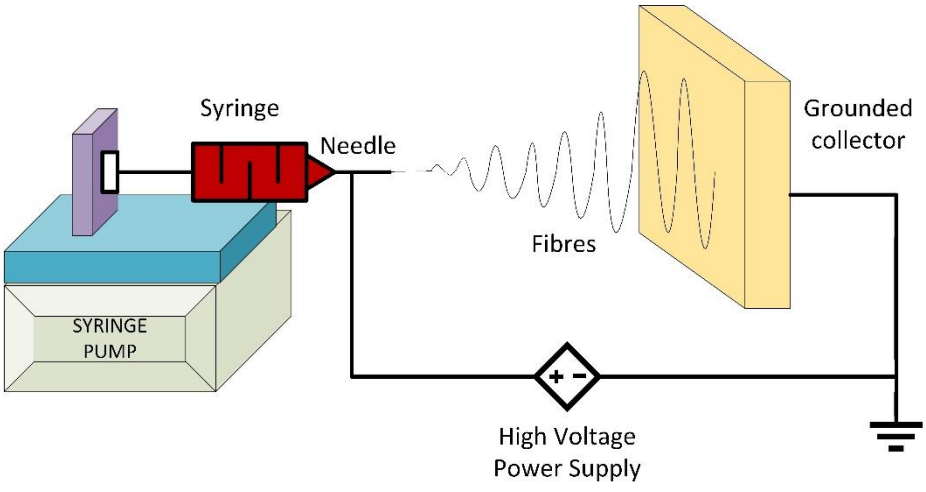

Figure 7.2. Schematic diagram of electrospinning setup

7.3.3. Synthesis of Fe_2O_3-Al_2O_3 composite nanoparticles

Pure Fe_2O_3 nanoparticles and its composite are prepared using mechanical mixing. The following steps demonstrates the synthesis of Fe_2O_3-Al_2O_3 composite nanoparticles. Pure Fe_2O_3 nanoparticles and Al_2O_3 nanoparticles are added in the weight ratio of 60:40 in deionized water. Then, the solution is stirred for 8 hours to get the uniform metal oxide composite slurry. The slurry is then dried in an oven at 80°C for 10 hours. After drying, these nanoparticles are calcined at 900 °C for 2 hours in muffle furnace.

7.3.4. CLC experimentation using nanostructured OCs and characterization

The main objective of this study is to test the thermal and redox cyclic stability of nanostructed OCs in CLC environment at 900 °C. Hence, hereafter the four prepared samples – pure Fe_2O_3 nanofibers, pure Fe_2O_3 nanoparticles, 60% Fe_2O_3 and 40% Al_2O_3 composite nanofibers and composite nanoparticles with 60% Fe_2O_3 and 40% Al_2O_3 are denoted as PNF, PNP, CNF, CNP respectively.

7.3.4.1. Thermal Cycling

In thermal cycling, the calcined nanofibers / nanoparticles are heated from ambient temperature to a typical CLC operating temperature of 900 °C at a heating rate of 10 °C/min and dwelled at 900 °C for 20 minutes inside the high temperature WEIBER muffle furnace (ACM-82301) and then cooled to room temperature. To assess the thermal stability of materials, twenty such thermal cycles are performed. The above thermal cycling process is followed for all the four synthesized samples.

7.3.4.2. Redox Cycling

A single redox cycle comprised of three steps: reduction, purging and oxidation. During the reduction, the nanofibers were exposed to a reducing environment by sending the 30 vol % CO and 70 vol % N_2 gases mixture at a flowrate of 0.2 LPM for 5 minutes. In the reduction process, CO gas reacts with oxygen present in Fe_2O_3 and reduces the metal oxide to Fe_3O_4 / FeO / Fe. After the reduction, the reactor was purged with an inert N_2 (99.99 vol%) gas at a flowrate of 0.8 LPM for 10 minutes to flush out any traces of reducing gases in the reactor. The reduced transition metal oxides were then oxidized in oxidation step by sending zero air at the flowrate of 0.8 LPM for 5 minutes. Twenty such continuous redox cycles were performed and samples after 10^{th} and 20^{th} redox cycles were collected to investigate the morphological stability and reactivity of the nanofibrous OCs. The same experimental procedure was followed to assess the performance of nanoparticle OCs. The morphological changes of these nanoparticle and

nanofibrous OCs after 10th and 20th redox cycles were analysed using SEM and XRD characterization techniques.

To conduct CLC redox cycle tests, the quartz tube reactor (outer diameter: 18 mm, inner diameter: 14 mm, length: 30 mm) was charged with synthesized OCs and both ends of the reactor was sealed with porous quartz wool (fiber size < 4 microns). The quartz tube reactor was placed inside a programmable tubular furnace as shown in Figure 7.3. A thermocouple was inserted inside the furnace tube to monitor the temperature near the test section. A PID controller (Honeywell, Model: DC1010) was connected to the thermocouple to control the furnace temperature. The gasses were passed at desired flow rates using the pre-calibrated rotameters. The conversion of the fuel with OCs was confirmed by the presence of CO_2 in outlet gas as detected from the gas analyser.

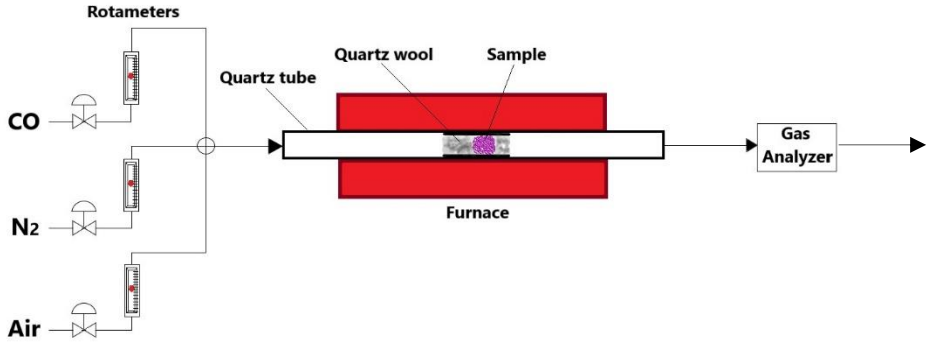

Figure 7.3. Schematic of experimental setup for CLC tests

The crystal phases of the metal oxides were identified using X-ray diffractometer (PANalytical, X'Pert Powder XRD) with a 2θ range of 10° to 80° at a speed of 5°/min. Scanning Electron Microscope (SEM, Tescan, Vega 3 LMU) was used to observe the morphological changes occurred in the metal oxides during the redox cycles. The surface mapping of the metal oxides was obtained using energy dispersive X-ray spectroscopy (EDAX, Tescan, Vega 3 LMU) to observe the distribution of the elements present on their surface.

7.3.4.3. Results and Discussion

SEM and EDAX characterization studies are being conducted for PNF, PNP, CNF, and CNP samples after thermal cycling. The performance in terms of cyclic stability of pure and composite nanofibers and nanoparticles is being analyzed and compared using the results from these characterization studies. The best-performing samples from this thermal analysis are further being considered for detailed redox cycling.

7.3.4.3.1 Thermal cycling

Figure 7.4 (a & b) and Figure 7.4 (c & d) depict the morphology of CNP and PNP respectively, after the 1st and 20th thermal cycle. It is evident from the figures that after 20th cycle, the particles sintered and their size increased manifold. Because of the presence of Al_2O_3 support in CNP, the extent of sintering is less compared to PNP. The morphology of CNF and PNF respectively, after the 1st and 20th thermal cycles is shown in Figure 7.5 (a & b) and Figure 7.5 (c & d). Interestingly, sintering is observed to be very minimal in case of the synthesized nanofibers (Figure 7.5) compared to nanoparticles (Figure 7.4). This could be because of the formation of entangled rigid nanofibrous structures, which minimizes the contact between the nanofibers. This increases the sintering resistance in nanofibers, whereas more particle to particle contact in nanoparticles aggravates the sintering during thermal cycling. The microstructural stability of the nanofibers is remarkable even after 20 thermal cycles, which can be observed from the retention of fibrous structure and negligible change in the fibre diameter as shown in Figure 7.5 (b & d). Among all the samples, CNF exhibited superior sintering resistance. In addition, PNF (Figure 7.5d) also has shown better sintering resistance compared to CNP (Figure 7.4b) and PNP (Figure 7.4d).

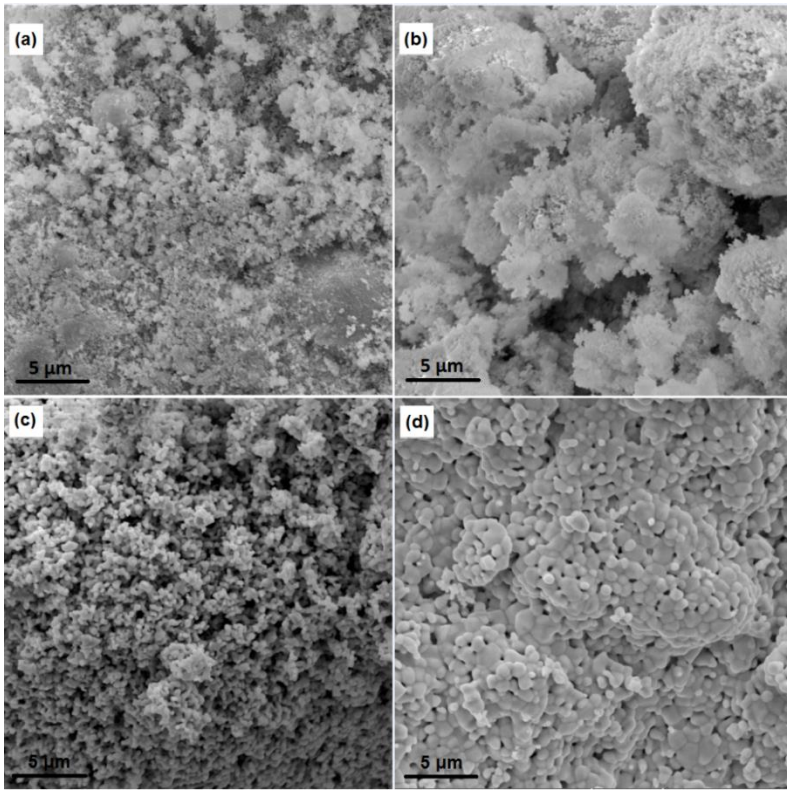

Figure 7.4. (a) SEM image of Fe_2O_3-Al_2O_3 nanoparticles with ratio 60:40 after 1st cycle (b) and after 20th cycle, (c) SEM image of pure Fe_2O_3 nanoparticles after 1st cycle (d) and after 20th cycle.

In addition to morphological investigation, Energy Dispersive X-ray Analysis (EDAX) is carried out for investigation of elements in nanostructured metal oxides. The presence of iron, aluminium and oxygen are clearly observed in all the samples before and after thermal cycles as can be seen from Table 7.1. The composition changes can be attributed to the random distribution of metal oxides. However, the elements present before and after thermal cycling confirm the absence of chemical changes in the prepared nanoparticles and nanofibers during the thermal cycling.

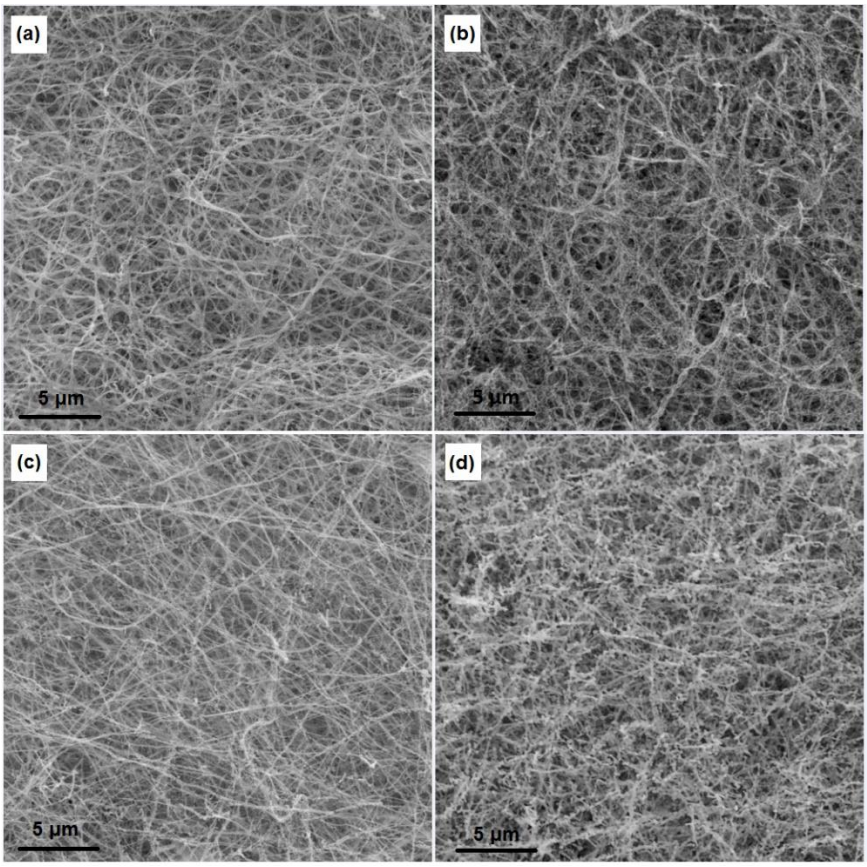

Figure 7.5. (a) SEM image of Fe_2O_3-Al_2O_3 nanofibers with ratio 60:40 after 1st cycle (b) and after 20th cycle, (c) SEM image of pure Fe_2O_3 nanofibers after 1st cycle (d) and after 20th cycle.

As the proposed novel nanofiber-based metal oxides exhibited good thermal cyclic stability and high sintering resistance, these can be used as promising oxygen carriers in the chemical looping combustion of gaseous or solid fuels. To further illustrate this, the CLC redox cyclic stability of CNF and CNP metal oxides are investigated under reduction with CO as the fuel and oxidation environment.

Table 7.1. EDAX analysis of nanostructured metal oxides before and after thermal cycling

S. No.	Sample	EDAX results			
1	Fe_2O_3-Al_2O_3 nanoparticles after 1st thermal cycle	Element	Weight%	Atomic%	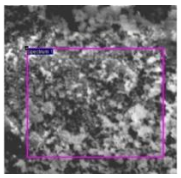
		O	41.34	63.51	
		Al	22.67	20.65	
		Fe	36.00	15.84	
2	Fe_2O_3-Al_2O_3 nanoparticles after 20th thermal cycle	Element	Weight%	Atomic%	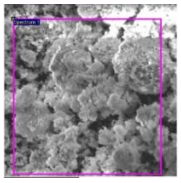
		O	36.09	59.58	
		Al	20.15	19.72	
		Fe	43.76	20.69	
3	Fe_2O_3-Al_2O_3 nanofibers after 1st thermal cycle	Element	Weight%	Atomic%	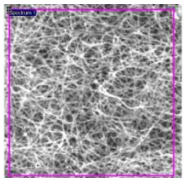
		O	31.84	59.30	
		Al	7.62	8.41	
		Fe	60.54	32.30	
4	Fe_2O_3-Al_2O_3 nanofibers after 20th thermal cycle	Element	Weight%	Atomic%	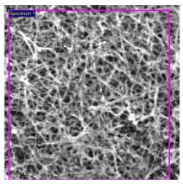
		O	35.23	61.15	
		Al	12.49	12.86	
		Fe	52.28	25.99	

7.3.4.3.2. Redox cycling

The SEM and EDAX characterization studies were performed for the Fe_2O_3-Al_2O_3 CNFs at the following different stages: fresh sample after calcination, after 1st reduction test and after 10th & 20th redox cycles. Using the XRD analysis, the elements present in fresh sample and the reduced forms of Fe_2O_3 in sample after 1st reduction test were identified. In addition, SEM analysis was also performed for the Fe_2O_3-Al_2O_3 composite CNPs after calcination, 10th and 20th redox cycles. The CLC performance in terms of cyclic stability of nanofibers and

nanoparticles were analysed and compared using the results from these characterization studies.

- **Characterization of fresh Fe_2O_3-Al_2O_3 CNFs after calcination and 1st reduction step**

SEM image of fresh Fe_2O_3-Al_2O_3 CNFs after calcination was presented in Figure 7.6 (a), where the formation of very fine cylindrical nanofibers with smooth surface and minimal contact among the nanofibers due to the entangled structure can be seen. These nanofibers have diameter in the range between 100-500 nm. The elemental composition of these nanofibers was presented in Figure 7.6 (b).

SEM analysis and surface mapping were performed on the nanofibers after the first reduction test to identify the changes in the morphology and surface elemental distribution due to the reaction of oxygen with fuel during the reduction process. The corresponding images were shown in Figure 7.6 (c) & (d). From the figures 7.6 (a) & (c), it can be observed that, the fibrous morphology is intact even after reduction step, however, diffusion of Fe cations towards the surface must have occurred. The same can be confirmed from the surface mapping image after 1st reduction test (Figure 7.6 (d)) where, the amount of Fe element present on the surface increased drastically as compared to that of fresh nanofiber surface (Figure 7.6 (b)).

The diffusion of Fe cations to the surface and depositing is generally observed in all OCs. However, this phenomena is more severe in nanosized OCs. These migrated Fe cations contact each other on surface and form agglomerates. This agglomeration reduces the active surface area and leads to sintering over a few redox cycles. However, the proposed novel metal oxide in the form of nanofibers with minimum fiber to fiber contact due to the entangled structure reduces the physical contact between the Fe particles. Hence, the fibrous morphology is expected to be retained without any significant change after multiple CLC cycles.

XRD analysis was performed to find the compounds present in fresh sample and their reduced forms after reduction step. XRD pattern of fresh Fe_2O_3-Al_2O_3 composite nanofibers after calcination along with standard XRD pattern of Hematite (Fe_2O_3) for (Dos Santos et al., 2016) is presented in Figure 7.7. The diffraction peaks aligned with Hematite (Fe_2O_3) standard diffraction peaks are marked with '*' symbol along with the respective miller indices. The other diffraction peaks aligned with Alumina (Al_2O_3) standard diffraction peaks are marked with '@' symbol. No other peaks are found related to other compounds which confirm that the nanofibers contain only Fe_2O_3 and Al_2O_3 components.

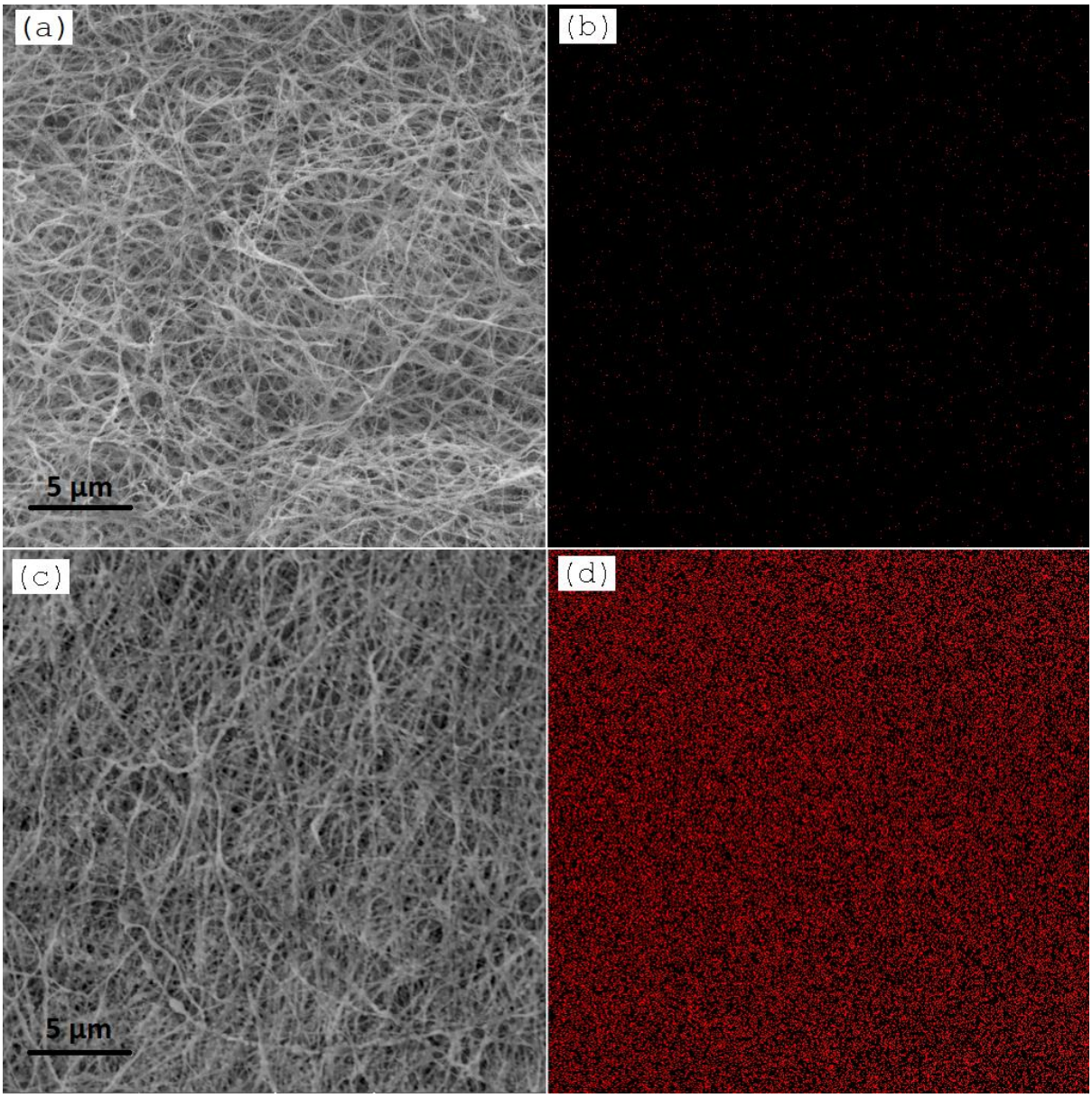

Figure 7.6. Fe_2O_3-Al_2O_3 composite nanofibers: SEM images (a) of fresh sample (c) after 1st reduction; Elemental mapping images of Fe (b) in fresh sample (d) after 1st reduction

The XRD pattern of Fe_2O_3-Al_2O_3 composite nanofibers after 1st reduction step along with XRD pattern of fresh Fe_2O_3-Al_2O_3 composite nanofibers were presented for comparison in Figure 7.8. The peaks of Fe_3O_4, FeO and Fe were visible in the XRD pattern, which confirmed that Fe_2O_3 was reduced to low oxygen level metal oxides during the reduction step. Only two peaks with very less intensities of Fe_2O_3 were found which indicated that most of the Fe_2O_3 had been reduced.

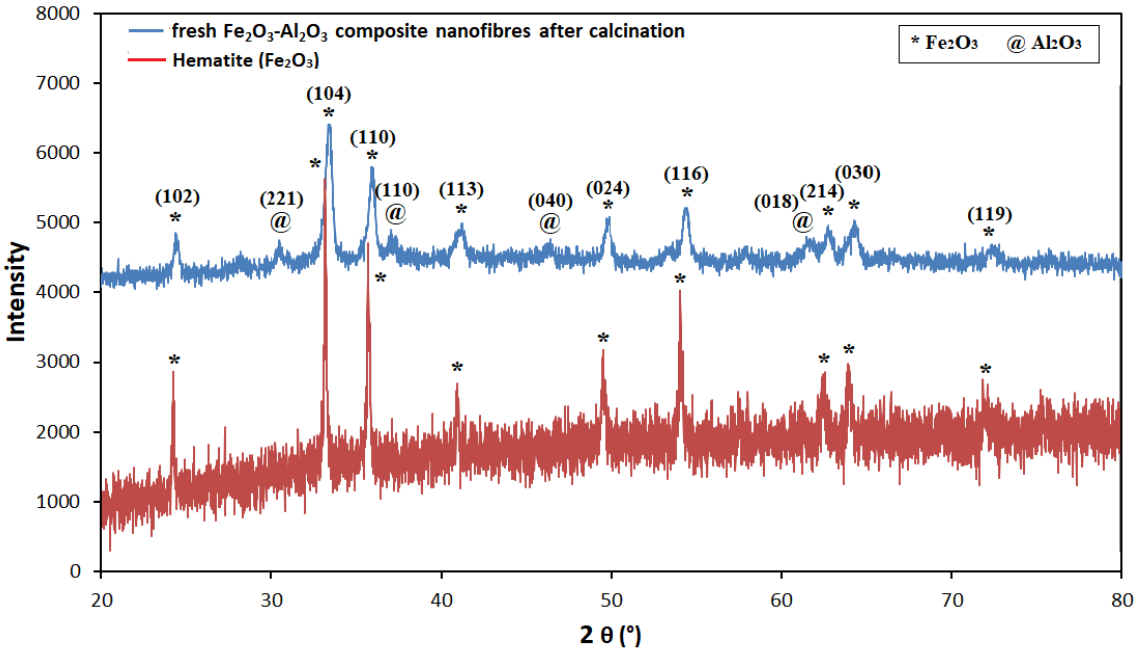

Figure 7.7. XRD pattern of fresh Fe_2O_3-Al_2O_3 composite nanofibers after calcination

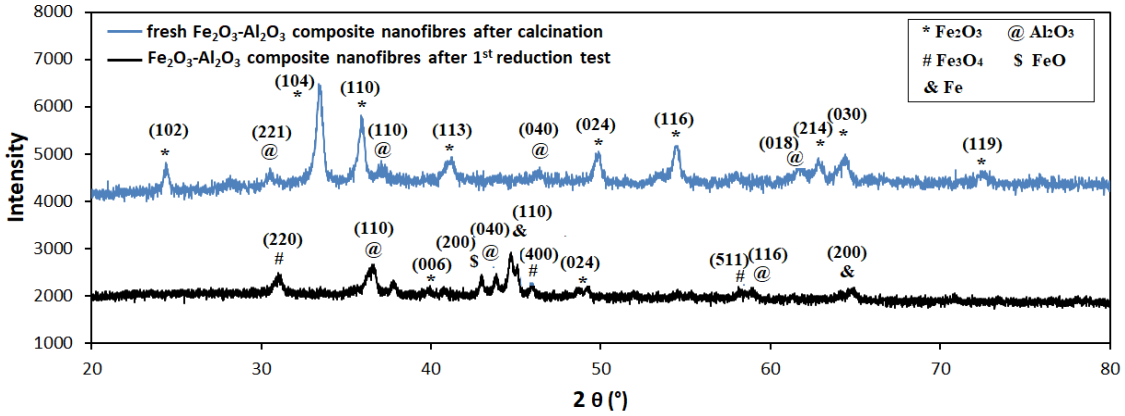

Figure 7.8. XRD pattern of Fe_2O_3-Al_2O_3 composite nanofibers after 1st reduction test

- **Comparison of cyclic stability of Fe_2O_3-Al_2O_3 nanofibers with Fe_2O_3-Al_2O_3 nanoparticles**

Multiple redox cycles were carried out at a typical CLC operating temperature of 900 ^oC in a tubular fixed bed reactor to assess the cyclic stability of the synthesized OCs. SEM images of the fresh Fe_2O_3-Al_2O_3 composite nanofibers and these nanofibers after 10 & 20 redox cycles were presented in Figure 7.9 (a, b & c). It can be observed from the Figure 7.9 (b) that the fibrous morphology after 10 redox cycles was still retained. This confirms that the fibers exhibited significant resistance towards thermal sintering. However,-after 20 redox cycles, the nanofibers had lost the continuous fibrous morphology as shown in Figure 7.9 (c). The grains

like morphology is observed which can be attributed to the appearance of broken fibers and their agglomeration due to sintering. From elemental mapping, Fe/(Fe + Al) atomic ratio was calculated as 0.5 and 0.78 after 10 and 20 redox cycles respectively. This significant increase in the ratio after 20 cycles can be ascribed to the migration of Fe cations to the surface during the redox process, loss of fibrous structure and agglomeration of the broken nanofibers.

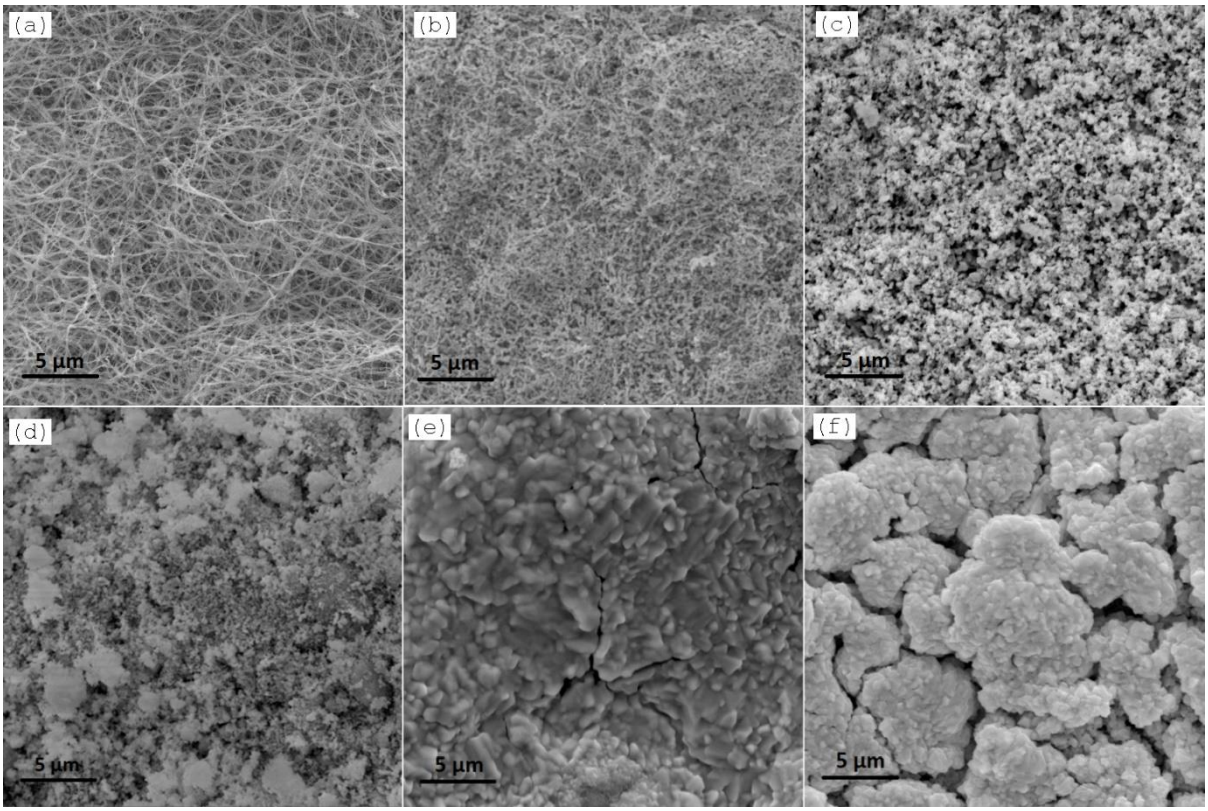

Figure 7.9. SEM images of Fe_2O_3-Al_2O_3 composite: (i) nanofibers after a) calcination, b) 10 redox cycles & c) 20 redox cycles; (ii) nanoparticles after d) calcination, e) 10 redox cycles & f) 20 redox cycles

SEM images of Fe_2O_3-Al_2O_3 composite nanoparticles after calcination, 10 and 20 redox cycles were presented in Figure 7.9 (d), (e) & (f), respectively. Lumps of different sizes and shapes can be observed in the Fe_2O_3-Al_2O_3 composite nanoparticles after 10 and 20 redox cycles. Severe sintering of composite nanoparticles and loss of grain boundaries resulted in the formation of lumps and reduction in active surface area after 10 redox cycles (Figure 7.9e) and this effect is even more noticeable after 20 redox cycles (Figure 7.9f). Nevertheless, the clear visibility of grain boundaries in the nanofibrous OCs even after 20 redox cycles shows better resistance to sintering.

The above analysis confirms that the nanofibers have shown better morphological stability during CLC redox cycles than the nanoparticles. Good cyclic stability was reported with

nanostructured OCs in the literature, but with high support and low transition metal oxide loadings. Nonetheless, OC composites possessing high metal oxide loadings (oxygen carrying capacities) along with cyclic stability are desirable for the successful operation of the CLC with minimum OC circulation rates and long operational time. The present study conducted with nanostructured OCs having relatively high transition metal oxide loading of 60% compared to that found in literature (<30%) clearly establishes that the Fe_2O_3-Al_2O_3 composite nanofibers are more resilient to deactivation caused by thermal sintering and they could sustain a greater number of redox cycles during high temperature CLC.

7.4. Summary

In this chapter, novel Fe_2O_3-Al_2O_3 metal oxides, structured in the form of nanofibers, have been fabricated through the application of the electrospinning technique. These nanofibrous materials have demonstrated remarkable thermal stability in comparison to their nanoparticle counterparts when subjected to a rigorous regimen of 20 thermal cycles, a procedure conducted at the conventional operating temperature of 900°C for chemical looping combustion. To further reinforce these findings, EDAX analysis has been employed, unequivocally substantiating the absence of any discernible chemical transformations occurring during the demanding thermal cycling experiments. This compelling evidence underscores the potential of the synthesized composite nanofibrous and particle-based metal oxides as viable candidates for serving as oxygen carriers (OCs) within the context of CLC, especially for the combustion of gaseous CO. These assessments have been carried out in a laboratory-scale fixed bed reactor.

Intriguingly, the morphological evolution of these OCs has been scrutinized following 10 and 20 redox cycles. A notable phenomenon observed is the substantial migration of Fe cations towards the material's surface during the reduction phase of the redox process. Upon the completion of 10 redox cycles, the fibrous morphology of the composite nanofibers remains pristine, devoid of any signs of sintering, signifying their robust structural integrity. Conversely, the composite nanoparticles experience substantial sintering challenges under identical conditions. However, upon extending the redox cycling to 20 cycles, the nanofibers gradually relinquish their continuous fibrous form and transition into a structure reminiscent of grains. These noteworthy findings gleaned from the study underscore the exceptional sintering resistance exhibited by OCs when they adopt a nanofibrous architecture, even in the presence of elevated temperatures and high concentrations of transition metal oxides. Notably, this includes a substantial loading of Fe2O3, amounting to 60% by weight. The results hold significant promise and pave the way for a new trajectory in the development of nanostructured OCs with the potential for achieving remarkable redox cyclic stability.

Chapter 8

Overall conclusions and scope for future work

8.1 Overall conclusions

This thesis is intended to demonstrate the feasibility of a chemical looping combustion and carbon dioxide and hydrogen utilization technologies in biomass fired power plants for zero CO_2 emissions. The overall performance of these plants is assessed based on energy, exergy and environmental analyses. The study is first conducted to check the feasibility of CLC-integrated biomass-fired power plant combined with an Organic Rankine Cycle (ORC) system as presented in *Chapter 4*. The CLC-integrated BFPP is further designed to co-generate hydrogen and power. This hydrogen co-generation CLC plant is then coupled with carbon dioxide and hydrogen utilization plants as presented in *Chapter 5*. Then, the performance of CLC-integrated BFPP is compared using different oxygen carriers to find out the most suitable one as presented in *Chapter 6*. Additionally, novel Fe2O3/Al2O3 composite nanofibrous oxygen carriers were developed using the electrospinning technique to confront the sintering issues associated with high temperature CLC operations as presented in *Chapter 7*.

The following works are done in this research work:

- Validation of aspenONE models
- Parametric analysis
- Energy, Exergy and Environmental analysis
- Synthesis of novel Fe2O3/Al2O3 composite nanofibrous oxygen carriers
- Thermal cycling and redox cycling of the Fe2O3/Al2O3 composite nanofibres
- SEM-EDAX and XRD analysis of the nanofibres

The key findings of the whole study presented in the previous chapters are summarized as follows:

- Based on the 3-E analyses study, it can be concluded that CLC integrated BFPP configuration is energetically, exergetically and environmentally efficient compared to the conventional BFPP.
- Based on the 3-E analyses, it can be concluded that the three-reactor CLC plant with hydrogen co-generation is energetically, exergetically and environmentally feasible and efficient.

- The CLC based plants integrated with methane and ammonia synthesis may not be a better choice for electricity production due to significant loss in energy.
- As iron ore is largely available in India at lower cost as compared to copper ore. Hence, the bimetallic oxygen carrier is preferable option as compared to CuO and Fe_2O_3 alone.
- Based upon the characterization results after 20 thermal and 20 redox cycles, it is evident that the Fe_2O_3/Al_2O_3 composite nanofibres are more resistant to thermal sintering than the nanoparticles. Hence, these nanofibres could be a promising option for oxygen carrier in lengthy CLC operations.

8.2 Scope for future work

In the present work, a steady state simulation of CLC integrated biomass fired power plant coupled with the CO_2 utilization plant is developed and analysed based on energy, exergy and environmental analyses. However, the work can be further continued, as there is a good scope for the future work. The scope for future work is given below.

- Equilibrium based Gibbs reactors are used in the CLC and CDU plants. These reactors may be replaced with the designed reactors with appropriate chemistries and kinetics to get better estimates.
- Experimental evaluation of the nanofibrous oxygen carriers for CLC of solid fuels and study the effect of ash on the performance on these nanofibrous oxygen carriers.
- Development of pilot scale plant for CLC integrated BFPP and all the CO_2 utilization plants separately and coupled with each other as given in the present work can be conducted.
- The proposed novel nanostructured metal oxide synthesis route can be investigated for the synthesis of specialized metal oxides for various chemical looping applications.
- The synthesis of nanostructured metal oxides using natural ores is also a potential area for further exploration.

List of Publications

INTERNATIONAL JOURNALS:

1. Performance assessment of novel nanofibrous Fe2O3/Al2O3 oxygen carriers for chemical looping combustion of gaseous fuel, Shailesh Singh Sikarwar , Kiran Donthula, Venkata Suresh Patnaikuni, Manohar Kakunuri , Ramsagar Vooradi, **Chemical Papers** (2023)

   doi: https://doi.org/10.1007/s11696-023-03199-z
2. Energy and Exergy analysis of Biomass Direct Chemical Looping Combustion for CO2 capture and Utilization, Shailesh Singh Sikarwar, Ramsagar Vooradi, Venkata Suresh Patnaikuni, **Computer Aided Chemical Engineering** 52 (2023) 3001-3006

   doi: https://doi.org/10.1016/B978-0-443-15274-0.50478-9
3. A novel thermally stable Fe_2O_3/Al_2O_3 nanofiber-based oxygen carrier for chemical-looping combustion, Shailesh Singh Sikarwar , Gajanan Dattarao Surywanshi , Venkata Suresh Patnaikuni, Manohar Kakunuri , Ramsagar Vooradi, **Chemical Papers** 76 (2022) 3987-3993

   doi : https://doi.org/10.1007/s11696-022-02129-9
4. Chemical looping combustion integrated Organic Rankine Cycled biomass-fired power plant - Energy and exergy analyses, Shailesh Singh Sikarwar , Gajanan Dattarao Surywanshi , Venkata Suresh Patnaikuni, Manohar Kakunuri , Ramsagar Vooradi, **Renewable Energy** 155 (2020) 931-949

   doi : https://doi.org/10.1016/j.renene.2020.03.114

INTERNATIONAL / NATIONAL CONFERENCES:

1. Energy and exergy analysis of CLC based biomass fired power plant with different oxygen carriers, Shailesh Singh Sikarwar, Ramsagar vooradi, Venkata Suresh Patnaikuni and Manohar Kakunuri, International Energy, Exergy, Environment symposium (IEEES-14), Istanbul, Turkey, Dec 24-27, 2023
2. Interaction between Coal-Ash and Iron-Ore in Chemical Looping Combustion, S.S. Sikarwar, Surywanshi Gajanan D, B. Basant K. Pillai, Venkata Suresh Patnaikuni, Manohar Kakunuri, Vooradi. R., International Conference on Sustainable Energy and Green Technology 2019 (SEGT 2019), Bangkok, Thailand, Dec 11-14, 2019.
3. Heat Integration of Chemical Looping Combustion based Biomass Fired Power plant, S.S. Sikarwar, Surywanshi Gajanan D, B. Basant K. Pillai, Venkata Suresh Patnaikuni, Sarath Babu Anne, Ramsagar Vooradi, 2nd International Conference on New Frontiers in Chemical, Energy and Environmental Engineering (INCEEE-2019), NIT Warangal, Feb 15-16, 2019
4. Thermodynamic Analysis of Chemical Looping Combustion Integrated Sugarcane Bagasse Based Biomass Power Plant, S.S. Sikarwar, Surywanshi Gajanan D, B. Basant K. Pillai, Venkata Suresh Patnaikuni, Sarath Babu Anne, Ramsagar Vooradi, International Conference on Advances and Challenges for Sustainable Ecosystem (ICACSE-2018), NIT Tiruchirappalli, 6-8, Dec., 2018.

References

1. Aasberg-Petersen, K., Nielsen, C. S., Dybkjær, I., & Perregaard, J. (2008). Large scale methanol production from natural gas. *Haldor Topsoe*, *22*.
2. Abdalla, A., Mohamedali, M., & Mahinpey, N. (2023). Recent progress in the development of synthetic oxygen carriers for chemical looping combustion applications. Catalysis Today, 407, 21-51.
3. Adanez, J., Abad, A., Garcia-Labiano, F., Gayan, P., & De Diego, L. F. (2012). Progress in chemical-looping combustion and reforming technologies. *Progress in energy and combustion science*, *38*(2), 215-282.
4. Adánez, J., Abad, A., Mendiara, T., Gayán, P., De Diego, L. F., & García-Labiano, F. (2018). Chemical looping combustion of solid fuels. *Progress in Energy and Combustion Science*, *65*, 6-66.
5. Adánez-Rubio, I., Abad, A., Gayán, P., De Diego, L. F., García-Labiano, F., & Adánez, J. (2014). Biomass combustion with CO2 capture by chemical looping with oxygen uncoupling (CLOU). *Fuel Processing Technology*, *124*, 104-114.
6. Aghaie, M., Mehrpooya, M., & Pourfayaz, F. (2016). Introducing an integrated chemical looping hydrogen production, inherent carbon capture and solid oxide fuel cell biomass fueled power plant process configuration. *Energy conversion and management*, *124*, 141-154.
7. Ahmadi, P., Dincer, I., & Rosen, M. A. (2013). Development and assessment of an integrated biomass-based multi-generation energy system. *Energy*, *56*, 155-166.
8. Akram, W., Sanjay, & Hassan, M. A. (2021). Chemical looping combustion with nanosize oxygen carrier: a review. *International Journal of Environmental Science and Technology*, *18*, 787-798.
9. Al Asfar, J., AlShwawra, A., Shaban, N. A., Alrbai, M., Qawasmeh, B. R., Sakhrieh, A., ... & Odeh, O. (2020). Thermodynamic analysis of a biomass-fired lab-scale power plant. *Energy*, *194*, 116843.
10. Al Mesfer, M. K., Danish, M., Fahmy, Y. M., & Rashid, M. M. (2018). Post-combustion CO2 capture with activated carbons using fixed bed adsorption. Heat and Mass Transfer, 54, 2715-2724.
11. Alalwan, H. A., & Alminshid, A. H. (2021). CO2 capturing methods: Chemical looping combustion (CLC) as a promising technique. *Science of The Total Environment*, *788*, 147850.
12. Alalwan, H. A., Cwiertny, D. M., & Grassian, V. H. (2017). Co3O4 nanoparticles as oxygen carriers for chemical looping combustion: a materials characterization approach to understanding oxygen carrier performance. *Chemical Engineering Journal*, *319*, 279-287.
13. Alalwan, H. A., Mason, S. E., Grassian, V. H., & Cwiertny, D. M. (2018). α-Fe2O3 nanoparticles as oxygen carriers for chemical looping combustion: an integrated materials characterization approach to understanding oxygen carrier performance, reduction mechanism, and particle size effects. *Energy & fuels*, *32*(7), 7959-7970.
14. Algieri, A. (2016). Comparative investigation of the performances of subcritical and transcritical biomass-fired ORC systems for micro-scale CHP applications. *Procedia Computer Science*, *83*, 855-862.
15. Algieri, A., & Morrone, P. (2014). Techno-economic analysis of biomass-fired ORC systems for single-family combined heat and power (CHP) applications. *Energy Procedia*, *45*, 1285-1294.
16. Al-Hitmi, K. M. R. (2012). QAFAC: Carbon dioxide recovery plant. *Sustainable Technologies, Systems and Policies*, *2012*(2), 22.

17. Ali, U., Font-Palma, C., Akram, M., Agbonghae, E. O., Ingham, D. B., & Pourkashanian, M. (2017). Comparative potential of natural gas, coal and biomass fired power plant with post-combustion CO2 capture and compression. *International Journal of Greenhouse Gas Control*, *63*, 184-193.
18. Al-Qayim, K., Nimmo, W. and Pourkashanian, M. (2015). Comparative techno-economic assessment of biomass and coal with CCS technologies in a pulverized combustion power plant in the United Kingdom. International Journal of Greenhouse Gas Control, 43, pp.82-92.
19. Al-Sulaiman, F. A., Dincer, I., & Hamdullahpur, F. (2012). Energy and exergy analyses of a biomass trigeneration system using an organic Rankine cycle. *Energy*, *45*(1), 975-985.
20. Annual report 2017-2018, Ministry of New and Renewable Energy Government of India https://mnre.gov.in/file-manager/annual-report/2017-2018/EN/index.htm
21. Aspen Tech. Aspen Physical Property System: Physical Property Methods, Methods. (2009) 1–234.
22. Azarpour, A., Suhaimi, S., Zahedi, G., & Bahadori, A. (2013). A review on the drawbacks of renewable energy as a promising energy source of the future. *Arabian Journal for Science and Engineering*, *38*, 317-328.
23. Babin, A., Vaneeckhaute, C., & Iliuta, M. C. (2021). Potential and challenges of bioenergy with carbon capture and storage as a carbon-negative energy source: A review. Biomass and Bioenergy, 146, 105968.
24. Bhattacharyya, D. (2022). Design and optimization of hybrid membrane–solvent-processes for post-combustion CO2 capture. Current Opinion in Chemical Engineering, 36, p.100768.
25. Bhui, B., & Vairakannu, P. (2019). Prospects and issues of integration of co-combustion of solid fuels (coal and biomass) in chemical looping technology. *Journal of environmental management*, *231*, 1241-1256.
26. Borsukiewicz-Gozdur, A., Wiśniewski, S., Mocarski, S., & Bańkowski, M. (2014). ORC power plant for electricity production from forest and agriculture biomass. *Energy Conversion and Management*, *87*, 1180-1185.
27. Brinkman, M.L., da Cunha, M.P., Heijnen, S., Wicke, B., Guilhoto, J.J., Walter, A., Faaij, A.P. and van der Hilst, F. (2018). Interregional assessment of socio-economic effects of sugarcane ethanol production in Brazil. Renewable and sustainable energy reviews, 88, pp.347-362.
28. Bu, X., Wang, L., & Li, H. (2013). Performance analysis and working fluid selection for geothermal energy-powered organic Rankine-vapor compression air conditioning. *Geothermal Energy*, *1*, 1-14.
29. Bui, M., Fajardy, M., & Mac Dowell, N. (2018). Bio-energy with carbon capture and storage (BECCS): Opportunities for performance improvement. *Fuel*, *213*, 164-175.
30. Bundela, P. S., & Vivek, C. (2010). Sustainable development through waste heat recovery. *American Journal of Environmental Sciences*, *6*(1), 83-89.
31. Carbon Recycling International, 2016. World's Largest CO2 Methanol Plant, http://carbonrecycling.is/george-olah/2016/2/14/worldslargest-co2-methanol-plant
32. Carpentieri, M., Corti, A., Lombardi, L., 2005. Life cycle assessment (LCA) of an integrated biomass gasification combined cycle (IBGCC) with CO2 removal. Energ. Convers. Manage. 46, 1790–1808.
33. Carraro, G., Bori, V., Lazzaretto, A., Toniato, G., & Danieli, P. (2020). Experimental investigation of an innovative biomass-fired micro-ORC system for cogeneration applications. *Renewable Energy*, *161*, 1226-1243.
34. Chang, F. C., Liao, P. H., Tsai, C. K., Hsiao, M. C., & Wang, H. P. (2014). Chemical-looping combustion of syngas with nano CuO–NiO on chabazite. *Applied energy*, *113*, 1731-1736.

35. Chao, C., Deng, Y., Dewil, R., Baeyens, J., & Fan, X. (2021). Post-combustion carbon capture. *Renewable and Sustainable Energy Reviews*, *138*, 110490.
36. Cheng, Z., Li, S., Liu, Y., Zhang, Y., Ling, Z., Yang, M., ... & Song, Y. (2022). Post-combustion CO2 capture and separation in flue gas based on hydrate technology: A review. *Renewable and Sustainable Energy Reviews*, *154*, 111806.
37. Colonna, P., Casati, E., Trapp, C., Mathijssen, T., Larjola, J., Turunen-Saaresti, T., & Uusitalo, A. (2015). Organic Rankine cycle power systems: from the concept to current technology, applications, and an outlook to the future. *Journal of Engineering for Gas Turbines and Power*, *137*(10), 100801.
38. Coppola, A., & Scala, F. (2021). Chemical looping for combustion of solid biomass: A review. *Energy & Fuels*, *35*(23), 19248-19265.
39. Cormos, A. M., & Cormos, C. C. (2014). Investigation of hydrogen and power co-generation based on direct coal chemical looping systems. *International journal of hydrogen energy*, *39*(5), 2067-2077.
40. Cormos, C. C. (2015). Biomass direct chemical looping for hydrogen and power co-production: Process configuration, simulation, thermal integration and techno-economic assessment. *Fuel processing technology*, *137*, 16-23.
41. Dale, S. *BP Statistical Review of World Energy 2021*, 70th ed.; BP Plc: London, UK, 2021; Available online: **https://www.bp.com/en/global/corporate/energy-economics/statistical-review-of-world-energy.html**
42. Daneshmand-Jahromi, S., Sedghkerdar, M. H., & Mahinpey, N. (2023). A review of chemical looping combustion technology: Fundamentals, and development of natural, industrial waste, and synthetic oxygen carriers. *Fuel*, *341*, 127626.
43. Darmawan, A., Ajiwibowo, M. W., Yoshikawa, K., Aziz, M., & Tokimatsu, K. (2018). Energy-efficient recovery of black liquor through gasification and syngas chemical looping. *Applied Energy*, *219*, 290-298.
44. De Diego, L.F., Gayán, P., García-Labiano, F., Celaya, J., Abad, A. and Adánez, J. (2005). Impregnated CuO/Al2O3 oxygen carriers for chemical-looping combustion: avoiding fluidized bed agglomeration. Energy & Fuels, 19(5), pp.1850-1856.
45. de Meyer, F., & Jouenne, S. (2022). Industrial carbon capture by absorption: recent advances and path forward. *Current Opinion in Chemical Engineering*, *38*, 100868.
46. De Vos, Y., Jacobs, M., Van Der Voort, P., Van Driessche, I., Snijkers, F., & Verberckmoes, A. (2019). Sustainable iron-based oxygen carriers for Chemical Looping for Hydrogen Generation. *international journal of hydrogen energy*, *44*(3), 1374-1391.
47. De Vos, Y., Jacobs, M., Van Der Voort, P., Van Driessche, I., Snijkers, F., & Verberckmoes, A. (2020). Development of stable oxygen carrier materials for chemical looping processes—a review. *Catalysts*, *10*(8), 926.
48. Del Grosso, M., Sridharan, B., Tsekos, C., Klein, S., & de Jong, W. (2020). A modelling based study on the integration of 10 MWth indirect torrefied biomass gasification, methanol and power production. *Biomass and bioenergy*, *136*, 105529.
49. Diego, M. E., Arias, B., & Abanades, J. C. (2016). Analysis of a double calcium loop process configuration for CO2 capture in cement plants. *Journal of Cleaner Production*, *117*, 110-121.
50. Dincer, I., & Acar, C. (2017). Smart energy systems for a sustainable future. *Applied energy*, *194*, 225-235.
51. Dos Santos, R., Patel, M., Cuadros, J., & Martins, Z. (2016). Influence of mineralogy on the preservation of amino acids under simulated Mars conditions. *Icarus*, *277*, 342-353.
52. Dwivedi, Y. K., Hughes, L., Kar, A. K., Baabdullah, A. M., Grover, P., Abbas, R., ... & Wade, M. (2022). Climate change and COP26: Are digital technologies and information

management part of the problem or the solution? An editorial reflection and call to action. *International Journal of Information Management*, *63*, 102456.
53. Dziejarski, B., Krzyżyńska, R., & Andersson, K. (2023). Current status of carbon capture, utilization, and storage technologies in the global economy: A survey of technical assessment. *Fuel*, *342*, 127776.
54. Erdem, H. H., Akkaya, A. V., Cetin, B., Dagdas, A., Sevilgen, S. H., Sahin, B., ... & Atas, S. (2009). Comparative energetic and exergetic performance analyses for coal-fired thermal power plants in Turkey. *International Journal of Thermal Sciences*, *48*(11), 2179-2186.
55. Fajardy, M. and Mac Dowell, N. (2017). Can BECCS deliver sustainable and resource efficient negative emissions?. Energy & Environmental Science, 10(6), pp.1389-1426.
56. Fan, L.S., (2010). Chemical Looping Systems for Fossil Energy Conversion, American Institute of Chemical Engineers.
57. Frauzem, R., Woodley, J. M., & Gani, R. (2017). Application of a computer-aided framework for the design of CO2 capture and utilization processes. In *Computer Aided Chemical Engineering* (Vol. 40, pp. 2653-2658). Elsevier.
58. Fu, B. R., Hsu, S. W., Liu, C. H., & Liu, Y. C. (2014). Statistical analysis of patent data relating to the organic Rankine cycle. *Renewable and Sustainable Energy Reviews*, *39*, 986-994.
59. Gerbens-Leenes, W., Hoekstra, A.Y. and van der Meer, T.H. (2009). The water footprint of bioenergy. Proceedings of the National Academy of Sciences, 106(25), pp.10219-10223.
60. Gholamian, E., Mahmoudi, S. S., & Zare, V. (2016). Proposal, exergy analysis and optimization of a new biomass-based cogeneration system. *Applied Thermal Engineering*, *93*, 223-235.
61. Gielen, D., Boshell, F., Saygin, D., Bazilian, M.D., Wagner, N., Gorini, R. (2019). The role of renewable energy in the global energy transformation Energy Strategy Reviews, 24, pp. 38-50.
62. Gizer, S. G., Polat, O., Ram, M. K., & Sahiner, N. (2022). Recent developments in CO2 capture, utilization, related materials, and challenges. *International Journal of Energy Research*, *46*(12), 16241-16263.
63. Gungor, B., & Dincer, I. (2021). Development of a sustainable community with an integrated renewable and waste to energy system for multiple useful outputs. *Journal of Cleaner Production*, *312*, 127704.
64. Gungor, B., & Dincer, I. (2022). A renewable energy based waste-to-energy system with hydrogen options. *International Journal of Hydrogen Energy*, *47*(45), 19526-19537.
65. Gür, T. M. (2022). Carbon dioxide emissions, capture, storage and utilization: Review of materials, processes and technologies. *Progress in Energy and Combustion Science*, *89*, 100965
66. Hafeez, S., Safdar, T., Pallari, E., Manos, G., Aristodemou, E., Zhang, Z., ... & Constantinou, A. (2021). CO 2 capture using membrane contactors: A systematic literature review. *Frontiers of Chemical Science and Engineering*, *15*, 720-754.
67. Hall, C.A., Lambert, J.G. and Balogh, S.B. (2014). EROI of different fuels and the implications for society. Energy policy, 64, pp.141-152.
68. Hayati, A. P., Zhafran, M., Sidiq, M. A., Rinaldi, A., Fitria, B., Tarisma, R., & Bindar, Y. (2020). Analysis of power from palm oil solid waste for biomass power plants: A case study in Aceh Province. *Chemosphere*, *253*, 126714.
69. He, Y., Zhu, L., Li, L., & Liu, G. (2020). Hydrogen and power cogeneration based on chemical looping combustion: Is it capable of reducing carbon emissions and the cost of production?. *Energy & Fuels*, *34*(3), 3501-3512.

70. Hossen, M. D., Islam, M. F., Ishraque, M. F., Shezan, S. A., & Arifuzzaman, S. M. (2022). Design and implementation of a hybrid solar-wind-biomass renewable energy system considering meteorological conditions with the power system performances. *International journal of photoenergy*, Article ID 8792732.
71. https://www.iea.org/publications/freepublications/publication/IndiaEnergyOutlook_WEO2015.pdf, 2015
72. https://www.iea.org/reports/energy-technology-perspectives-2010, License: CC BY 4.0 IEA (2023a), CO_2 Emissions in 2022, IEA, Paris https://www.iea.org/reports/co2-emissions-in-2022, License: CC BY 4.0
73. Hu, J., Galvita, V. V., Poelman, H., Detavernier, C., & Marin, G. B. (2017). A core-shell structured Fe2O3/ZrO2@ ZrO2 nanomaterial with enhanced redox activity and stability for CO2 conversion. *Journal of CO2 Utilization*, *17*, 20-31.
74. Hu, S., Chen, Q., Xiang, J., Su, S., Sun, L., Wang, Y., Xu, B. and Chi, H. (2016). Modification of iron oxide to promote reaction property for chemical looping combustion with CO. Combustion Science and Technology, 188(8), pp.1319-1330.
75. Hu, Z., Wang, X., Zhang, L., Yang, S., Ruan, R., Bai, S., ... & Tan, H. (2020). Emission characteristics of particulate matters from a 30 MW biomass-fired power plant in China. *Renewable Energy*, *155*, 225-236.
76. Huang, Z., He, F., Feng, Y., Zhao, K., Zheng, A., Chang, S., & Li, H. (2013). Synthesis gas production through biomass direct chemical looping conversion with natural hematite as an oxygen carrier. *Bioresource technology*, *140*, 138-145.
77. IEA (2010), Energy Technology Perspectives 2010, IEA, Paris
78. IEA (2020), Key World Energy Statistics 2020, IEA, Paris https://www.iea.org/reports/key-world-energy-statistics-2020, License: CC BY 4.0
79. IEA (2023b), Tracking Clean Energy Progress 2023, IEA, Paris https://www.iea.org/reports/tracking-clean-energy-progress-2023, License: CC BY 4.0
80. Ismail, M., Liu, W., Dunstan, M.T. and Scott, S.A. (2016). Development and performance of iron based oxygen carriers containing calcium ferrites for chemical looping combustion and production of hydrogen. International journal of hydrogen energy, 41(7), pp.4073-4084.
81. Jain, V. (2019). Fossil fuels, GHG emissions and clean energy development: Asian giants in a comparative perspective. Millennial Asia, 10(1), 1-24.
82. Jang, Y., & Lee, J. (2018). Optimizations of the organic Rankine cycle-based domestic CHP using biomass fuel. *Energy Conversion and Management*, *160*, 31-47.
83. Joshi, A., Shah, V., Mohapatra, P., Kumar, S., Joshi, R. K., Kathe, M., ... & Fan, L. S. (2021). Chemical looping-A perspective on the next-gen technology for efficient fossil fuel utilization. *Advances in Applied Energy*, *3*, 100044.
84. Kanoğlu, M., Çengel, Y. A., & Dinçer, İ. (2012). *Efficiency evaluation of energy systems*. Springer Science & Business Media.
85. Keller, M., Arjmand, M., Leion, H., & Mattisson, T. (2014). Interaction of mineral matter of coal with oxygen carriers in chemical-looping combustion (CLC). Chemical Engineering Research and Design, 92(9), 1753-1770.
86. Kevat, M. D., & Banerjee, T. (2018). Process simulation and energy analysis of chemical looping combustion and chemical looping with oxygen uncoupling for sawdust biomass. *Energy Technology*, *6*(7), 1237-1247.
87. Khanmohammadi, S., & Atashkari, K. (2018). Modeling and multi-objective optimization of a novel biomass feed polygeneration system integrated with multi effect desalination unit. *Thermal Science and Engineering Progress*, *8*, 269-283.

88. Khanmohammadi, S., Atashkari, K., & Kouhikamali, R. (2016). Modeling and assessment of a biomass gasification integrated system for multigeneration purpose. *International Journal of Chemical Engineering*. ID 2639241.
89. Khatri, P., & Pandit, A. B. (2022). Systematic review of life cycle assessments applied to sugarcane bagasse utilization alternatives. Biomass and Bioenergy, 158, 106365.
90. Kobayashi, N., & Fan, L. S. (2011). Biomass direct chemical looping process: a perspective. *Biomass and Bioenergy*, *35*(3), 1252-1262.
91. Kumar, A., Kumar, N., Baredar, P., & Shukla, A. (2015). A review on biomass energy resources, potential, conversion and policy in India. *Renewable and sustainable energy reviews*, *45*, 530-539.
92. Lewis, W. K., & Gilliland, E. R. (1954). *U.S. Patent No. 2,665,972*. Washington, DC: U.S. Patent and Trademark Office.
93. Li, F., Zeng, L., & Fan, L. S. (2010). Biomass direct chemical looping process: Process simulation. *Fuel*, *89*(12), 3773-3784.
94. Li, G., Liu, F., Liu, T., Yu, Z., Liu, Z., & Fang, Y. (2019). Life cycle assessment of coal direct chemical looping hydrogen generation with Fe2O3 oxygen carrier. *Journal of Cleaner Production*, *239*, 118118.
95. Lin, J. C. M. (2007). Combination of a biomass fired updraft gasifier and a stirling engine for power production. *J. Energy Resour. Technol*, 129(1), 66-70.
96. Liu, D., Liu, M., Xiao, B., Guo, X., Niu, D., Qin, G., & Jia, H. (2020). Exploring biomass power generation's development under encouraged policies in China. *Journal of Cleaner Production*, *258*, 120786.
97. Liu, H., Shao, Y., & Li, J. (2011). A biomass-fired micro-scale CHP system with organic Rankine cycle (ORC)–Thermodynamic modelling studies. *Biomass and Bioenergy*, *35*(9), 3985-3994.
98. Liu, W., Liu, C., Gogoi, P., & Deng, Y. (2020). Overview of biomass conversion to electricity and hydrogen and recent developments in low-temperature electrochemical approaches. *Engineering*, *6*(12), 1351-1363.
99. Liu, Y., Kirchesch, P., Graule, T., Liersch, A., & Clemens, F. (2015). Nanoparticle prepared mechanically stable hierarchically porous silica granulates and their application as oxygen carrier supports for chemical looping combustion. *Journal of Materials Chemistry A*, *3*(22), 11863-11873.
100. Liu, Y., Long, Y., Tang, Y., Gu, Z. and Li, K. (2019). Effect of preparation method on the structural characteristics of NiO-ZrO2 oxygen carriers for chemical-looping combustion. Chemical Research in Chinese Universities, 35(6), pp.1024-1031.
101. Liu, Y., Qin, L., Cheng, Z., Goetze, J. W., Kong, F., Fan, J. A., & Fan, L. S. (2019). Near 100% CO selectivity in nanoscaled iron-based oxygen carriers for chemical looping methane partial oxidation. *Nature Communications*, *10*(1), 5503.
102. Luo, M., Yi, Y., Wang, S., Wang, Z., Du, M., Pan, J., & Wang, Q. (2018). Review of hydrogen production using chemical-looping technology. *Renewable and Sustainable Energy Reviews*, *81*, 3186-3214.
103. Lyngfelt, A. (2014). Chemical-looping combustion of solid fuels–status of development. *Applied energy*, *113*, 1869-1873.
104. Lyngfelt, A. (2020). Chemical looping combustion: status and development challenges. *Energy & Fuels*, *34*(8), 9077-9093.
105. Lyngfelt, A., Brink, A., Langørgen, Ø., Mattisson, T., Rydén, M., & Linderholm, C. (2019). 11,000 h of chemical-looping combustion operation—Where are we and where do we want to go?. *International Journal of Greenhouse Gas Control*, *88*, 38-56.
106. Ma, Z., Zhang, S., & Xiao, R. (2019). Insights into the relationship between microstructural evolution and deactivation of Al2O3 supported Fe2O3 oxygen carrier in chemical looping combustion. *Energy Conversion and Management*, *188*, 429-437.

107. Madejski, P., Chmiel, K., Subramanian, N., & Kuś, T. (2022). Methods and techniques for CO2 capture: Review of potential solutions and applications in modern energy technologies. *Energies*, *15*(3), 887.
108. Malico, I., Pereira, R. N., Gonçalves, A. C., & Sousa, A. M. (2019). Current status and future perspectives for energy production from solid biomass in the European industry. *Renewable and Sustainable Energy Reviews*, *112*, 960-977.
109. Mattisson, T., Johansson, M. and Lyngfelt, A. (2006). The use of NiO as an oxygen carrier in chemical-looping combustion. Fuel, 85(5-6), pp.736-747.
110. Maya, J.C., Chejne, F. and Bhatia, S.K. (2017). Effect of sintering on the reactivity of copper-based oxygen carriers synthesized by impregnation. Chemical Engineering Science, 162, pp.131-140.
111. Mazari, S. A., Ali, B. S., Jan, B. M., Saeed, I. M., & Nizamuddin, S. (2015). An overview of solvent management and emissions of amine-based CO2 capture technology. *International Journal of Greenhouse Gas Control*, *34*, 129-140.
112. Mei, D., Soleimanisalim, A. H., Lyngfelt, A., Leion, H., Linderholm, C., & Mattisson, T. (2022). Modelling of gas conversion with an analytical reactor model for biomass chemical looping combustion (bio-CLC) of solid fuels. Chemical Engineering Journal, 433, 133563.
113. Mendiara, T., Abad, A., De Diego, L. F., García-Labiano, F., Gayán, P., & Adánez, J. (2013). Biomass combustion in a CLC system using an iron ore as an oxygen carrier. *International Journal of Greenhouse Gas Control*, *19*, 322-330.
114. Mendiara, T., Adánez-Rubio, I., Gayán, P., Abad, A., De Diego, L. F., García-Labiano, F., & Adánez, J. (2016). Process comparison for biomass combustion: in situ gasification-chemical looping combustion (iG-CLC) versus chemical looping with oxygen uncoupling (CLOU). *Energy Technology*, *4*(10), 1130-1136.
115. Mendiara, T., Pérez, R., Abad, A., De Diego, L. F., García-Labiano, F., Gayán, P., & Adánez, J. (2012). Low-cost Fe-based oxygen carrier materials for the i G-CLC process with coal. 1. Industrial & engineering chemistry research, 51(50), 16216-16229.
116. Mendiara, T., Pérez-Astray, A., Izquierdo, M. T., Abad, A., De Diego, L. F., García-Labiano, F., ... & Adánez, J. (2018). Chemical looping combustion of different types of biomass in a 0.5 kWth unit. *Fuel*, *211*, 868-875.
117. Mercado, J. P., Ubando, A. T., Gonzaga, J. A., and Naqvi, S. R. (2023). Life cycle assessment of a biomass based chemical looping combustion. Environmental Research, 217, 114876.
118. Meyer, D., Wong, C. S., Engle, F., & Krumdieck, S. (2013). Design and build of a 1 kilowatt organic Rankine cycle power generator. 35th New Zealand Geothermal Workshop: 2013 Proceedings.
119. Mikkelsen, M., Jørgensen, M., & Krebs, F. C. (2010). The teraton challenge. A review of fixation and transformation of carbon dioxide. *Energy & Environmental Science*, *3*(1), 43-81.
120. Mishra, A., & Li, F. (2018). Chemical looping at the nanoscale—challenges and opportunities. *Current opinion in chemical engineering*, *20*, 143-150.
121. Mok, L-F.(1982). Sensitivity Study of Energy Consumption in Am Operation, H.S. Thesis, Univ. of California, Berkeley.
122. Moriarty, P. and Honnery, D. (2017). Assessing the climate mitigation potential of biomass. AIMS Energy, 5(1), pp.20-38.
123. Morrone, P., Algieri, A., Castiglione, T., Perrone, D., & Bova, S. (2018). Investigation of integrated organic rankine cycles and wind turbines for micro-scale applications. *Energy Procedia*, *148*, 986-993.
124. Mukherjee, S., Kumar, P., Yang, A., & Fennell, P. (2015). Energy and exergy analysis of chemical looping combustion technology and comparison with pre-combustion and oxy-

fuel combustion technologies for CO2 capture. *Journal of environmental chemical engineering*, *3*(3), 2104-2114.
125. Nielsen, A. (1968). *An Investigation on Promoted Iron Catalysts for the Synthesis of Ammonia*, 3rd ed., Jul. Gjellerups Forlag.
126. Nur, T. B., Setiawan, A., Yudanto, B. G., & Ependi, S. (2019). Techno-economic analysis of organic rankine cycle fueled biomass waste from palm oil mill. In *AIP Conference Proceedings* (Vol. 2085, No. 1). AIP Publishing.
127. Odunlami, O. A., Vershima, D. A., Oladimeji, T. E., Nkongho, S., Ogunlade, S. K., & Fakinle, B. S. (2022). Advanced techniques for the capturing and separation of CO2–a review. *Results in Engineering*, *15*, 100512.
128. Olabi, A. G., Obaideen, K., Elsaid, K., Wilberforce, T., Sayed, E. T., Maghrabie, H. M., & Abdelkareem, M. A. (2022). Assessment of the pre-combustion carbon capture contribution into sustainable development goals SDGs using novel indicators. *Renewable and Sustainable Energy Reviews*, *153*, 111710.
129. Oruc, O., & Dincer, I. (2020). Evaluation of hydrogen production with iron-based chemical looping fed by different biomass. *International Journal of Hydrogen Energy*, *45*(60), 34557-34565.
130. Osman, A. I., Abdelkader, A., Farrell, C., Rooney, D., & Morgan, K. (2019). Reusing, recycling and up-cycling of biomass: A review of practical and kinetic modelling approaches. *Fuel Processing Technology*, *192*, 179-202.
131. Otto, A., Grube, T., Schiebahn, S., & Stolten, D. (2015). Closing the loop: captured CO 2 as a feedstock in the chemical industry. *Energy & environmental science*, *8*(11), 3283-3297.
132. Otto, S. K., Kousi, K., Neagu, D., Bekris, L., Janek, J., & Metcalfe, I. S. (2019). Exsolved nickel nanoparticles acting as oxygen storage reservoirs and active sites for redox CH4 conversion. *ACS applied energy materials*, *2*(10), 7288-7298.
133. Ozdil, N. F. T., Segmen, M. R., & Tantekin, A. (2015). Thermodynamic analysis of an Organic Rankine Cycle (ORC) based on industrial data. *Applied Thermal Engineering*, *91*, 43-52.
134. Pan, P., Zhang, M., Xu, G., Chen, H., Song, X., & Liu, T. (2020). Thermodynamic and economic analyses of a new waste-to-energy system incorporated with a biomass-fired power plant. *Energies*, *13*(17), 4345.
135. Park, C. H., Lee, C. H., Guiver, M. D., & Lee, Y. M. (2011). Sulfonated hydrocarbon membranes for medium-temperature and low-humidity proton exchange membrane fuel cells (PEMFCs). *Progress in Polymer Science*, *36*(11), 1443-1498.
136. Pérez-Astray, A., Mendiara, T., de Diego, L. F., Abad, A., García-Labiano, F., Izquierdo, M. T., and Adánez, J. (2021). Behavior of a manganese-iron mixed oxide doped with titanium in reducing the oxygen demand for CLC of biomass. Fuel, 292, 120381.
137. Peu, S. D., Das, A., Hossain, M. S., Akanda, M. A. M., Akanda, M. M. H., Rahman, M., ... & Salah, M. M. (2023). A comprehensive review on recent advancements in absorption-based post combustion carbon capture technologies to obtain a sustainable energy sector with clean environment. Sustainability, 15(7), 5827.
138. Pezzuolo, A., Benato, A., Stoppato, A., & Mirandola, A. (2016). Fluid selection and plant configuration of an ORC-biomass fed system generating heat and/or power. *Energy Procedia*, *101*, 822-829.
139. Pillai, B. B. K., Surywanshi, G. D., Patnaikuni, V. S., Anne, S. B., & Vooradi, R. (2019). Performance analysis of a double calcium looping-integrated biomass-fired power plant: Exploring a carbon reduction opportunity. *International Journal of Energy Research*, *43*(10), 5301-5318. IEA, India energy outlook.

140. Portugal-Pereira, J., Soria, R., Rathmann, R., Schaeffer, R. and Szklo, A. (2015). Agricultural and agro-industrial residues-to-energy: Techno-economic and environmental assessment in Brazil. Biomass and bioenergy, 81, pp.521-533.
141. Prabowo, B., Aziz, M., Umeki, K., Susanto, H., Yan, M., & Yoshikawa, K. (2015). CO2-recycling biomass gasification system for highly efficient and carbon-negative power generation. *Applied Energy*, *158*, 97-106.
142. Preißinger, M., Heberle, F., & Brüggemann, D. (2012). Thermodynamic analysis of double-stage biomass fired Organic Rankine Cycle for micro-cogeneration. *International Journal of Energy Research*, *36*(8), 944-952.
143. Pröll, T. and Zerobin, F. (2019). Biomass-based negative emission technology options with combined heat and power generation. Mitigation and Adaptation Strategies for Global Change, 24(7), pp.1307-1324.
144. Qasim, M., Ayoub, M., Ghazali, N. A., Aqsha, A., & Ameen, M. (2021). Recent advances and development of various oxygen carriers for the chemical looping combustion process: a review. *Industrial & Engineering Chemistry Research*, *60*(24), 8621-8641.
145. Quoilin, S., Van Den Broek, M., Declaye, S., Dewallef, P., & Lemort, V. (2013). Techno-economic survey of Organic Rankine Cycle (ORC) systems. *Renewable and sustainable energy reviews*, *22*, 168-186.
146. Rahman, A., Farrok, O., & Haque, M. M. (2022). Environmental impact of renewable energy source based electrical power plants: Solar, wind, hydroelectric, biomass, geothermal, tidal, ocean, and osmotic. *Renewable and Sustainable Energy Reviews*, *161*, 112279.
147. Razi, F., & Dincer, I. (2022). Renewable energy development and hydrogen economy in MENA region: A review. *Renewable and Sustainable Energy Reviews*, *168*, 112763.
148. Ridha, F.N., Duchesne, M.A., Lu, X., Lu, D.Y., Filippou, D. and Hughes, R.W. (2016). Characterization of an ilmenite ore for pressurized chemical looping combustion. Applied energy, 163, pp.323-333.
149. Sahoo, B. D., Mukherjee, D., Joshi, K. D., Kaushik, T. C., & Gupta, S. C. (2016). Pressure induced phase transition and thermo-physical properties in LuX (X= N, P). *Materials Research Express*, *3*(4), 046502.
150. Scarlat, N., Dallemand, J.F., Taylor, N. and Banja, M., 2019. Brief on biomass for energy in the European Union.
151. Sharif, A., Bhattacharya, M., Afshan, S., & Shahbaz, M. (2021). Disaggregated renewable energy sources in mitigating CO2 emissions: new evidence from the USA using quantile regressions. *Environmental Science and Pollution Research*, *28*(41), 57582-57601.
152. Shen, L., Wu, J., Xiao, J., Song, Q., & Xiao, R. (2009). Chemical-looping combustion of biomass in a 10 kWth reactor with iron oxide as an oxygen carrier. *Energy & Fuels*, *23*(5), 2498-2505.
153. Sifat, N. S., & Haseli, Y. (2019). A critical review of CO2 capture technologies and prospects for clean power generation. *Energies*, *12*(21), 4143.
154. Sikarwar, S., Surywanshi, G., Patnaikuni, V., Kakunuri, M., & Vooradi, R. (2020). Chemical looping combustion integrated Organic Rankine Cycled biomass-fired power plant e Energy and exergy analyses. *Renewable Energy*, *155*, 931-949.
155. Singh, J. (2015). Overview of electric power potential of surplus agricultural biomass from economic, social, environmental and technical perspective—A case study of Punjab. *Renewable and Sustainable Energy Reviews*, *42*, 286-297.
156. Singh, J. (2016). A roadmap for production of sustainable, consistent and reliable electric power from agricultural biomass-An Indian perspective. *Energy Policy*, *92*, 246-254.

157. Siriwardane, R., Benincosa, W., Riley, J., Tian, H. and Richards, G. (2016). Investigation of reactions in a fluidized bed reactor during chemical looping combustion of coal/steam with copper oxide-iron oxide-alumina oxygen carrier. Applied Energy, 183, pp.1550-1564.
158. Situmorang, Y. A., Zhao, Z., An, P., Rizkiana, J., Prakoso, T., Abudula, A., & Guan, G. (2021). A small-scale power generation system based on biomass direct chemical looping process with organic rankine cycle. *Chemical Engineering and Processing-Process Intensification*, *163*, 108361.
159. Situmorang, Y. A., Zhao, Z., Yoshida, A., Abudula, A., & Guan, G. (2020). Small-scale biomass gasification systems for power generation (< 200 kW class): A review. *Renewable and sustainable energy reviews*, *117*, 109486.
160. Skorek-Osikowska, A., Bartela, Ł., & Kotowicz, J. (2017). Thermodynamic and ecological assessment of selected coal-fired power plants integrated with carbon dioxide capture. *Applied Energy*, *200*, 73-88.
161. Song, T., & Shen, L. (2018). Review of reactor for chemical looping combustion of solid fuels. *International Journal of Greenhouse Gas Control*, *76*, 92-110.
162. Song, T., Shen, T., Shen, L., Xiao, J., Gu, H., & Zhang, S. (2013). Evaluation of hematite oxygen carrier in chemical-looping combustion of coal. *Fuel*, *104*, 244-252.
163. Sotomonte, C. A. R., Ribeiro, S., Oliveira, E., Lora, E. E. S., & Venturini, O. J. (2011). Organic Rankine cycle associated with an absorption chiller for biomass applications. *Revista de Engenharia Térmica*, *10*(1-2), 15-22.
164. Staničić, I., Hanning, M., Deniz, R., Mattisson, T., Backman, R., & Leion, H. (2020). Interaction of oxygen carriers with common biomass ash components. Fuel processing technology, 200, 106313.
165. Statistical-Review-of-World-Energy, Statistical-Review-of-World-Energy @ Www.Bp.Com, (2017). https://www.bp.com/en/global/corporate/energy-economics/statistical-review-of-world-energy.html
166. Sun, Y., Jiang, E., Xu, X., Wang, J., Tu, R. and Fan, F. (2019). Influence of synthesized method on the cycle stability of NiO/NiAl2O4 during chemical looping combustion of biomass pyrolysis gas. Industrial & Engineering Chemistry Research, 58(29), pp.13163-13173.
167. Sun, Z., & Aziz, M. (2021a). Comparative thermodynamic and techno-economic assessment of green methanol production from biomass through direct chemical looping processes. *Journal of cleaner production*, *321*, 129023.
168. Sun, Z., & Aziz, M. (2021b). Thermodynamic analysis of a tri-generation system driven by biomass direct chemical looping combustion process. *Energy Conversion and Management*, *244*, 114517.
169. Sun, Z., Wang, S., & Aziz, M. (2022). Highly integrated system for ammonia and electricity production from biomass employing direct chemical looping: exergy and exergoeconomic analyses. *Energy Conversion and Management*, *251*, 115013.
170. Suresh, M. V. J. J., Reddy, K. S., & Kolar, A. K. (2010). 3-E analysis of advanced power plants based on high ash coal. *International Journal of Energy Research*, *34*(8), 716-735.
171. Surywanshi, G. D., Pillai, B. B. K., Patnaikuni, V. S., Vooradi, R., & Anne, S. B. (2019). 4-E analyses of chemical looping combustion based subcritical, supercritical and ultra-supercritical coal-fired power plants. *Energy Conversion and Management*, *200*, 112050.
172. Tahir, F., Saeed, M. A., & Ali, U. (2023). Biomass energy perspective in Pakistan based on chemical looping gasification for hydrogen production and power generation. *International Journal of Hydrogen Energy*, 48, 18211-18232.

173. Tchanche, B. F., Lambrinos, G., Frangoudakis, A., & Papadakis, G. (2011). Low-grade heat conversion into power using organic Rankine cycles–A review of various applications. *Renewable and Sustainable Energy Reviews*, *15*(8), 3963-3979.
174. U.S. Geological Survey. Mineral Commodity Summaries. Iron Ore 2017;1:2016–7. https://minerals.usgs.gov/minerals/pubs/commodity/iron_ore/mcs-2017-feore.pdf.
175. Wang, D., Chen, S., Xu, C., & Xiang, W. (2013). Energy and exergy analysis of a new hydrogen-fueled power plant based on calcium looping process. *International journal of hydrogen energy*, *38*(13), 5389-5400.
176. Wang, P., Means, N., Shekhawat, D., Berry, D., & Massoudi, M. (2015). Chemical-looping combustion and gasification of coals and oxygen carrier development: a brief review. Energies, 8(10), 10605-10635.
177. Wang, Q., Wu, W., & He, Z. (2019). Thermodynamic analysis and optimization of a novel organic Rankine cycle-based micro-scale cogeneration system using biomass fuel. *Energy Conversion and Management*, *198*, 111803.
178. Wei, X., Manovic, V., & Hanak, D. P. (2020). Techno-economic assessment of coal- or biomass-fired oxy-combustion power plants with supercritical carbon dioxide cycle. *Energy Conversion and Management*, *221*, 113143.
179. Wen, Y. Y., Li, Z. S., Xu, L., & Cai, N. S. (2012). Experimental study of natural Cu ore particles as oxygen carriers in chemical looping with oxygen uncoupling (CLOU). Energy & fuels, 26(6), 3919-3927.
180. Yan, L., Cao, Y., & He, B. (2019). Energy, exergy and economic analyses of a novel biomass fueled power plant with carbon capture and sequestration. *Science of The Total Environment*, *690*, 812-820.
181. Zaini, I. N., Nurdiawati, A., & Aziz, M. (2017). Cogeneration of power and H2 by steam gasification and syngas chemical looping of macroalgae. *Applied Energy*, *207*, 134-145.
182. Zhang, S., Wang, X., Mao, Z., Li, Y., Jin, B. and Xiao, R. (2020). Effect of calcination condition on the performance of iron ore in chemical-looping combustion. Fuel Processing Technology, 203, p.106395.
183. Zhu, Y., Liang, J., Yang, Q., Zhou, H., & Peng, K. (2019). Water use of a biomass direct-combustion power generation system in China: A combination of life cycle assessment and water footprint analysis. *Renewable and Sustainable Energy Reviews*, *115*, 109396.